M 2014

U.PORTO
FEUP FACULDADE DE ENGENHARIA
UNIVERSIDADE DO PORTO

THE CROSS-TALK BETWEEN ENDOTHELIAL CELLS AND MESENCHYMAL STEM CELLS IN A 3D MICROENVIRONMENT

DAVID BOAVENTURA TEIXEIRA GOMES

DISSERTAÇÃO DE MESTRADO APRESENTADA
À FACULDADE DE ENGENHARIA DA UNIVERSIDADE DO PORTO EM
ENGENHARIA BIOMÉDICA

Faculdade de Engenharia da Universidade do Porto

The cross-talk between endothelial cells and mesenchymal stem cells in a 3D microenvironment

David Boaventura Teixeira Gomes

Dissertação realizada no âmbito do
Mestrado em Engenharia Biomédica

Orientador: Doutora Cristina Barrias
Co-orientador: Doutora Aureliana Filipa Sousa

31 de Julho de 2014

"Eles não sabem, nem sonham,
que o sonho comanda a vida,
que sempre que um homem sonha
o mundo pula e avança
como bola colorida
entre as mãos de uma criança."

António Gedeão

This Thesis is dedicated to my Grandfather Dario who taught me the best skills a man can have: to be creative and to be a dreamer, always.

Resumo

As terapias celulares baseadas no transplante de células endoteliais (ECs) dentro de hidrogéis são hoje em dia vistas com grande interesse em estratégias de regeneração de tecidos, nomeadamente para o tratamento de tecidos isquémicos, visando a promoção da rápida (re)vascularização do implante usado para regenerar esse mesmo tecido.

O objetivo deste trabalho prendeu-se com a optimização de um microambiente tridimensional (3D), capaz de proporcionar sinais celulares e de matriz, que correctamente estimulem a sobrevivência das ECs, e promovam a sua organização em estruturas pré-vasculares. Neste trabalho, foram usados hidrogéis de alginato modificado com o péptido de adesão RGD, previamente desenvolvidos, para cultivar diferentes tipos de ECs. Células endoteliais do cordão umbilical (HUVECs) e células endoteliais progenitoras (EPCs) derivadas do sangue do cordão umbilical (UCB) foram cultivadas em 3D, em mono-cultura ou em combinação com outros tipos celulares.

Utilizando um protocolo já publicado para o isolamento de duas populações de EPCs, uma menos madura (er-EPCs) e outra mais madura (la-EPCs também chamadas de OECs), foram obtidas, respectivamente, duas populações distintas aqui designadas por UCB cells A e UCB cells B. As UCB cells A não expressaram o marcador endotelial CD31 e apresentaram uma morfologia idêntica a fibroblastos e células mesenquimais (MSCs). As UCB cells B apresentaram duas populações de células distintas que expressam os marcadores CD31, CD34, CD14 e CD45 e ainda foram capazes de internalizar ac-Dil-LDL. Estas células, apresentaram uma morfologia redonda e alguns agregados celulares foram detectados no poço, características idênticas às er-EPCs.

Com objetivo de otimizar um microambiente num hidrogel que fosse o melhor para o transplante de ECs, foram estabelecidas culturas em 3D dos diferentes tipos celulares, tanto em mono-cultura como em co-cultura com as MSCs, utilizadas como células de suporte. Foram testadas as seguintes combinações: HUVECs+MSCs, UCB cells A+MSC, UCB cells B+HUVEC e UCB cells B+HUVECs+MSC. A presença das MSCs na cultura pareceu aumentar tanto a sobrevivência quanto a funcionalidade das HUVECs. Este processo poderá ter sido devido ao efeito que as MSCs tiveram na reorganização da matriz, uma vez que estas foram capazes de migrar para o centro dos discos e de criar agregados multicelulares. Estes resultados, juntamente com o facto de ter sido também detectada a expressão de α-SMA actina, sugerem que as MSCs em co-cultura com as HUVECs possam adotar um papel idêntico ao dos pericitos. Apesar das ECs terem sido capazes de formar estruturas tubulares nos dias 1 e 3, estas estruturas deixaram de ser detetadas ao dia 7. Este resultado mostra a necessidade de melhorar o sistema de cultura com vista a aumentar a estabilização destas estruturas ao longo do tempo. Quando cultivadas em 3D, as UCB cells A mantiveram uma atividade metabólica alta e foram capazes de contrair substancialmente a matriz, um comportamento

típico de fibroblastos/MSCs, organizando-se em agregados multicelulares com algumas células estendidas, tanto em mono-cultura como quando co-cultivadas com as MSCs. No que diz respeito às UCB cells B, estas não foram capazes de aumentar a sobrevivência das HUVECs quando em co-cultura, mas foram capazes de promover tanto a migração das células como a contracção da matriz, quando tri-cultivadas com as MSCs e as HUVECs. Este aumento foi detectado pela formação de um grande agregado no centro do disco que apresentava estruturas celulares bem organizadas na sua periferia.

Apesar dos avanços descritos anteriormente, a cultura em condições 3D revelou ser uma tarefa desafiante, com o envolvimento de múltiplas variáveis. Assim sendo, a última parte desta tese foi dedicada ao desenvolvimento de uma nova plataforma de detecção de alto rendimento (HTS) em que uma matriz de micro-gotas de gel é produzida por uma técnica de bioimpressão assistida por laser (LAB). Após otimização das condições necessárias para a bioimpressão, foi possível bioimprimir, soluções com diferentes concentrações de alginato-RGD (1 e 2% m/V), combinadas com agentes de gelificação ($CaCO_3$ and GDL) e MSCs. Este sistema manteve-se estável durante 7 dias em cultura, período durante o qual foi mantida também a viabilidade celular. Com o objetivo de validar este sistema, as MSCs bioimpressas foram induzidas a diferenciar ao longo da linhagem osteogénica e os respectivos resultados foram correlacionados com os resultados obtidos em paralelo com o sistema normal de médio rendimento (MT). Por último, foram bioimpressas micro-gotas de HUVECs co-cultivadas com MSCs, obtidas pela adição dos dois tipos de células à solução de alginato. Estes resultados representam o primeiro passo no processo de validação da plataforma de HST proposta, que poderá servir com uma ferramenta útil na análise do comportamento celular em 3D, e consequente otimização de microambientes para a cultura de ECs.

Abstract

Endothelial cell-based therapies in which endothelial cells (ECs) populations are delivered within hydrogel vehicles provide an interesting approach to the treatment of ischemic tissues, and can also be useful to promote the rapid vascularization of tissue-engineered constructs. The aim of this study was to establish optimized three-dimensional (3D) microenvironments, providing adequate matrix/cellular cues, for enhancing ECs survival and promoting their organization into pre-vascular structures. Previously developed RGD-alginate hydrogels were used for the 3D culture of different types of ECs, namely human umbilical vein endothelial cells (HUVECs) and umbilical cord blood (UCB)-derived endothelial progenitor cells (EPCs), which were cultured alone or in combination with other cell types.

Following a previously published protocol for the isolation of early-EPCs and of late-EPCs (also known as outgrowth endothelial cells, OECs), two distinct UCB cells populations were isolated and characterized – hereafter designated as UCB cells A and B, respectively. Unexpectedly, UCB cells A lacked the expression of CD31, a prototypical endothelial marker, and presented a fibroblast/mesenchymal-like morphology. In contrast, UCB cells B were composed by two distinct cell populations that expressed CD31, CD34, CD14 and CD45, were able to uptake Ac-Dil-LDL and presented a round shape, forming some aggregates, thus resembling early-EPCs.

To define an optimal hydrogel-based microenvironment for ECs delivery, 3D cultures of the various cell types were then established, either in monoculture or in coculture with mesenchymal stem cells (MSCs), used as supportive cells. Different cell combinations were tested, namely: HUVECs+MSCs, UCB cells A+MSC, UCB cells B+HUVEC and UCB cells B+HUVECs+MSCs. The presence of MSCs seemed to enhance the survival and functionality of cocultured HUVECs, possibly by changing the matrix environment as they migrated towards the center of the disks forming multicellular aggregates. They possibly also acted as pericyte-like cells, as suggested by the expression of α-smooth muscle actin (α-SMA). Yet, while ECs tubular-like assemblies were detected at days 1 and 3, these were no longer present at day 7, showing that further improvements of the system have to be made towards the stabilization of these structures. In 3D, UCB cells A cells maintained high metabolic activity and were able to substantially contract the matrix, a typical fibroblastic/mesenchymal feature, organizing into aligned multicellular aggregates with some sprouting cells, both in mono- and MSCs coculture. UCB cells B were not able to improve the survival of cocultured HUVECs, but enhanced cell migration/matrix contraction when triple-cultured with MSCs and HUVECs, forming a large aggregate at the center of the disk that presented several sprouting multicellular structures at its periphery.

The optimization of 3D culture conditions revealed to be a quite challenging task, involving the concomitant analysis of different variables. Thus, in the final part of this thesis, a new

high-throughput screening (HTS) platform was developed, consisting on cell-in-gell 3D microarrays produced by laser-assisted bioprinting (LAB). After optimizing the bioprinting set-up, it was possible to print self-gelling RGD-alginate solutions at different concentrations (1 and 2% w/v), combined with crosslinking agents ($CaCO_3$ and GDL), and loaded with MSCs. Cell viability and microarray stability were preserved for up to 7 days in culture. To validate the system, the osteogenic differentiation of printed MSCs was tested and the results correlated with those observed in a standard medium-throughput (MT) assay (hydrogel disks) run in parallel. Finally, microarrays of cocultured HUVECs and MSCs were obtained by printing alginate solutions containing both cell types. These results represent a first step towards the validation of the proposed HTS platform, which might provide a very useful tool for analyzing cell behavior in 3D and, consequently, for the development of optimized 3D microenvironments for ECs culture.

Acknowledgements

Any successful thing in life is always accomplished as the result of a common effort. The fundamental basis of science is to contribute with each single research to a common goal promoting a higher input. According to this thought, this work was accomplished with the effort of many to whom I would like to address my deep gratitude.

First of all I would like to address my sincere gratitude to my supervisor Cristina Barrias. She accepted me in this journey as her master student, gave me the opportunity to grow as a researcher and as a person, but most of all she transmitted to me her passion, wisdom, care and excellence that are the key elements to be successful in science as in life. Along these two years, it never ceased to amaze me how Cristina was able to solve all the problems, to help me with everything, to have a friend and encouraging word, and to make me want to be better and better.

To my co-supervisor, Filipa Sousa, I would like to thank all the time she spent with me, patience, care, and wisdom. Not less importantly, I would like to thank her for all the friendship, talking, laughing, crying, crazy times, crazy thoughts and ideas and for helping me to find myself when I was lost. I shall never forget the encouraging words, the refreshing talks on the lab yard, and all the other amazing moments passed together along this thesis.

To all my team colleagues, namely Raquel Maia, Silvia Bidarra, and Ana Luísa Torres, I would like to express my deep gratitude for all the help and team work, talks, and scientific discussions which contributed a lot to the present work and for the researcher that I have become today.

To my group leader, Pedro Granja, I would like to thank, one more time, for the opportunity he gave me to work in our team and for allowing me to engage on several projects which were essential for my knowledge growing and my mind opening to new ideas.

To Raquel Gonçalves I would like to thank the help with the umbilical cord cells isolation and characterization, and for all her time and availability to help me with all my doubts.

To Isabel Amaral, I would like to thank the availability to discuss protocols and to explain me the details of the techniques, and also for sharing with me the antibodies that were crucial for the experiments.

To Dra. Carla Ramalho and Susana Guerreiro, I would like to thank the availability to supply us umbilical cord blood, and to ensure that all the communication between the Serviço de Urgência da Obstréticia could be done smoothly.

To INSERM team, at Bordeaux, I would like to thank all the time spent in teaching me and introducing me to the lab life. But most of all I would like to express my deep gratitude to Hugo Oliveira, Maritie Grellier, and especially to a little fluffy tiny human, Emma, for helping me through all the time I was at Bordeaux and for making me feel welcomed as friend. I really miss you guys!

To all my INEB fellows and friends I do not know how to express how thankful I am for everything. After four years sharing work and life, I could not be more grateful; I consider this Institution as my second family. Thank you my INEB friends for all the time, love, friendship, and sharing. Particularly, I would like to thank Sara Neves, with whom I share a deep friendship and affection. Sara, there are no words that can express how important you were when I was feeling bad and alone in Bordeaux. Thank you for all the conversations, discussions, work talk, for all we have accomplished together, for our adventures, and for all that is yet to come. Thank you for everything.

At last, but not the least, I would like to thank my family and friends (especially Leandro Machado in the final phase), as without them I would not be able to do this thesis and, more importantly, to finish its last step. Thank you, Mom, Dad, Guilherme, Miguel for all the indescribable support, patience, encouragement, and love. You know I love you all.

Index

List of Figures

List of tables

Abbreviations

List of abbreviations (alphabetic order)

2D	*Two-dimensional*
3D	*Three-dimensional*
A	*Ampere*
Ac-LDL	*acetylated – Low Density Lipoprotein*
ALP	*Alkaline Phosphatase*
BM	*Basal Medium*
BMw	*Bone Marrow*
BSA	*Bovine Serum Albumin*
CD	*Cluster of Differentiation*
CLSM	*Confocal Laser Scanning Microscope*
CPDA-1	*Citrate, Phosphate, Dextrose and Adenine*
ECM	*Extracellular Matrix*
ECs	*Endothelial Cells*
EDC	*1-Ethyl-3-(3-dimethylaminopropyl)carbodiimide*
EDTA	*Ethylenediaminetetraacetic acid*
EGM2	*Endothelial Growth Medium 2*
EGM2-MV	*Endothelial Growth Medium 2 – Microvascular*
eNOS	*endothelial Nitric Oxide Synthase*
EPCs	*Endothelial Progenitor Cells*
Eph	*Ephrin*
Er-EPCs	*early-Endothelial Progenitor Cells*
FACS	*Fluorescence-activated Cell Sorting*
FDA	*Food and Drug Administration*
Flt-1	*Vascular endothelial growth factor receptor-1*
Fn	*Fibronectin*
G units	*a-L-guluronic acid*
G4RGDSP	*(Glycine)4-Arginine-Glycine-Aspartic acid-Serine-Proline*
GDL	*D-glucono-δ-lactone*
GVHD	*Graft-versus-Host Disease*
HBSS	*Hank's Balanced Salt Solution*
HDMECs	*Human Dermal Microvasculature Endothelial Cells*
HLA	*Human Leukocyte Antigen*
hMSCs	*human Mesenchymal Stem Cells*
HMW	*High Molecular Weight*
HSCs	*Hematopoietic Stem Cells*

HT	*High-Throughput*
HTS	*High-Throughput Screening*
HUVECs	*Human Umbilical Vascular Endothelial Cells*
HVECs	*Human Vasculature Endothelial Cells*
IgG	*Immunoglobulin G*
IHC	*Immunohistochemistry*
INSERM	*Institut National de la Santé et la Recherche Médicale*
IR	*Infra-red*
KDR	*Kinase Insert Domain Receptor*
LAB	*Laser-assisted Bioprinting*
LMW	*Low Molecular Weight*
M units	*(1-4)-linked-B-D-mannuronic acid*
MAPLE-DW	*Matrix-assisted Pulse Laser Evaporation- Direct Write*
MNCs	*Mononuclear Cells*
MSCs	*Mesenchymal Stem Cells*
MT	*Medium-throughput*
OECs	*Outgrowth Endothelial Cells*
PB	*Peripheral Blood*
PCs	*Pericytes*
PDGF	*Platelet Derived Growth Factor*
PECAM-1	*Platelet Endothelial Cell Adhesion Molecule-1*
PLL	*Poly-L-Lysine*
PVCs	*Perivascular Cells*
RGD	*Arg-Gly-Asp*
RT	*Room Temperature*
SMCs	*Smooth Muscle Cells*
TBS	*Tris-buffered Saline*
TRI	*Time Resolved Imaging*
TSB-1	*Thrombospondin-1*
UCB	*Discrete Fourier Transform*
UV	*Ultraviolet*
VE-cad	*Vascular Endothelial-cadherin*
VEGF	*Vascular Endothelial Growth Factor*
vWF	*van Willebrand Factor*
α-SMA	*alpha-Smooth Muscle actin*

Introduction

Tissue engineering has been growing as an independent field over the last two decades. The emergence of new biomedical technologies together with advances in cell biology have led this field to develop as a helping tool for both normal injured tissues and tissues with impaired repair/regenerative ability.

These advances have a great impact in clinical practice, allowing the development of procedures that were impossible to be performed until now which are starting to be used as well accepted therapies. For example, in 2008, a decellularized trachea was implanted in a patient for the first time, and latter, in 2011, the development of the first synthetic tissue-engineered trachea was also reported. In what concerns decellularized tissues, an allogenic iliac vein scaffold was implanted in a 10-years-old patient, seeded with autologous endothelial and smooth muscle cells (SMCs) that were differentiated *in vitro* from bone marrow stromal cells, showing how promising decellularized tissues can be serving as scaffolds for cell therapies (*1*). Advances in the manipulation and creation of different types of biomaterials have also made possible therapies for cartilage and bone regeneration, employing several different strategies. Most of these therapies use biomaterials with autologous cells filling the existing defect in the tissues thus promoting their regeneration. These therapies have been used for microfractures and craniofacial reconstruction, among other types of applications, improving/increasing/saving patient's lives (*1*).

Despite these progresses in tissue engineering strategies, the available therapies are in many cases only applicable for specific tissues, which are not characterized by complex vascular and/or nervous networks, as it is the case of cartilage, which is a highly avascular tissue lacking nervous terminals (*2*). Mimicking the highly complex structure of vasculature or nervous system is so complex that, until now, there are no sufficiently advanced strategies being used in clinical practice. Thus, in order to regenerate other tissues and organs, the development of more robust therapeutic approaches that stimulate correct vascularization and integration of the implant with the host vasculature are crucial (*3*).

Without a perfusion blood supply, a new tissue is not able to survive and engraft correctly. Cells only survive if they have a capillary residing within 150-200 μm of distance (*4*) (**Figure 1**), which means that any biomaterial either has to degrade rapidly to allow vessels to grow inside and nourish the newly formed tissue, or has to create its own vascular structures that will eventually anastomose with the pre-existing vasculature of the host tissue. In the latter case, these biomaterials should be loaded with vessel-forming ECs.

1. Microvascular network, vasculogenesis and angiogenesis

Multicellular organisms need to distribute nutrients throughout their entire system. In humans, there is a complex vascular network system composed of arteries dividing consecutively into smaller branches like meta-arterioles (80–100mm), until finally forming capillaries (10–15mm) that distribute nutrients and oxygen inhaled by the lungs, recollect by-product wastes produced by cells and have other functions like immune protection, cellular signalling, and endocrine interactions (*5*) (**Figure 1**). After capillaries interact with all the

tissues in our body, they unite into post-capillaries venules, venules and finally veins returning the waste products to be filtered and excreted by the excretory system, and returning the blood to the lungs to be oxygenated (*4*).

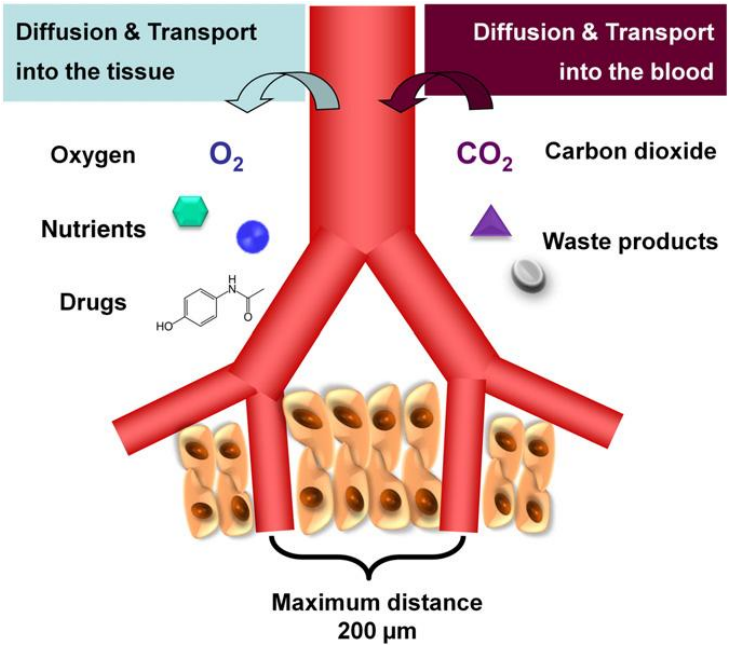

Figure 1 – Schematic description of vascularized tissues *in vivo*. Diffusion and transport processes occur throughout all body and the surrounding tissues are supplied with oxygen, nutrients and molecular signaling via the vasculature. Waste products, CO_2, and molecules produced by cells are exchanged with blood to enter into the circulation system (adapted from (*6*)).

During gestation, angioblasts, that derive from the mesenchyma, cluster together, eventually start to form solid tubes that are the preliminary tubular structures that will originate arteries and veins. This process, called vasculogenesis, is responsible for the formation of the body blood vessel network during gestation. The formation of new vessels from the previous ones occurs with sprouting of cells from previous vessels, a process called angiogenesis, which only occurs during adulthood in pathological situations like ischemia, inflammation, wound healing, and hypoxia (*4, 7*).

Vessels are composed of several cell types and a specific extracellular matrix (ECM) that functions as a scaffold where cells are going to be anchored. ECs form the lumen of vessels and are the main cell type responsible for the formation of the vessel network. These cells align with each other forming a tubular structure that will mature into capillaries. These are the main site of exchange of nutrients between blood and tissue, due to their capacity of extravasion and high surface-to-volume ratio. ECs in capillaries are covered by a basement membrane that is a specific ECM found in epithelial structures. In order to stabilize this capillary architecture, pericytes (PCs) enlace ECs and the basement membrane leading to a tighter structure and close interaction, allowing as well their contractile role. As capillary's

diameter increases, capillaries start to be called arterioles, occurring some specific changes in their cellular content. The number of mural cells (PCs and SMCs) increases and precapillary arterioles are completely covered with SMCs that have their own basement membrane and interact tightly with the endothelium (*8*). These two cell types, SMCs and PCs, have been described as having an important role in stabilizing newly formed capillaries.

Despite published descriptions that in adulthood angiogenesis only occurs in body stress situation and that ECs are a slow or non-replicative population (*9*), since 1997, a new paradigm has been established for vascularization in adulthood. The discovery of a new circulating blood cells population with postnatal vasculogenesis potential was reported by Ashara *et al* (*10*). These cells showed the ability of promoting or making new blood vessels (*11-12*). It was shown that not only they display several surface markers characteristic of endothelial lineage, but also the expression of hematopoietic antigens. These cells also demonstrate colony-forming ability *in vitro*, and are described as being promoters of vascular regeneration at sites of ischemia upon transplantation, which led to define these cells as EPCs. Since this remarkable discovery, many studies have been conducted to define EPCs and distinguish different populations and/or subpopulations that resemble EPCs. However, a definite characterization of an EPCs population is still lacking, and although some populations are being referred as EPCs, they can actually be other populations with some similar features (*11, 13*).

EPCs have been explored in several therapeutic strategies (*14*) and are currently being explored in the cancer field for their role in promotion/participation in angiogenesis (*8*). This subject will be further addressed in more detail in next section.

2. ECs in pro-angiogenic therapies: types and sources

As previously mentioned, the biggest challenge in tissue engineering is the fabrication and regeneration of more complex and thicker tissues, as there is a need for blood supply. Since ECs are the main cells composing the vessels' endothelium, much research has been developed aiming at using these cells to promote angiogenesis and neovascularization.

The different ECs populations that have been used up to now have slight differences between them, depending on the place from where they were isolated and on the role they have to play. However, in general, mature ECs express a panel of common phenotypic markers, including von Willebrand factor (vWF), platelet endothelial cell adhesion molecule-1 (PECAM-1 or CD31), CD34, and vascular endothelial (VE)-cadherin (VE-cad), and effectively uptake ac-LDL (*15*). Although other markers can be used to identify ECs (*15*), these are the most commonly used to identify this type of cells by flow cytometry or immunohistochemistry (IHC) techniques (**Table 1**).

Table 1 - Endothelial Constitutive Markers (adapted from (*15*)).

Endothelial Constitutive Markers			
Markers	**Species**	**Cell Type**	**Reference**
Factor VIII-related antigen	h/m	ECs (irregularly expressed by capillaries and tumor vessels), platelets, megakaryocytes	(*16*)
CD31/PECAM-1	h/m	ECs, platelets, megakaryocytes, B and T lymphocyte subsets, monocytes, neutrophils	(*17-18*)
Angiotensin-converting enzyme	h/m	ECs, epithelial cells, monocyte-macrophages, T lymphocytes	(*16*)
Type I scavenger receptor (acetylated-LDL uptake)	h/m	ECs, macrophages, SMCs, pericytes, fibroblasts	(*19*)
Ulex europaeus I agglutinin binding/O(H) blood-type antigen	h	ECs, erythrocytes	(*20*)
Bandeirea simplicifolia lectin binding	m	ECs	(*16*)
*Griffonia simplicifolia*agglutinin binding	m	ECs	(*21*)
Weibal-Palade bodies	h/m	ECs	(*22*)
Vascular endothelial cadherin	h/m	ECs, trophoblasts, PLN sinus macrophages	(*23*)
CD34	h/m	ECs, hemopoietic precursors	(*24*)
CD102/ICAM-2	h/m	ECs, lymphocytes, monocytes, platelets	(*25*)
CD51/61 (vitronectin receptor)	h/m	ECs (overexpressed in tumor ECs), platelets, megakaryocytes, osteoclasts, mast cells, B lymphocytes	(*26*)
CD105/endoglin	h	ECs (overexpressed in tumor ECs), monocyte-macrophages, B lymphocytes, syncytiotrophoblasts	(*27*)
CD36	h	Microvascular ECs, monocyte-macrophages, erythroid cells, platelets, megakaryocytes	(*28*)
CD73/VAP-2	h	ECs, T and B lymphocytes, tonsillar epithelium	(*29*)
S-ENDO 1/MUC18	h/m	ECs, SMCs, dendritic cells, leukocytes, melanoma cells, carcinoma cells	(*30*)
Thrombomodulin	h/m	ECs, SMCs	(*31*)
HEMCAM	m	Microvascular ECs, hemopoietic progenitors	(*32*)
Sca-1	m	ECs, hemopoietic precursors	(*33*)
AAMP	h	ECs, cytotrophoblasts, mononuclear inflammatory cells, melanoma cells, adenocarcinoma cells	(*34*)

Interestingly, most of the markers found to be expressed by ECs, are also common to hematopoietic precursors or to mature blood cells, showing that both lineages have a common precursor (*15*) (**Table 1**).

Human mature ECs can be isolated from different endothelium structures and cultured *in vitro*. Some populations like HUVECs, human dermal microvasculature ECs (HDMECs) and human vasculature ECs in general (HVECs) can be isolated and cultured with a proper endothelial-specific medium supplemented with adequate growth factors. However, ECs present slightly different behaviors, when they are sparse in culture, or confluent. When confluent, ECs establish cell-to-cell contact that inhibits both spontaneous and growth factor-induced cell growth and their metabolism has some changes, like the alterations of the arachidonic acid metabolism, or the release of lytic enzymes or growth factors (*15*). These changes are in accordance with their normal *in vivo* behavior. In the endothelium, ECs are stable and not expected to proliferate until an injury occurs, and the endothelium is disrupted, leading to ECs proliferation and changing of their metabolism to recover the endothelium integrity, where cells establish cell-to-cell contacts, similar to what happens when they are confluent *in vitro*.

However, it is still technically challenging to isolate mature ECs. Isolating them from a patient to use them as an autologous setting would cause morbidity at the donor site, as cells would have to be isolated from healthy vessels, and ultimately the number of cells isolated would be very low due to their challenging expansion process, since these cells exhibit low proliferation rates (*6, 35*).

To overcome these difficulties, EPCs have more recently emerged as a promising source of ECs for neovascularization in tissue engineering strategies, due to their higher proliferative capacity and ability of integrating the formation of new blood vessels (*11-12, 36-37*). EPCs can be isolated from human peripheral blood (PB), bone marrow (BMw), umbilical cord blood (UCB) and placental tissue (*36*). Among all these possible sources, PB and UCB have been considered as the most adequate options, as both are easily collected from adult blood donors, or from umbilical cord blood upon birth, respectively. EPCs collected from those different sources share common features, such as being recruited to injured sites, and integrating the newly formed vessels in sites where ischemia occurs (*36*).

EPCs still lack a concise, widely accepted definition, despite the advances made since the discovery of endothelial circulating cells with various clinical trials still ongoing. It seems that in blood there are different circulating cell populations that can represent EPCs in different stages of differentiation. The lack of a unique protocol for the isolation of these cells, and the lack of specific markers for their characterization, have led to different interpretations of different EPC-like cell populations (*11*). Due to this difficulty in defining what are EPCs, these cells are not yet postulated as a validated clinical stategy. Clinical applications require a high level of characterization and definition of the cells being used, as demanded by authorities such as the Food and Drug Administration (FDA).

EPCs from PB have been described as heterogeneous populations of cells and at least two different populations can be identified according to their appearance and morphological characterization (*38*). The first population, called er-EPCs, can be obtained from the mononuclear cells (MNCs) fraction of blood, after centrifugation with Ficoll gradient, upon being cultured for 4-7 days in fibronectin coated plate (*11-12, 39-41*). When in standard two-dimensional (2D) cell culture setup, this fraction is characterized by a round to fibroblastic-like morphology, with the formation of some cell agglomerates. These cells are thought to derive from blood cells and more specifically from myeloid lineages, as they are described to express CD45 and CD14 (*38-39, 41*). er-EPCs express the most common endothelial markers such as CD31, CD34, vWF, and VE-cad and are able to uptake ac-LDL, but are not able to form tubular-like structures in matrigel assay. Even though they are described to have a low proliferative potential, they are able to secrete proangiogenic molecules that stimulate angiogenesis and neovascularization (*37, 42-43*). In hind limb ischemia, these cells effectively helped the restoration of the blood network to the injured limb (*37, 42-43*).

Late-EPC (la-EPCs) or, the so-called OECs is the other population that can be obtained from the seeding of MNCs. Using collagen type I-coated plates, as it was used here in this work, these cells are usually kept for 2-3 weeks in culture in an endothelial growth medium (EGM2) after initial sub culturing steps (*39-41, 44-49*). Then, the colonies start to form with cells with cobblestone-like morphology, very identical to mature ECs. These colonies are then isolated and replated to have a culture pure in OECs. In contrast to mature ECs and er-EPCs, OECs have a high proliferative potential, are able to form tubular-like structures in a matrigel assay, and also to integrate into newly-formed vessels. Like er-EPCs, OECs express CD31, vWF, and VE-cad, and are able to uptake ac-LDL. However, they lose CD14 and CD45 expression, which means that they are ECs, but do not share the myeloid and blood markers, respectively, as er-EPCs do. Regarding CD34 expression, OECs have been described by some authors as expressing this hematopoietic marker (*41, 48-49*), while other authors demonstrated that these cells are CD34-negative (*44, 46*). CD34 expression is such an ambiguous characteristic to define OECs that Cheng *et al (39)* characterized their isolated population as having only 50 per cent OECs $CD34^+$. These results altogether can lead to two conclusions: either there are OECs that descend from hematopoietic stem cells (HSCs) (belonging to the hematopoietic lineage) and OECs that do not, or all OECs are descendents from HSCs, but *in vitro* might start diverging and losing the stem potential that is characteristic of $CD34^+$ cells.

Although both EPCs populations are different, they are both capable of rescuing an ischemic limb when injected in an animal. This shows how these cells can be a very important tool for tissue engineering in the promotion and participation in neovascularization for regeneration therapies. All this information is summarized in a table adapted from Fuchs *et al* (*38*) and Yoon *et al* (*50*) (**Table 2**).

Table 2 - Overview on characteristics that distinguish between EPCs and OECs. Adapted from (*38*) and (*50*)

	EPCs	OECs	Marker functions
Morphology	Spindle shaped morphology (*50-52*)	Cobblestone-like morphology (*44, 53-55*)	
	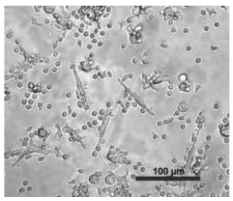	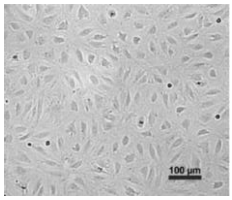	
Appearance in culture	After 7 days in culture (*50, 56*)	After 2-3 weeks in culture (*51, 53, 56*)	
Human phenotypic markers	CD31+ (*10, 52, 57*)	CD31+ (*53, 55, 58*)	Cell contact protein that mediates homotypic EC adhesion.
	CD45+ (*52, 59*)	CD45- (*59*)	Surface transmembrane phosphatase expressed in hematopoietic lineage cells.
	CD34+ (*10, 50, 57*)	CD34+ (*50, 59-60*)	Stem-cell-related marker.
	CD14+ (*50, 52-53*)	CD14- (*50, 53*)	Monocyte surface marker.
	CD146+ (*61*)	CD146+ (*58, 61*)	Adhesion molecule that mediates homotypic EC adhesion.
	CD133+ (*60, 62-63*)	CD133- (*59*)	Stem-cell-related surface marker.
	Flt-1+ (*56*)	Flt-1+ (*56*)	VEGF receptor-1.
	eNOS (*56*)	eNOS (*53, 56*)	Modulates VEGF-induced angiogenesis and vascular permeability in vivo.
	vWF+ (*55-56, 64*)	vWF+ (*55-56, 58*)	Constitutive glycoprotein of the endothelium.
	VE-cadherin+ (*52, 56-57*)	VE-cadherin+ (*51, 56, 58*)	Cell contact protein that mediates homotypic EC adhesion.
	KDR+ (*56-57, 64*)	KDR+ (*50, 56, 59*)	VEGF receptor-2.
	CD36+ (*51*)	CD36+ (*51*)	Receptor of TSP-1 and mediator of its anti-angiogenic activity
	Tie2+ (*10, 53*)	Tie2+ (*53*)	Cell surface receptor that bind and is activated by the angiopoietins.
		Caveolin-1 (*53, 58*)	Marker of endothelial differentiation. Upregulated during vessel formation.
Proliferative potential	Low (*50, 52, 56*)	High (*50, 56*)	
Tube formation	No (*50, 65*)	Yes (*50, 65*)	
Paracrine augmentation of angiogenesis	Yes (*66*)	No (*66*)	

As already stated, UCB and PB seem to be the more promising sources for the isolation of EPCs for tissue engineering, due to their availability and easier harvesting process. However, when comparing these two sources, some authors described that UCB-EPCs present higher anti-oxidant and migration ability with higher therapeutic efficacy comparing to PB-EPCs, in a hind limb ischemic disease model (*36*). This effect was reported as being caused by specifically up-regulated factors in EPCs derived from UBC, such as STMIN 1, CFL 1, PARK 7, NME 1, GLO 1, HSP 27 and PRDX 2. These factors seem to be key elements that could be functionally active in ischemic regions and promote an enhanced neovascularization process (*36*). Not only UCB-EPCs induce more neovascularization, but they also provide a safer source of cells in terms of immune rejection. Nuzzolo *et al* (*67*) described that UCB-EPCs have a lower pro-inflammatory and pro-thrombotic profile than adult EPCs. Due to the fact that EPCs

represent a very small fraction of the blood cells and that for cell therapies the number of cells necessary to a successful engraft is very high, sometimes the use of cells from different donors is necessary. In fact, for HSCs therapies, it was described the same pattern. HSCs from UCB divide more and faster than HSCs from BMw and lose less $CD34^{+}CD38^{-}$ stem cell population throughout *ex vivo* expansion *(68)***.** In terms of HLA-mismatch, UCB-HSCs have less rejection, leading also to less graft-versus-host-disease (GVHD) and the possibility of using a wider-range of donors for transplantation (*69*). Finally, UCB-HSCs have a higher differentiation potential than BMw-HSCs, which is also extremely important for transplantation (*70*). Altogether this knowledge about cells derived from UCB lead to conclude that this source seems to be the safest and the best for tissue engineering. It is also important to emphasize that UCB is many times discarded as a biological waste in hospitals, although this has been decreasing due to the creation of private and public UCB banks.

3. Coculture of ECs with supportive cells

As it was discussed above, capillaries are formed by an endothelium composed of tightly connected ECs that is the immediate structure to contact with blood elements. However, this tube is covered with a specific matrix, and more importantly, by mural cells that play active roles in the capillaries and vessels dynamics and are now known to have a crucial role in angiogenesis (*71-72*).

In the microvasculature, PCs are the major mural cells found in capillaries, while SMCs are found in precapillary arterioles. Although ECs migrate and make sprouts without mural cells' help during angiogenesis, PCs are among the first cells responsible for the invasion of newly vascularized tissues and appear located at the growing front of the endothelial sprouts. They determine the location of sprout formation and guide newly formed vessels by interaction with EC via paracrine communication (*72-73*). Actually, PCs have a close molecular interaction with ECs. Betsholtz *et al* (*74*) described ECs as producers of platelet derived growth factor – B (PDGF-B) and PCs as expressing PDGF receptor-ß (PDGFR-ß). PDGF-B recruits PCs from the surroundings of the sprouting vessel to participate in angiogenesis. This process is also accomplished by vascular endothelial growth factor (VEGF) released upon hypoxia, that not only stimulates ECs to proliferate and migrate, but also directly induces proliferation and migration of PCs (*72, 75*). Other interactions between ligands and their receptors are also responsible for the tight relation between PCs and ECs. NG2 and Notch-3 system and Ephrins (Eph) and Eph receptors system are also responsible for endothelial cell motility, mural cell migration, spreading and adhesion during vessel wall assembly, and PCs and ECs assembly (*72*). Thus, it is clear that mural cells, in this case PCs, have a crucial role in vessel organization and stabilization. Moreover, these cells act in angiogenesis and in vessel remodeling processes showing the importance of mural cells for neovascularization strategies.

In fact, the latest research performed in terms of neovascularization strategies, uses the recent findings regarding the crosstalk between supportive/mural cells and ECs, to create more functional vascularized systems. The interaction of mural cells with ECs has been the subject of study of many research teams. When cultured alone, ECs proliferate and grow until confluence, establishing cell-to-cell contacts and forming a monolayer. If these cells are not passaged, they detach, remaining in suspension and ultimately die. This phenomenon does not resemble the tubular-like structures found in vessels *in vivo,* which are barely seen and highly unstable in 2D culture systems, and even in 3D cultures (*76-82*). However, when ECs are cocultured with supportive cells such as fibroblasts, MSCs, PCs or SMCs, their organization is achieved and tubular-like structures are formed that resemble the normal ECs alignment (*76-82*).

Recent findings about phenotypic characterization of PCs and perivascular cells (PVCs) have led to a great discussion whether these cells are MSCs. Crisan *et al (83)* and Corselli *et al* (*84*) showed that PVCs and PCs that reside in the outmost layer of blood vessels are the *in vivo* counterparts of MSCs (*71*). Regardless where these cells are isolated in the human body, they all express MSCs phenotypic markers and present multipotency, having the ability to differentiate into various mesenchymal lineages, including the osteogenic, chondrogenic, and adipogenic. Moreover, when cultured *in vitro* and stimulated with angiogenic factors (e.g. when cultured in EGM2), adventitial MSCs acquire a pericytic-like phenotype (*84*), which suggests that these cells upon a proper signaling by angiogenic factors (or under a hypoxia situations), adopt a pericytic-like phenotype to differentiate into PCs that need to be recruited for the angiogenesis process.

Indeed, many studies have explored the potential of MSCs as mural cells for ECs survival, angiogenesis enhancement, and neovascularization (*77-80, 85-87*). Carrion *et al* (*77*) described the role of α6 integrin subunit in MSC-mediated angiogenesis. When this molecule was knockdown, capillary sprouting of ECs was significantly reduced, causing the failure of MSCs to associate with the nascent vessels (*77*). A distinct property that defines MSCs is their ability to produce factors that act by a paracrine effect. Aguirre *et al* (*79*) described the transference of fluorescent dyes between MSCs and EPCs in coculture, probably by vesicles transport. Initially, cells were dyed with two different lipophilic fluorescent dyes, and over time cells with two dyes were increasingly detected suggesting a vesicle transport phenomena. Indeed, the transfer of cellular material has been recently described by Liu *et al* (*88*). MSCs were added to HUVECs that suffered oxygen deprivation and reoxygenation. This anoxia suffered by HUVECs has led MSCs to transfer mitochondria to HUVECs by tunneling nanotubes in order to rescue HUVECs from oxygen deprivation. This data emphasizes the crucial role that mural cells play in enhancing ECs survival and can explain why MSCs, when injected in schemia situations improve blood reperfusion. Moreover, not only MSCs secrete key cytokines and growth factors that will affect ECs in a paracrine way, but they also produce a vast number of matrix proteins that participate in the assembly of a new ECM at the wounded tissue and serve as cues for them and for other cells (*89*). The molecular

signaling from this new matrix is essential for ECs survival, as the endothelium organization is highly dependent on the ECM surrounding it, as discussed above. In fact, our group has also reported that MSCs in 3D are able to produce a complex fibronectin (Fn) mesh (*90*), an essential ECM protein that serves as an important cue for correct ECs anchorage and alignment. A very good review of the data regarding MSCs and ECs cross-talk and MSC angiogenesis promotion can be read for further information (*91*).

4. Three-dimensional cultures of ECs

4.1. Three-dimensional hydrogel-cultures

In 1983, Montesano *et al* (*92*) have shown the importance of a 3D environment for ECs. Bovine ECs were cultured on top of collagen gels for 3 days and the results presented suggest that these cells displayed a behavior similar to that observed in a 2D environment, showing some interaction, forming a few agglomerates but without the formation of tubular-like structures. However, when covered with another layer of collagen on top, i.e. in a real 3D environment, cells started to form interconnecting cords of cells, resembling what happens *in vivo*.

In fact, there are several aspects of the cell microenvironment that 2D systems fail to mimic. These differences were first described in a study by Elsdale and Bard (*93*), where fibroblasts were cultured within a 3D structure composed of collagen type I. Under such conditions, but not in 2D, these cells were able to create a 3D organization that partially mimicked connective tissue cells *in vivo*. Since then, several studies on the behavior of 3D cultured cells have been performed (*94-99*).

Nowadays, it seems clear that 3D cell cultures are essential models for the study of cell biology, as they can incorporate mechanical and biochemical stimuli directly conveyed by the matrix. In fact, it is now evident that in order to harmoniously create a tissue, cells must interact not only with each other but also with their ECM (*94-99*).

Thus, to culture cells under “real” 3D conditions, i.e. entrapped, it is necessary to use as culture substrate a material that can mimic the ECM, and recapitulate some key aspects of the native cellular microenvironment.

Taking this in consideration, an optimal material should provide a high content of water and good permeability in order to facilitate the diffusion of oxygen and transport of nutrients and other soluble factors throughout the matrix, reaching all the cells within it, and at the same time allowing the outward diffusion of cellular metabolites. Hydrogels are very interesting materials for this kind of application, as they exhibit all these essential properties. Among them, some types of hydrogels are intrinsically “inert”, but can be specifically functionalized with key bioactive moieties (*100-102*).

4.2. ECs cultured within 3D hydrogel matrices

As it was discussed before, there are several cell processes that cannot be recapitulated in 2D cultures. Angiogenesis is a process highly dependent on the surrounding microenvironment, as ECs must concomitantly establish integrin-mediated adhesive interactions with matrix-bound ligands. These adhesive interactions are important for the subsequent shape changes that will activate actomyosin-dependent contractile responses (*103*). Motogenic, proliferative, and morphogenic programs are all triggered by the tight relation between matrix and cells, and neovascularization only occurs with the interplay of all these actors (*103*). Thus, the 3D microenvironment has great importance for the correct ECs behavior. For tissue engineering this knowledge is extremely important. In order to have a system that can generate new vessels *in vitro*, or in an *in vivo* implantation, a 3D culture system is mandatory.

The work of Zhou *et al* (*103*) shows the importance of ECM and 3D environment. Indeed, ECs when cultured in 3D conditions were able to initiate neovascularization by unfolding soluble Fn and depositing a pericellular network of fibrils. This network served to support cytoskeletal organization, actomyosin-dependent tension, and the viscoelastic properties of the embedded cells in a 3D-specific fashion. The same process was not accomplished by cells in 2D conditions, as these cells are unable to produce a pericellular network of fibrils leading to a lack of cytoskeletal organization that ultimately leads ECs to sense the environment differently, not being able to undergo apoptosis and senescence because of the ECM signaling is not interpreted correctly by cells (*103*).

The ECM also influences ECs behavior through physical signaling. Changing the mechanical properties of ECM has great impact on cells, and for ECs the impact is crucial for the formation or the absence of tubular-like structures *(104)*. Urech *et al (104)* observed that when fibrin ECM was stiffer, the cells were not able to form tubular-like structures, despite remaining viable. This result reflects the physical input that ECM has on ECs when cultured in a 3D environment. Indeed, the exogenous and endogenous forces are critical regulators of endothelial cell health and blood vessel maintenance (*105*). These forces can only be correctly mimicked if cells are surrounded by a 3D matrix as it was demonstrated in the above examples. For tissue engineering therapeutic purposes, the understanding of biochemical and biophysical cues that regulate ECs behavior, and their respective assembling for formation of a functional endothelium, is mandatory for a system capable of neovascularization usable in clinical practice.

Hydrogels matrices are often used to culture ECs under 3D conditions. Collagen gels (*106-108*), purified fibrin (*108-110*), Matrigel (*111*), or a mixture of these proteins with others, are among the hydrogels most commonly used. As mechanical properties can be tuned to some extent in hydrogels, these 3D systems can be easily optimized to culture ECs. Not only these properties can be changed by crosslink extent of the polymer or the polymer content itself,

but hydrogels are also permissive to mechanical changing through the embedded cells (*90, 112*). These properties can be tuned to favor ECs organization into tubular structures, often with lumens, that can be quantified and monitored in real time by videomicroscopy, as hydrogels can be monitored by a confocal microscope (*113*).

Another material that has been used for ECs culture is alginate (*114-117*). Alginate is a naturally derived polysaccharide, composed of (1-4)-linked ß-D-mannuronic acid (M units) and α-L-guluronic acid (G units) monomers, varying in amount and sequential distribution along the polymer chain. The alginate molecule is a block copolymer of GG, GM and MM sequences. Divalent cations such as Ca^{2+} bind the GG regions of adjacent alginate chains, resulting in ionic crosslinking, and the formation of a hydrogel from aqueous alginate solutions. Crosslinking may be promoted *in situ*, under mild conditions, and a variety of techniques can be used to control gelling and mechanical properties of the resulting hydrogels (*118*). In order to have a cell-interactive hydrogel, alginate can be chemically modified with the peptide sequence RGD (*119-123*), an adhesion motif present in several ECM molecules that interacts with adhesion molecules present at the cell's surface. This kind of functionalization provides an integrin-mediated interaction between the ECM mimic and the cells entrapped within it (*120*).

In particular, our group has been studying how HUVECs behave in a 3D RGD-alginate hydrogel. Bidarra *et al* (*124*) showed that ECs were able to proliferate and maintained 80% of viability for at least 48 h, after being embedded. ECs were also able to organize into 3D cellular networks inside the hydrogel and, when in contact with matrigel, cells migrated out of the hydrogel forming tubular-like structures (**Figure 2**). Thus, this work shows that alginate hydrogels can be used as an adequate substrate to culture ECs in a 3D fashion, and be used not only for mechanistic *in vitro* studies, but also as an ECs delivery system.

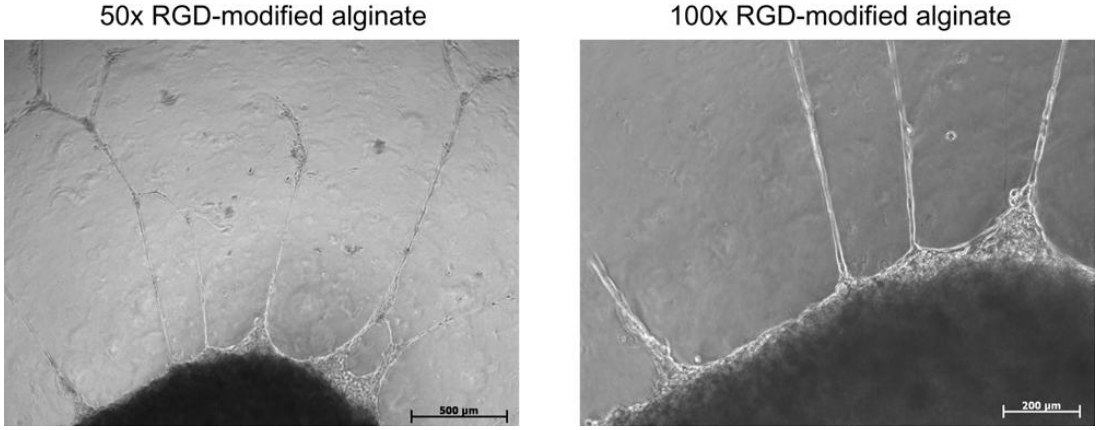

Figure 2 – Representative phase-contrast micrographs of HUVECs. Cells have migrated out from the alginate matrix into the surrounding tissue mimic (Matrigel), where they formed tubular-like structures. Images at different magnifications were taken after 24h of incubation (adapted from (*124*)).

5. Cell-in-gel 3D microarrays

Understanding the mechanisms of microenvironmental cellular regulation in 3D, which include not only the effect of soluble factors and cell–cell interactions, but also cell-matrix interactions, is quite challenging (*125*). In order to capture a more global picture of extrinsic control of cells fate, it is necessary to systematically deconstruct the role of each of these signals and their interplay, which is very time-consuming. Moreover, for this kind of set-up, huge amounts of materials and cells are needed, which greatly increases the cost of the experiments. One possible solution to these issues is the use of HTS platforms. Essentially, the aim is to miniaturize the experimental set-up to allow the concomitant parallelization of different trial conditions, ideally on a single microscope slide (*126*). HTS can then be used to scan the influence of various physical, chemical, and biological properties on the cellular behavior (*127*). Instead of individually test each parameter, these approaches aim to take information from the complexity of biological systems through combinations of various parameters (*127*).

Up to know, a few microarray platforms for HTS of cell behavior have been developed. For example, Flaim et al (*128*) have used these platforms for screening the effects of ECM proteins in stem cell differentiation. Other authors have used similar methods to analyze the influence of growth factors (*129*) and biomaterials (*130*) on stem cell growth and differentiation in a high-throughput (HT) manner. However, the majority of the "cellular microarrays" that have been described in the literature are in 2D ("cell-on-gel"). In order to add the 3rd dimension to such assays, "cell-in-gel" microarray formats have to be created. Only a few groups have attempted to do that in a HT set-up. For example, Fernandes *et al* used microarray-spotting techniques to deposit nanodrops of cell-laden alginate solutions (*131-133*). Although the authors were able to take an important step towards HT screening, they have mainly achieved the patterning of multiple, repeated samples in an array, without combinatorial complexity, which still remains a major challenge in the field. (*90*) Recently, Dolatshahi-Pirouz *et al* (*134*) described a robotic microarray spotter capable of printing different hydrogel formulations with hMSCs embedded within methacrylated gelatin hydrogels. The authors used this platform to combine different ECM compositions with different media in order to evaluate the best condition that enhances the expression of osteogenic markers. This work represented an important advance in the HTS for studying cell-ECM communication in 3D. It showed that a rather simple technique can be used to study how hMSC interact with important ECM proteins, making it possible to screen 96 different combinations in only one assay. With such a tool, it is possible not only to reduce the material needed to perform an experiment, but also the time spent in defining the best possible condition (*134*).

Advances in bioprinting technologies have been crucial to develop this type of systems. Bioprinting is defined as the use of printing technology to deposit living cells, ECM

components, biochemical factors, proteins, drugs, and biomaterials on a receiving solid or gel substrate or liquid reservoir (*135*).

In comparison to other patterning methods, bioprinting presents some advantages as a technique to produce cellular microarrays. First of all it is simple to use and works with several systems previously optimized for other purposes. Since these technologies are relatively simple, the process to obtain geometrically well-defined patterns with polymers or ceramics is inexpensive and rapid (*136*), leading to HT deposition of ECM analogues (*137*). Last, but not least, also being a revolutionary technology, bioprinting provides 3D complexity by multi-layer printing (*137-139*). There are several possible methods that can be used for this type of bioprinting. Acoustic (*140-141*), inkjet (*142-143*), valve-based (*139, 144-146*), and laser printing technologies (*147-150*) are the most commonly used ones (**Figure 3**).

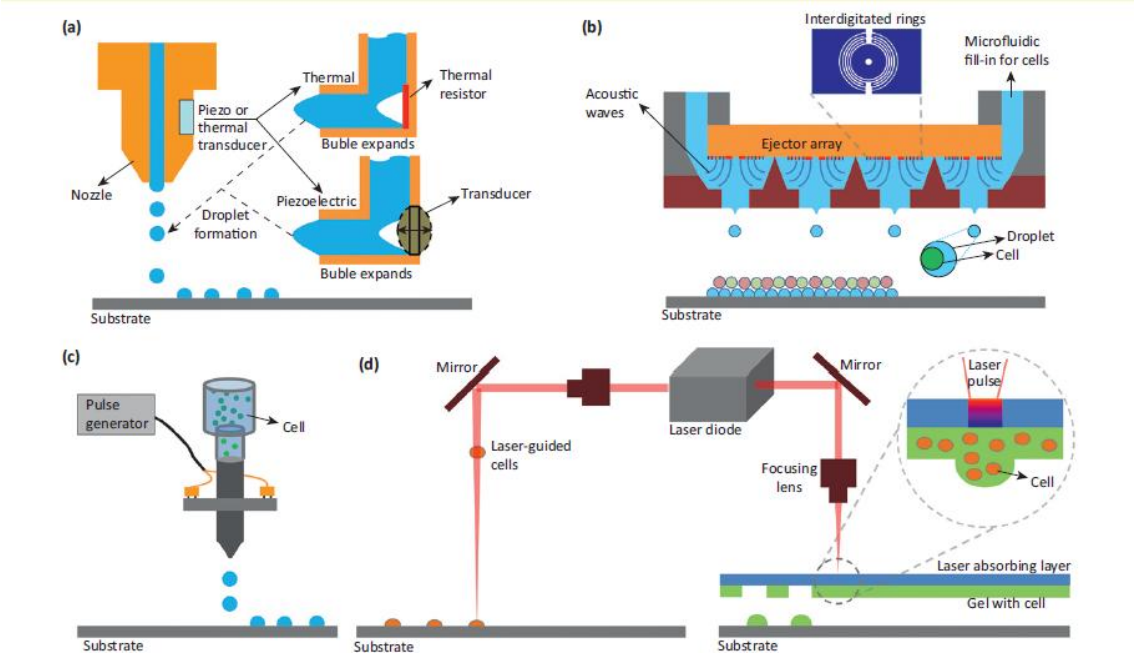

Figure 3 – **Sketch of bioprinting technologies**. (**a**) Thermal and piezoelectric ink-jet printing. Two major methods to jet the bio-ink are demonstrated. (**b**) Setup for acoustic pico-liter droplet generation. Droplets can be deposited drop-on-demand with predetermined separation and locations. (**c**) Sketch of the valve- based printing setup. (**d**) Sketch of the laser printing setup. (Left) Laser-guided direct cell printing. (Right) (adapted from (*135*)).

The first approach to construct a bioprinter actually came from the common concept of a printer. Wilson and Boland (*151*) have reported how they modified a common HP printer to start to print biomolecules and cells. Since this pioneer idea, a lot of efforts have been made for improving all the technologies involved in the bioprinting field. Following this idea of an inkjet system, some authors have used this technology to place a cell suspension in a cartridge connected to a computer, allowing the controlled printing of the cell suspension in the substrate, creating a controlled pattern (*142-143*). This method has a good throughput,

since it can print very fast, but unfortunately lacks of single cell control and spatial resolution (**Table 3**).

Table 3 – Comparison of commonly used bioprinting technologies based on performance (adapted from (*135*))

Performance metric	Valve-based bioprinting [7,24–26]	Laser –induced bioprinting (LIFT, BioLP, MAPLE) [19,21,40–44]	Laser-guided bioprinting [18,39]	Inkjet bioprinting [16,17]	Acoustic bioprinting [5,23]
Throughput	Medium	Medium	Low	High	High
Droplet size	100 μm–1 mm	>20 μm	>10 μm	50–300 μm	10–500 μm
Spatial resolution	Medium	Medium	High	Medium	Medium
Single Cell Control	Medium	Medium	High	Low	High

Another method to print cell-in gel constructs is the valve-based droplet ejection method (*144-145*). The hydrogel droplets are ejected onto a surface, in a drop-on-demand fashion, allowing the control of the number of cells printed per droplet and also the number of droplets wanted to be printed. However, in this case the printable droplet sizes are too large for a developing microarray platforms and the throughput is not so high. In order to have a precise spatial resolution with a cell printing controlled at the unit level, laser-guided direct printing is the best option leading to constructs very well spatial organized. This technique uses the power of photons from a laser beam to trap and guide cells by exploiting the differences in refractive indexes of cells and cell media (*147*). The spatial resolution is so high that this technique is being used for the construction of 3D cell structures like vascular structures composed of HUVECs printed in parallel layers of matrigel (*152*), and also the micropatterning of liver sinusoid-like structures with micrometer resolution *in vitro* (*147*). Despite the great advantages of this technique its throughput is very low. An alternative to this, that combines HT and high single cell control, is the acoustic bioprinting. Via acoustics this technique is capable of printing 100 000 droplets per second (*140*) and make well-defined patterns. Also, this technique is not harmful to the cells, since the wave's energy does not affect cell viability. Regarding the spatial range, it can goes from 10 to 500 μm which enables a great variety of different formulations (Further reading: Tasoglu and Demirci review (*135*)). The last technique referred in this brief description is the laser-induced biopriting (**Figure 4**). This was the bioprinting technique explored in this work, and it is therefore described in more detail.

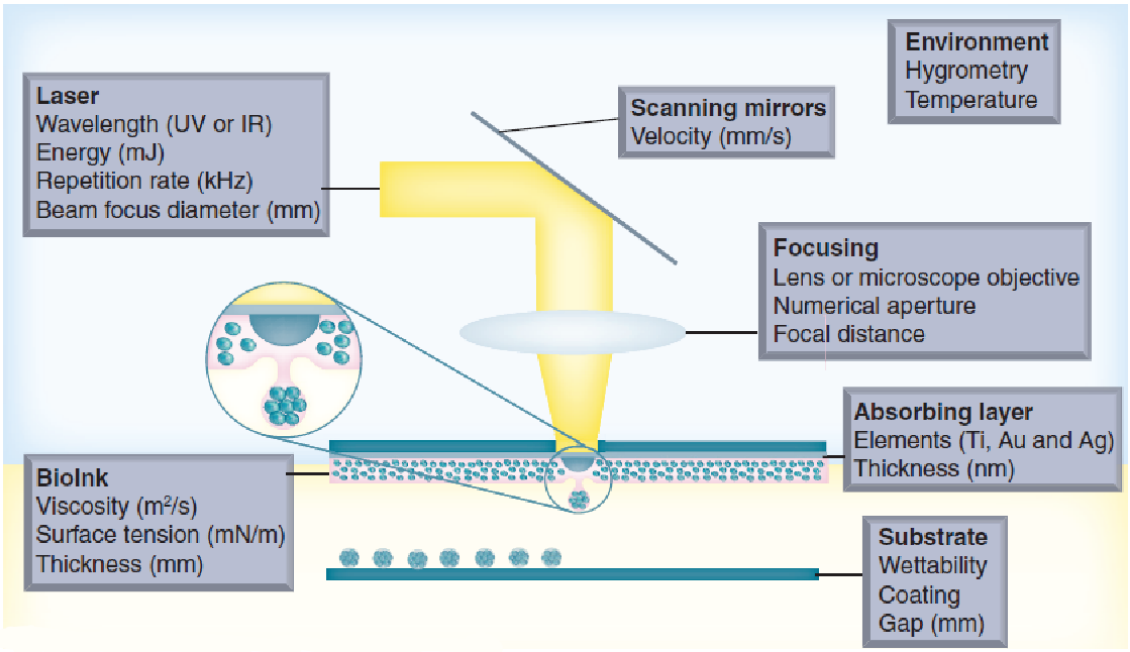

Figure 4 – **Laser-assisted bioprinting, featuring all the parameters involved in the process** (adapted from (*153*)).

Laser-assisted or laser-induced bioprinting is usually composed of three elements: a pulsed laser source, a target coated with the material to be printed (the ribbon) and a receiving substrate (**Figure 4**) (*153*). The ribbon is a multilayer component (**Figure 5**) that has a support transparent to laser radiation wavelength and a layer that is going to be transferred – bioink. This layer will transport the biomolecules, cells or biomaterials so it has to be sensitive to the heat caused by the laser beam.

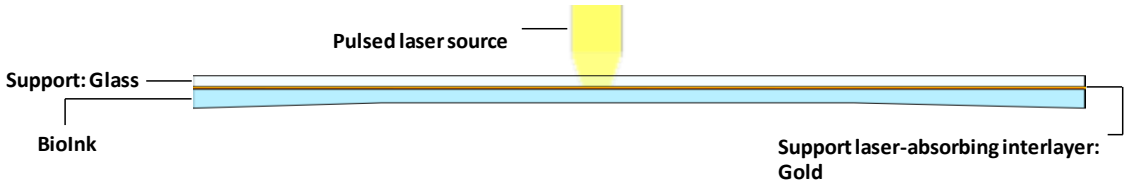

Figure 5 – Laser-assisted Biopriting composition.

As schematized in **Figure 5**, there is the need to use a laser-absorbing interlayer, since sometimes the bioink itself is not transferable by the laser energy. This layer is going to absorb the energy and induce the transfer of the bioink. Hence, this technique is also called matrix-assisted pulse laser evaporation- direct write (MAPLE-DW) (*154*). This interlayer that is first vaporized eliminates direct interaction between the laser beam and the bioink. Usually this layer consists of a thin film (tens of nm) of metal (Au, Ti, Ag), metal oxide (TiO2) or photo-decomposing volatile polymer (triazene) (*153*).

This technique – LAB – appears has an attractive alternative to inkjet and micro-pen printing devices. In fact, these other techniques present some problems like the clogging (due to the viscosity, cell agglomeration, ink drying or even gelation) of the printing heads or capillaries used by these printers to achieve micron-scale resolution. Also, comparing to the laser-guided bioprinting referred above, LAB is capable of making the rapid deposit of material at a rate of kHz and works with mild-viscous solutions (*153*).

The printing process used in LAB is schematized in **Figure 6**. Briefly, a pulsed (typically 1-20 μJ per pulse) ultra-violet (UV) or infra-red (IR) Laser will cross the transparent material (frequently glass) (**Figure 6.1**). The interlayer composed of gold will absorb the laser's energy and starts to evaporate (including normal boiling and phase explosion) forming a plasma that may further form a vapor bubble that expands towards the free surface (**Figure 6.2**).

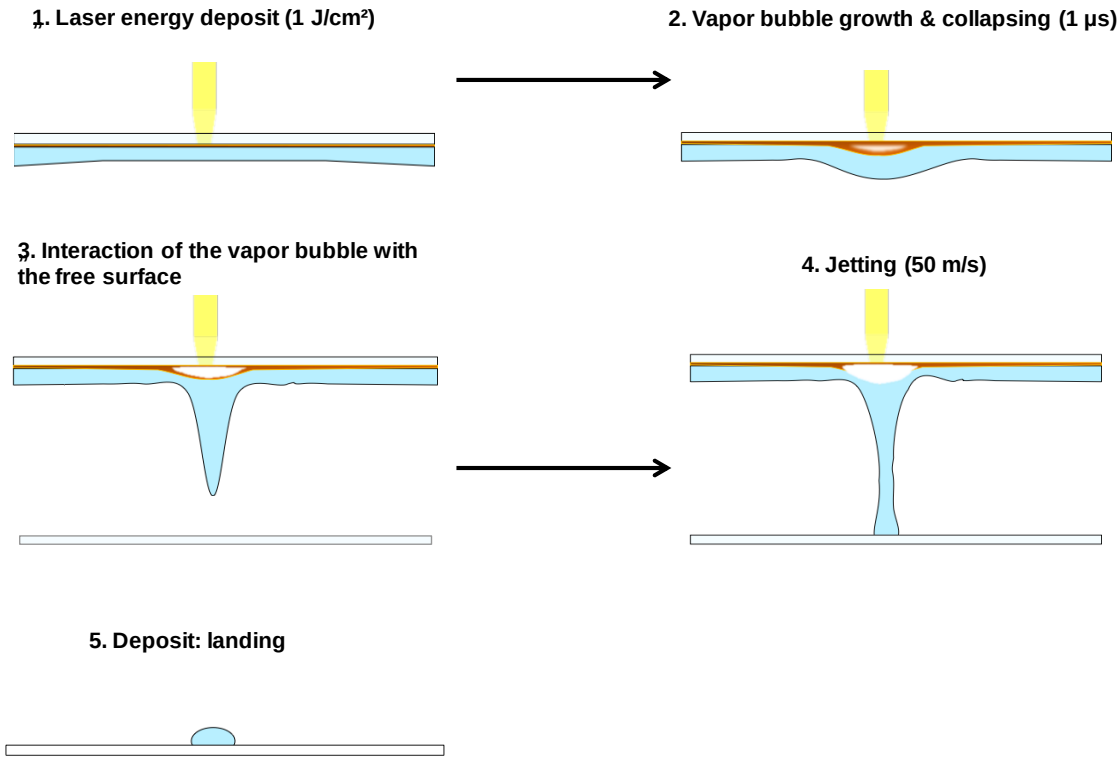

Figure 6 – Step-by-step mechanism of laser-assisted bioprinting.

The bubble collapses due to a high-pressure region generated in the bubble apex and a jet may be formed (**Figure 6.3**). This jet advances at a constant velocity (20–150 m/s, depending on experimental conditions) until it reaches the receptor substrate leading to material deposition (**Figure 6.4**). Depending of the landing, the jet conditions and, most importantly, the surface properties, the formation of little droplets in the range of pico-to-nano liters, occurs in an HT manner (**Figure 6.5**) (*153*).

As it is possible to see in **Figure 6**, there are a large number of conditions that may affect all the process. These conditions are yet to be all decoded and a lot of effort has been done by

Guillemot's team at INSERM to unravel the influence of several parameters in the bioprinting. In this work, we tried to correlate some of these conditions with the printing outcome. Duocastella *et al* (*155*) have been studying the influence of viscosity and surface tension in the LAB performance. It appears that when the viscosity of the bioink solutions is increased, the energy input necessary for the bubble formation has to be higher. This means that all the process is not only related to the laser beam power, but also with the rheological properties of the bioink (*153, 156*).

Other important aspects that can influence the printing are surface properties. The gap between the bioink and the susbtrate was shown to be finite, since the jet has to reach the surface of the susbtrate (*155*).

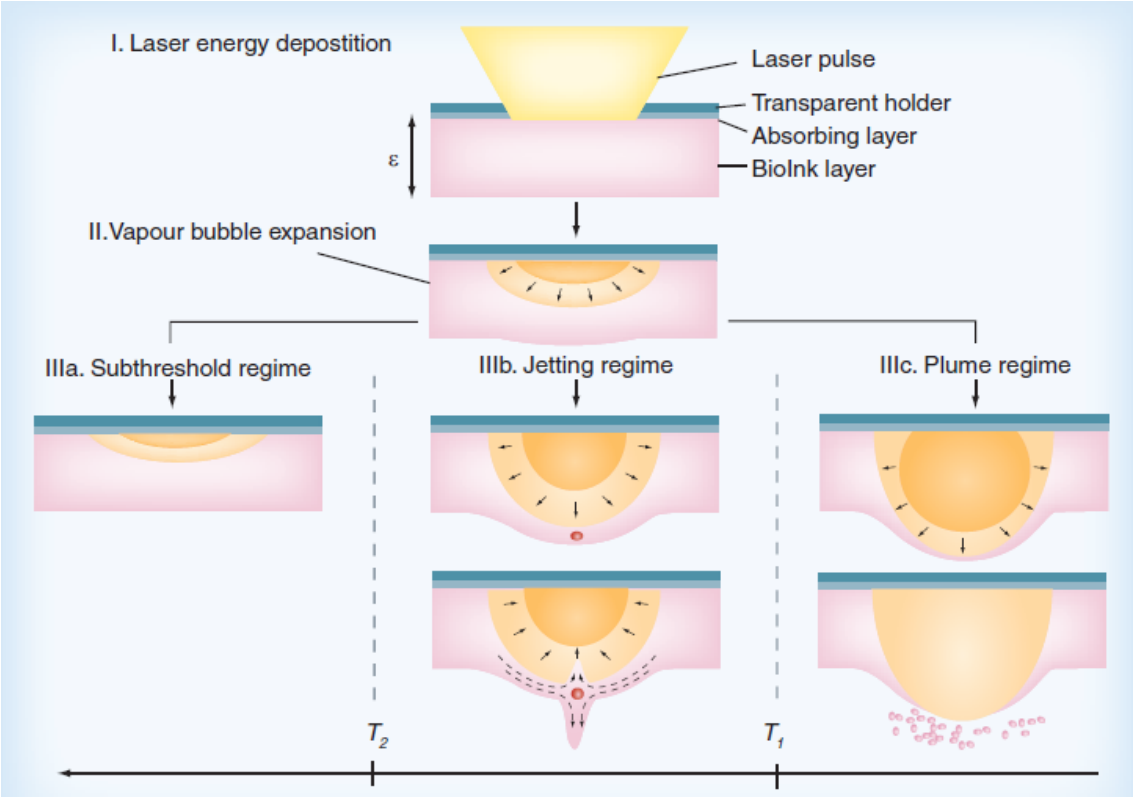

Figure 7 - Laser-induced droplet ejection regimes (adapted from (*153*)).

Also the wettability and possible coating of the surface will not only affect the jet deposit by physicochemical affinity, but also the formation of proper droplets that can be used for cell culture and microarrays production. For instance, a more hydrophilic surface is going to have an impact in the droplets diameters and heights, since hydrogels tend to spread more in this kind of surfaces. Also in terms of stability overtime, the hydrogel droplets of the microarray have to persist adhered to the substrate surface. These and other parameters are going to be discussed further in this work (*153*).

The parameters involving the ribbon, the bioink, and the laser beam are very important to control. As it was described above, these parameters will ultimately affect the laser dynamics

affecting the laser regime (**Figure 7**). There are three possible regimes: sub-threshold regime, jetting regime, and plume regime. For a certain viscosity and film thickness, the jetting regime is observed only for intermediary laser fluencies. For lower fluencies, the bubble collapses far from the free surface without generating a jet. The opposite behaviour occurs for high fluencies. In this case the bubble bursts to the surface, generating sub-micrometer droplets. These correlations between film thickness and bioink viscosities force the operator to optimize all the bioprinting parameters for a certain bioink (*153, 156*).

Recently, LAB is being used for several tissue engineering applications, namely for 3D tissue formation and organization (*157*); for the study of the molecular mechanisms involved in stem cell fate and commitment (*131*); to print engineered tissue substitutes directly into in vivo models (*158*); to allow robotic-assisted medical intervention (*159*), and to create *in vitro* models for the characterization of cell-environment effects (*160-161*).

However, until now, there are no studies that have fully addressed the potential of LAB as a technique to develop microarray systems in 3D. Moreover, no attempts have been made to make complex studies combining such strategies with the use advanced artificial ECMs with tunable biochemical and mechanical properties. In the present work, we intended take a first step towards that end. In brief, we have tried to combine the advantages of using the tunable ECM-like 3D matrices, developed by our team (*120, 124, 162*) with LAB, for the creation of a cell-in-gel 3D microarray platform. To produce the microarrays, bioinks with different polymer concentrations (1% and 2% w/v alginate) and different cellular densities were used to study the impact of these parameters in the bioprinting process and on cells behavior. Another innovation tested here was the use of self-gelling bioinks, composed of alginate and cells combined with gelation agents ($CaCO_3$ and GDL). This allows the printing process to be made in just one step, with the gelation of the droplets occurring slowly after the spotting has been made. In particular, in this work we wanted to establish whether LAB could be use to: (a) print bioinks with different cell densities and variable viscosities; (b) obtain a controlled cell patterning (equidistant and regular micro-spots); (c) maintain cell viability along the printing procedure; (d) produce microarrays that remained stably attached to the receiving substrate along the subsequent period of culture. Next we wanted to validate the microarray culture (cell-in-gel micro-spots) by comparing some of the obtained results with those obtained using a MT assay (cell-in-gel disks), previously established in our team. The final goal was to use this new HTS platform for the analysis of EC-MSC crosstalk in 3D.

Material and Methods

1. Isolation and characterization of UCB cells A and UCB cells B

1.1. Isolation of EPCs and OECs from UCB samples

UCB samples were collected during labor at Hospital São João. All of the donors signed an informed consent form that is in compliance with the Portuguese legislation and the ethical committee of the referred hospital, approving the collection. After collection, the samples were stored and transported in 250 mL sterile bags that contained 35 mL of CPDA-1 (Citrate, Phosphate, Dextrose and Adenine) anti-coagulant solution (Mollitia). MNCs were isolated from blood using Ficoll (Histopaque-1077 Hybri Max; Sigma-Aldrich) density gradient separation (**Figure 8**) as previously described (*163*). Briefly, blood samples were diluted 1:1 with Hank's Balanced Salt Solution (HBSS, Alfagene) and gently dropped on top of 20 mL of Histopaque® solution.

To obtain OECs, centrifugation was performed at 780 *x g* for 30 min. Mononucleated Cells (MNCs) rings were then transferred onto 50 mL Falcon tubes, washed with twice their volume of HBSS and afterwards resuspended in supplemented Microvascular Endothelial Cell Growth Medium-2 (EGM2-MV, Lonza), with 10% FBS. Cells were plated onto collagen type-I–treated plates (Enzifarma) at a cellular density of approximately $1x10^6$ cells/cm^2 and cultured for 18-21 days at 37ºC, in a humidified atmosphere with 5% v/v CO_2 in air, with medium change every day, until the formation of colonies. Cells were then detached by tripsinization (0.25% w/v trypsin/ethylenediamine tetraacetic acid (EDTA) solution, Sigma), cultured in uncoated 6-well plates with EGM2-MV. When confluent, cells were either frozen or expanded until passage 3, when they were used. These cells will be hereafter designated as UCB Cells A.

To obtain EPCs, centrifugation was performed at 400 *x g* for 30 minutes. MNCs rings were then pipetted onto 50 mL tubes, washed with twice their volume of HBSS and afterwards resuspended in supplemented EGM2-MV, with 10% FBS and without hydrocortisone supplement. Cells were plated onto Fn-treated plates (normal plates were incubated for 30 min with Fn solution (Enzifarma) at 1 mg/mL and let dry at room temperature (RT)) at a cellular density of about $1x10^6$ cells/cm^2 and then cultured for 5 days at 37ºC, in a humidified atmosphere with 5% v/v CO_2 in air, without medium change. After tripsinization, cells were immediately used for experiments. These cells will be hereafter designated as UCB Cells B.

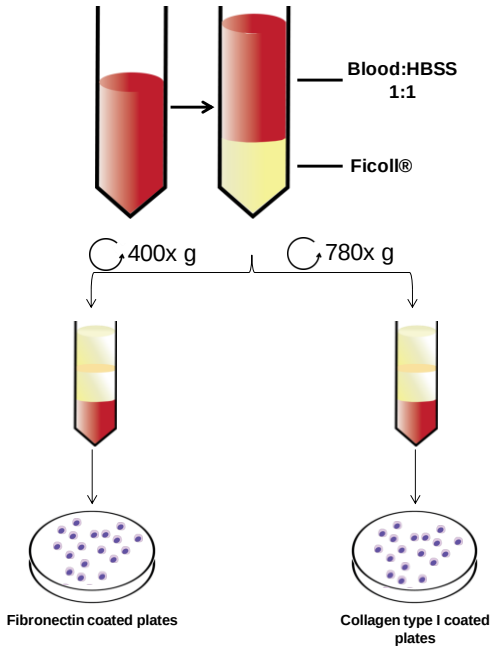

Figure 8 – Protocol isolation for er-EPCs and OECs.

1.2. Fluorescence-activated cell sorting analysis (FACS) of UCB cells A and UCB cells B

After tripsinization (0.25%), both UBC cells A and B were aliquoted (10^5 cells per condition), centrifuged, and resupended in FACS buffer (PBS; 0.5% w/v bovine serum albumin; 0.01% w/v azide, Sigma-Aldrich). After being washed twice, cells were incubated for 30 minutes at 4ºC with isotype controls (Mouse IgG1 FITC and Mouse IgG1 R-PE; both from Caltag Medsystems), or antigen-specific mouse anti-human antibodies: CD31-APC (Myltenyi Biotec), CD34-FITC, (Caltag Medsystems), CD45-FITC (Imunno Tolls), and CD14-APC (Imunno Tolls). A control with non-stained cells was also performed. After incubation, all samples were centrifuged and washed twice and markers expression analysis was carried out by three-color flow cytometry on a FACSCalibur flow cytometer (BD Biosciences). Data analysis was made using FlowJo® software.

1.3. Immunofluorescence analysis of expression of ECs markers in UCB cells A and B

Immunofluorescence staining was performed to assess the expression of ECs markers. Both UCB cells A and B were fixed with 4% v/v paraformaldehyde (PFA; Merck Millipore, Darmstadt, Germany) for 30 min at RT, washed with PBS, and permeabilized with 0.2% v/v Triton X-100 (Sigma-Aldrich) in PBS for 10 min. For VE-cad analysis, samples were incubated for 10 min in ammonium chloride (50 mM NH_4Cl, Sigma-Aldrich) before permeabilization. After washing with PBS, the samples were incubated for 1 h at room temperature in blocking solution (4% v/v FBS in 1% w/v BSA in PBS) and incubated overnight at 4ºC with the following primary anti-human antibodies: monoclonal mouse CD31 (PECAM1; Dako, 1:50), monoclonal mouse VE-cad (VE-cad; Santa Cruz Biotechnology, 1:100), and polyclonal rabbit vWF (Dako, 1:300). Excess antibody was removed by washing with PBS and samples were incubated with the secondary antibodies (Alexa Fluor® 594 anti-mouse, Alexa Fluor® 488 anti-rabbit, Alexa Fluor® 488, and Alexa Fluor® 647, Invitrogen, 1:1000) for 1 h at RT. The nuclei of cells was stained with 4',6-diamidino-2-phenylindole (FluoroShield™ with DAPI; Sigma-Aldrich). Negative controls were also performed with only secondary antibody staining to validate the assay. Samples were visualized under a Zeiss inverted fluorescence microscope (IFM, Zeiss Axiovert 200, Carl Zeiss International) and the resulting images were processed using Fiji Imaging Software.

1.4. Endothelial functional assay

Samples were incubated with 10 µg/mL of DiI-labeled ac-LDL (Bioquote) for 4 h at 37ºC and washed three times with EGM2 or EGM2-MV. The uptake of Ac-LDL was visualized under an inverted fluorescence microscope.

2. Establishment of hydrogel-based 3D cultures

2.1. Cell cultures

HUVECs and MSCs (Lonza) were routinely kept in culture at 37ºC in a humidified atmosphere with 5% v/v CO_2 in air. Media was changed every two days: HUVECs were cultured in complete M199 (Sigma-Aldrich) with 10% v/v FBS, 0.1 mg/mL Heparin (Heparin Sodium Salt; Sigma-Aldrich), 1% v/v Pen/Strep. Endothelial Cell Growth Supplement (ECGS; BD Biosciences) at a concentration of 3 µL/mL was added every time the media was changed. MSCs were cultured in Dulbecco's Modified Eagle medium (DMEM; Invitrogen) with 10% FBS and 1% P/S. Both HUVECs and MSCs were trypsinized when they reached confluence. For the following experiments, cells from passages 6 and 7 were used. Regarding UCB cells A and B, isolation was made according to the method described in **Section 1.1.** and there was no incubation period prior to cell embedment.

2.2. Preparation of peptide-grafted alginate

Ultra pure alginate with high content of guluronic vs mannuronic acid units (>60%, NovaMatrix, FMC Biopolymers) and different molecular weights were used. High molecular weight alginate (HMW; 150 kDa) was oxidized and modified as previously described (*164*). The cell-adhesion peptide sequence (glycine)4-arginine-glycine-aspartic acid-serineproline (G4RGDSP, GenScript), hereafter abbreviated as RGD, was coupled to oxidized High Molecular Weight (HMW) alginate using carbodiimide chemistry, as described in detail in previous studies (*162*). Briefly, a 1 % (w/v) alginate solution in 0.1 M MES buffer (Sigma) was prepared and stirred overnight Sulfo-NHS (Thermo Scientific) and EDC (Sigma) at 1:2 molar ratio were then sequentially added and stirred for 15 min, to activate polymer COOH- groups before addition of the RGD peptide (17 mg/g alginate). After stirring for 24 h, the reaction was quenched with Hydroxylamine (NH_2OH, Sigma). Nonreacted species were separated by dialysis (MWCO 3500 membrane, Spectrum Lab) against solutions of decreasing concentration of Sodium Cloride (NaCl, Merck) and finally in deionized water. The recovered solution was lyophilized and the RGD-alginate was stored at -20ºC until further use.

2.3. Preparation of RGD-alginate self-gelling hydrogel disks

To prepare *in situ* crosslinking hydrogel matrices an internal gelation strategy adapted from Kuo *et al*. was used (*165-166*). The alginate gel precursor solution was a 50:50 v/v binary mixture of RGD-grafted oxidized HMW alginate and unmodified Low Molecular Weight (LMW) alginate, prepared at a total alginate concentration of 1 an 2% (w/v) in 0.9 wt.% NaCl (Sigma-

Aldrich). This formulation has been previously optimized by our team (*162, 167*) with final concentration of RGD peptide of 200 μM. The solution was sterile-filtered (0.22 μm) and thoroughly mixed with an aqueous suspension of $CaCO_3$ (Fluka) at a $CaCO_3$/COOH molar ratio of 1.6. To trigger gel formation, a fresh solution of GDL (Sigma) was added. The $CaCO_3$/GDL molar ratio was set at 0.125. The pre-gel solution was then added to the cell suspension with the correct number of cells and hydrogel disks (15 μL) were casted between Teflon plates with spacers of 700 μm. The cell-laden mixture was left to crosslink for 1 h at 37ºC under a humidified atmosphere, and placed in 24 well plates before medium was added. The medium was changed 30 min after to stabilize the pH and the final constructs were incubated at 37ºC in a humidified atmosphere with 5% v/v CO_2.

For cocultures, either HUVECs or UCB cells A in suspension were mixed (1:1 ratio) with MSCs at a final cellular density of 10 million/mL, while in triple-cultures, the same final density and ratio between HUVECs and MSCs was maintained, but UCB cells B were also added at a final cellular density of 10 million/mL. Controls of monocultures were also performed for HUVECs, MSCs, UCB cells A and UCB cells B at a final cellular density of 10 million/mL of gel precursor solution. For cocultures of HUVECs and MSCs, cells were maintained in EGM2 medium during the culture period, while for cocultures of MSCs and UCB cells A, cocultures of HUVEC and UCB cells B, and triple-cultures, cells were maintained in EGM2-MV medium.

3. Cell behaviour in 3D cell cultures

3.1. Metabolic activity and cellular viability

The metabolic activity of entrapped cells in alginate matrices was assessed by resazurin assay. Resazurin (resazurin sodium salt at 0.1 mg/mL; Sigma-Aldrich) was diluted (20% v/v) in the respective medium (EGM2 or EGM2-MV) and incubated with the disks for 3 h at 37ºC. A fluorometer (Synergy MX; Biotek, Winooski, US) was used to excite the samples at 530 nm and read the fluorescence at 590 nm. EGM2 or EGM2-MV with resazurin (20% v/v) were used as blank samples.

Cell viability within alginate disks was determined with a Live/Dead assay. CyTRAK Orange™ and DRAQ7™ (both from Biostatus) were used as dyes for live cell and dead cells, respectively. CyTRAK Orange™ was diluted in medium at 10 μM as final concentration, while DRAQ7™ was diluted in medium at 3 μM as final concentration. Both dyes were incubated for 10 min at RT. Disks were then visualized under a laser scanning microscope (CLSM, Leica TCS-SP2 AOBS; Leica Microsystems, Wetzlar, Germany). The resulting images were processed using Fiji Imaging Software.

3.2. Matrix contraction

After gelification and at day 3, photographs of the disks were taken using a stereoscopic microscope (Olympus SZX10). Percentage of contraction was calculated by the difference of diameter between day 0 and day 3. Measurement calculations were processed using Fiji Imaging Software.

3.3. Cell labelling

Cells were suspended in serum-free medium and labelled with CellTracker™ (Invitrogen) Blue (MSCs) or Green (HUVECs) by incubation with 15 μL of the stock solution (prepared according to the manufacturer) during 30 min (stirring the solution each 10 min). After centrifugation the cells were ressuspended with complete medium and incubated for 30 min. Cells were embedded in disks as described in **Section 2.3.** and disks were then visualized under a laser scanning microscope (CLSM, Leica TCS-SP2 AOBS; Leica Microsystems, Wetzlar, Germany). The resulting images were processed using Fiji Imaging Software.

3.4. Immunocytochemistry

Ac-LDL uptake was used to assess ECs rearrangement and functionality in 3D (as described in **Section 1.4.**). For visualization, disks were washed twice with a solution of TBS 1x/7.5 mM $CaCl_2$ and fixed in 4% PFA in TBS/$CaCl_2$.

Immunocytochemistry of 3D constructs was performed by fixing with 4% v/v PFA in TBS/$CaCl_2$ for 30 min at room temperature, disks were then washed with TBS/$CaCl_2$ and permeabilized with 0.2% v/v Triton X-100 (Sigma-Aldrich) in TBS/$CaCl_2$ for 10 min. For VE-cadherin analysis, samples were incubated for 10 min in ammonium chloride (50 mM NH_4Cl, Sigma-Aldrich) before permeabilization. The samples were then incubated for 1 h at room temperature in blocking solution (4% v/v FBS in 1% w/v BSA in TBS/$CaCl_2$) and left overnight at 4ºC with primary antibodies. Excess antibody was removed by washing with TBS/$CaCl_2$. The secondary antibodies and phalloidin (Alexa Fluor®-488 Phalloidin; Invitrogen) (when the case) were incubated for 1 h at room temperature. Samples were counterstained with DAPI and visualized under a CLSM and the resulting images were handled using Fiji Imaging Software.

Primary antibodies against mouse α-SMA (Dako, 1:100), mouse VE-cad (1:50), rabbit vWF (1:150), mouse CD31 (1:50), and mouse CD45 (1:100) were used and detected with secondary antibodies referred in **Section 1.3**.

4. Establishment of cell-in gel 3D microarrays: bioprinting setting

4.1. Preparation of RGD-alginate bioinks

Bioinks with 1 % (w/v) or 2 % (w/v) alginate in 0.9 wt.% NaCl were prepared and combined or not with cross-linking agents and cells (MSCs or HUVECs), as described in **Section 2.3.** In some assays (at INSERM), a MSCs cell line (D1) expressing Tomato protein was used (see section 2.5.1.) **Figure 9** illustrates how the bioinks are prepared and applied onto the receiver substrate.

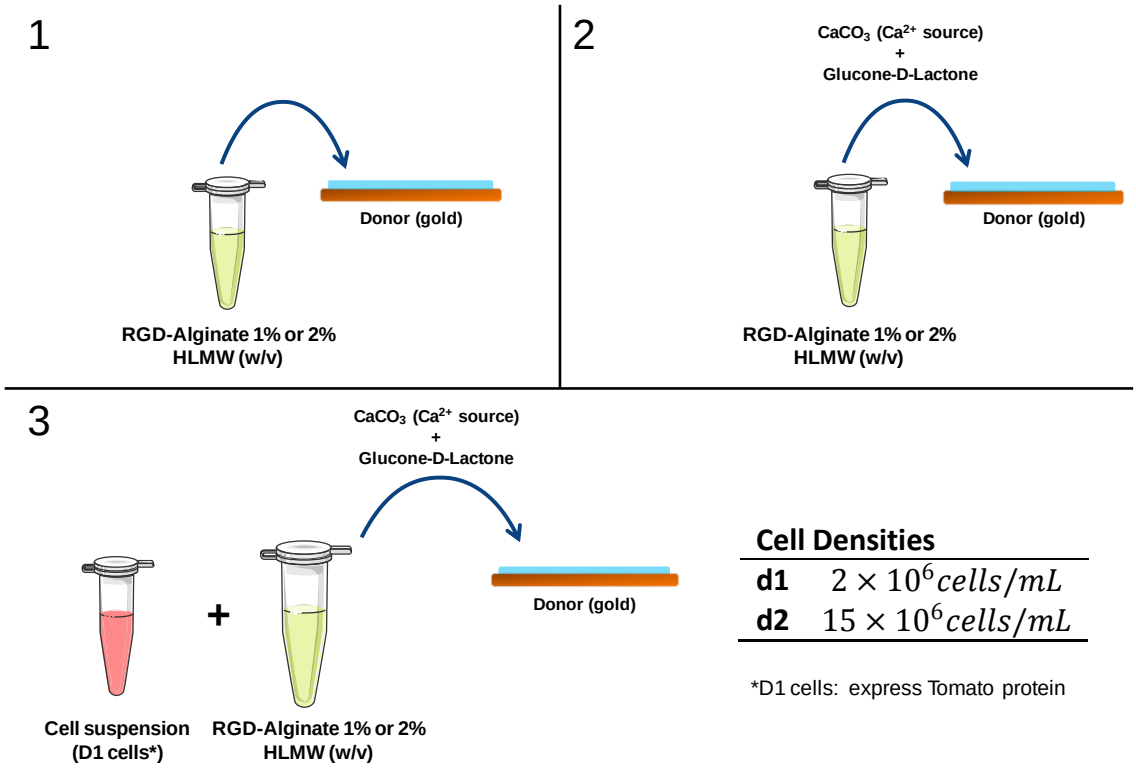

Figure 9 - Printing optimization strategy. (**1**) Printing of alginate only; (**2**) printing of alginate with gelation agents; (**3**) printing of alginate with gelation agents and cells at different cell densities.

4.2. Bioink rheological characterization

The viscosities of the alginate solutions (1 % (w/v) and 2 % (w/v), with two different cell densities - 2 x 10^6 cells/mL or 15 x 10^6 cells/mL) were determined with a Kinexus Pro rheometer (Malvern Instruments, Malvern, UK), using cone and plate (40 mm cone diameter, 1° cone angle). The sample solutions were prepared in a similar way as for cell entrapment

studies but without the addition of GDL as no gelation triggering should occur. 150 µl of sample solution were used for each measurement and the plate was lowered to a measuring gap size of 0.015 mm. The temperature was set to 25°C to simulate the temperature at which the alginate drops are printed. The evaporation was prevented using a water ring around (but not contacting) the sample. The temperature was maintained and the evaporation was prevented by the rheometer active hood. The shear viscosity was recorded by applying a shear rate ramp from 0.01 to 1000 s^{-1}.

4.3. Bioprinting behavior

Time-resolved imaging (TRI) was used to assess bioink printability. For these experiments the bioink with the higher viscosity (2% w/v alginate) was used. A laser energy of 28 Ampere (A) and a film thickness of 20 µm were selected. The system used a laser light and a CCD camera to take pictures at exact precise times.

4.4. LAB Workstation

The LAB workstation consisted of a solid Nd:YAG crystal laser (Navigator I, Newport Spectra Physics) was selected with the following specifications (k = 1064 nm, s = 30 ns, f = 1–100 kHz, q = 3.4 mrad, TEM00, ptp < 1.5% rms, P= 7 W).

A sophisticated five-axe positioning system was integrated into the workstation (NovaLase, SA, Canéjan, France) with the purpose of printing multi-color patterns and building 3D biostructures. The substrate was held with a (x, y, z) motorized micrometric translation stage whose resolution is 1 lm for the (x, y) axis and 5 lm for the z axis. In order to achieve multi-color printing, a high resolution (1° angular resolution) motorized carousel with a loading capacity of five different ribbons was designed (see **Figure 10**). The substrate positioning system and carousel were held on the same vertical axis with the aim of varying focusing conditions without changing the gap distance.

Droplet generation from the ribbon surface was performed by driving the laser beam by means of a high speed scanning system composed of two galvanometric mirrors (SCANgine 14, ScanLab), with a scanning speed reaching 2000 mm s-1, and a large field optical F-theta lens (S4LFT, Sill Optics, France) (F = 58 mm). Focal setting in the ribbon and (x, y, z) substrate positioning were carried out via a CCD camera through the optical scanning system.

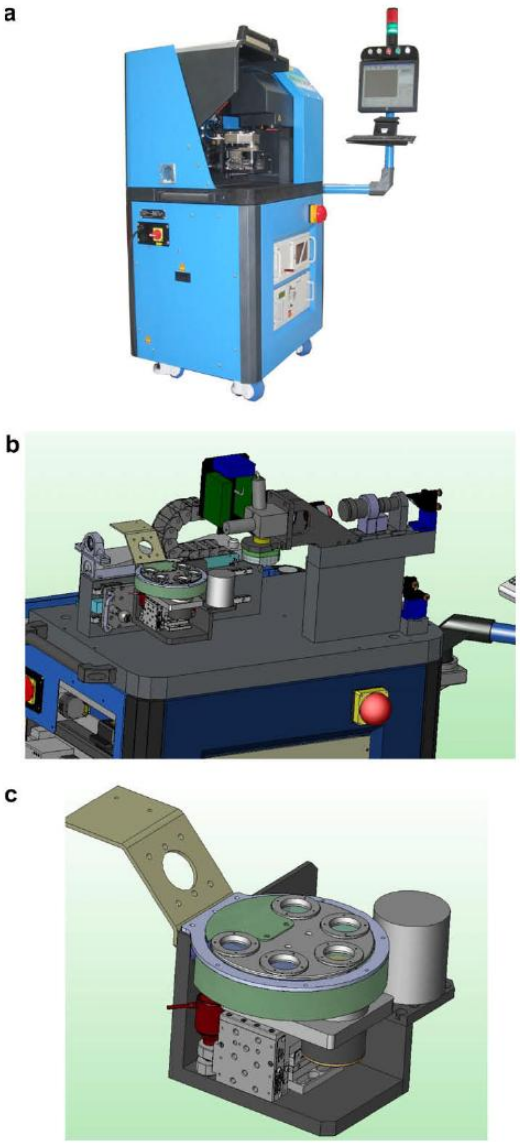

Figure 10 – LAB workstation (**a**) View of the HT biological laser printer, (**b**) optomechanical set-up and (**c**) high resolution positioning system placed below the carousel holder with a loading capacity of five different ribbons (adapeted from (*153*))

The integration of the laser and all above-mentioned components was made possible using Solidworks software. Substrate positioning, carousel driving, video observation and pattern designs were monitored with dedicated software developed with Delphi software.

Finally, this CAD/CAM workstation (**Figure 10**) was placed in a cell culture room in order to facilitate cell transfer experiments (*9*).

4.5. Ribbon preparation

As described above, the ribbon is made of three layers: a support, a thin metal absorbing layer and a solution of hydrogel. The support is a 30 mm diameter disk made of IR-transparent quartz. This disk was sputter coated with 20–30 nm of gold using an Emscope SC500 coating unit. The thickness was chosen to be higher than the optical skin depth (17 nm) at near-IR wavelengths (1064 nm). Then the hydrogel film, composed of a suspension of the desired materials, was spread onto the gold-coated quartz disk with a micrometric film blade (3570, Elcometer). Typical film thickness was 20 - 30 µm.

4.6. Substrate preparation

Two different substrates (receivers) were used. For printing optimization, the printing elements were collected on a quartz disk, whose characteristics were the same as the support. For cell culture, microarrays were printed directly into LabTek® (Nunc* Lab-Tek* II Chamber Slide* System), which were pre-treated with 0.1% w/v PLL solution (Sigma) for 1h, washed 3 time and left to dry overnight.

4.7. Characterization of the transferred materials

Droplets shape, diameters, and cell number per spot counts were measured by contrast microscopy and fluorescence microscopy.
Droplets' heights were measured by TRI images. Images show a droplet with its reflection. Half of the value measured was considered the real height.
In order to calculate droplets volume, an approximate formula was used (**Expression 1**). With volume values, approximate cellular densities were estimated.

$$V = \left[\frac{1}{6}\pi h\left(3\frac{D^2}{4} + h^2\right)\right]$$

Expression 1 – Calculation used to obtain the approximated droplet's volume

5. Establishment of cell-in gel 3D microarrays: cell culture studies

5.1. Culture of mouse mesenchymal stem cells (D1 cells)

D1 mouse mesenchymal stem cells (D1 cells) (Lonza) expressing tomato protein were routinely cultured in a basal medium (hereafter designated as BM) composed of low-glucose Dulbecco's Modified Eagle Medium with glutamax (DMEM, Gibco) supplemented with 10% v/v Fetal Bovine Serum (Lonza) and 1% v/v Penicillin/Streptomycin (Pen/Strep, Gibco). Cultures were maintained at 37ºC under a humidified atmosphere of 5% v/v CO_2 in air, with culture medium being changed twice a week, and were trypsinized when reaching 70% confluence. For some studies, osteogenic differentiaton was induced by culturing cells in induction media (freshly made basal medium supplemented with 10 nM dexamethasone (Sigma), 10mM ß -glycerophosphate (Sigma) and 50 μg/mL 2-phospho-L-ascorbic acid (Fluka). HUVECs, routinely cultured as described before (**Section 2.1.**) were also used in some assays.

5.2. Microarrays stability assay

The stability of microarrays bioprinted onto poly-L-lysine (PLL)-treated slides was analyzed. Samples were left in basal culture medium under standard culture conditions over one week. Contrast microscopy images were taken at day 0, 3, 5 and 7.

5.3. Microarrays cell culture assays

Bioprinted microarrays of 1 % (w/v) and 2 % (w/v) alginate in Superfrost™ and LabTek® slides were left in culture for a period of one week under basal or osteogenic conditions. Cell viability was analyzed using the Live/Dead Assay (Invitrogen®) according to the manufacturer instructions. Osteogenic differentiation was analyzed by alkaline phosphatase (ALP) staining. Briefly, slides were washed three times with TBS-Ca (TBS, 50 mM Tris in 150 mM NaCl, pH 7.4 with 5 mM $CaCl_2$) and fixed with 4% v/v PFA in TBS/$CaCl_2$ for 20 min at RT, followed by another washing step, and incubated for 30 min in Naphtol AS-MX phosphate/Fast Violet B salt (Sigma) at 37ºC (protected from light). Pictures were taken by confocal microscope (Leica®) and fluorescence microscope, and by inverted microscope (Zeiss®), respectively.
As a comparison test, the bioinks used for each assay were also used for making hydrogel microdiscs (MT set-up) and the live/dead assay and ALP staining were also performed as described above.

5.4. Microarrays coculture printing

Using a 1 % (w/v) alginate solution, microarray cocultures of HUVECs and MSCs were established. Both cell types were printed at a final cellular density of 25 million/mL, making a total cellular density of 50 million/mL. The two cell types could be distinguished by using a combination of fluorescence/bright field microscopy (fluorescence emitted by D1 cells but not by HUVECs).

Results and Discussion

Results and Discussion – Part I – *In Vitro* 3D cross-talk between ECs and MSCs

1. Isolation and characterization of EPCs from umbilical cord blood

In this study, we attempted to isolate two different endothelial progenitor cell populations from UCB, EPCs and OECs, according to the protocol described by Silva *et al* (*163*) (in detail in **Material and Methods section**). MNCs were isolated from whole UCB using a density gradient. For OECs isolation, cells were centrifuged at 780 x *g* and plated on collagen type I-coated plates (hereafter designated as UCB Cells A), while for EPCs isolation, cells were centrifuged at 400 x *g* and plated on Fn-coated plates (hereafter designated as UCB cells B). After a differentiation period of around 21 days followed by colony isolation and further culture for UCB cells A, and 5 days culture for UCB cells B, both cell types were characterized by flow cytometry.

As depicted in **Figure 11A,** UCB cells A presented a single population of cells with some diversity of size and complexity. From this data, it is possible to see that UCB cells A did not express two of the most common blood lineage markers: CD45 and CD14 (**Figure 11B and C**). CD45 is the pan-marker for blood cells, while CD14 is expressed only by the myeloid lineages, which indicates that the isolated cells are not blood cells. The absence of blood markers expression was also described by Silva *et al* (*163*). CD34, which is a marker for HSCs, has been described for some authors to be expressed by OECs (*40, 48-49*), while other authors describe the absence of this marker at the cell membrane of OECs (*44, 46*). In fact, there is a lot of controversy around the expression markers that are characteristic of OECs and for CD34, there is no consensus. The authors that describe CD34 expression defend that these cells have differentiated from a HSCs ancestral, while the opposite is defended by the other authors. In this work, CD34 expression was not detected in UCB cells A, what is in accordance with Silva *et al* (*163*). Another important feature of OECs is their high mitotic rate. Silva *et al* (*163*) have described OECs as being highly proliferative cells, with low senescence and high telomerase activity. Here, when expanded in 2D culture, UCB cells A seemed to grow rapidly and easily in EGM2-MV medium. However, proliferation, and doubling time studies were not performed, which will need to be further pursued in the future. Regarding CD31, a phenotypic marker characteristic of ECs and highly expressed in mature ECs such as HUVECs,

almost all authors describe a wide expression of this marker in OECs (*39*, *44-49*). In particular, according to Silva *et al* (*163*), the differentiation protocol tested here should have yielded CD31 positive cells.

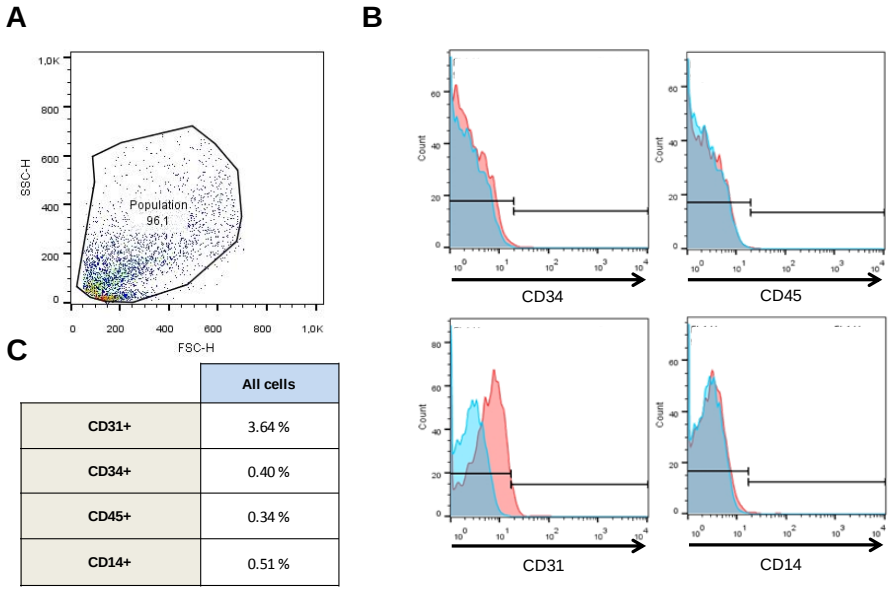

C

	All cells
CD31+	3.64 %
CD34+	0.40 %
CD45+	0.34 %
CD14+	0.51 %

Figure 11 – Flow cytometry analysis of UCB cells A. (**A**) Forward and side scatter plot of UCB cells A. (**B**) Histogram analysis for CD34, CD45, CD31, and CD14 expression markers of UCB cells A. UCB cells A population in red, while isotype control is in blue. (**C**) Table with percentages of CD31, CD34, CD45, and CD14 expression markers of UCB cells A.

However, here, almost no CD31 expression was found in UCB cells A, with only 3.24% of cells being positive for this marker (**Figure 11C**), which was an unexpected result.

Regarding UCB cells B, their phenotypic profile is completely different. As depicted in **Figure 12**, the Forward/Side scatter plot shows two different sub-populations of cells that were analyzed separately for their phenotypic markers expression (**Figure 12B and 12C**). Population 1 presented 49.6% of CD31 expression, which is in accordance with other authors who describe low expression of CD31 for EPCs populations (*39-40*). Despite Silva *et al* (*163*) have classified EPCs as CD31 positive cells, in his study nothing is said about the percentage of positive cells, and this information was only supported by immunocytochemistry. UCB cells B from population 1 were also positive for CD45 and CD14, which means that cells came from the myeloid lineage. Silva *et al* (*163*) also showed that EPCs are CD14 positive, however, in his study, nothing is said about their CD45 expression. Yet, CD45 expression by EPCs has been described in many different studies, as reviewed by Richardson and Yoder (*11*). The expression profile of UCB cells B suggests that these cells share phenotypic markers from both hematopoietic lineage and endothelial lineage. Taking this in account and also that 15.5% of the cells expressed CD34, lead us to hypothesize that some cells from this population might

come from a common cell called hemangioblast (*13*), a cell described on ontology as being able to differentiate both in endothelial and blood lineages (*37*). Another important aspect is the difference between populations 1 and 2. Er-EPCs that are the ones yielded upon a short period of endothelial differentiation, are described as a heterogeneous cell population. So, the presence of two distinct populations as shown in **Figure 12A** is in accordance with that heterogeneity. Here, populations 1 and 2 only differed in their CD34 and CD14 expression. Population 2 had lower expression of CD34, which indicates that this population has less progenitor features, while CD14 expression indicates that population 2 has less cells derived from the myeloid lineage.

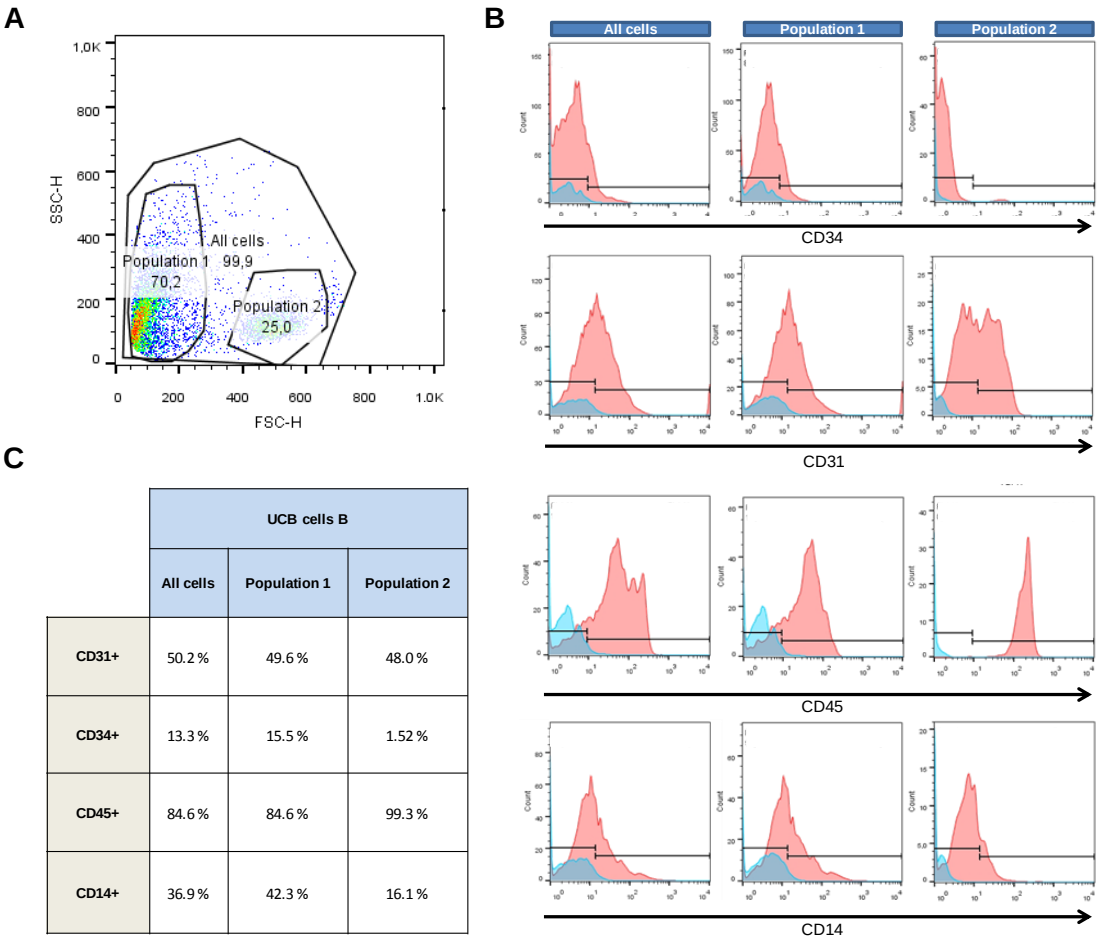

	UCB cells B		
	All cells	Population 1	Population 2
CD31+	50.2 %	49.6 %	48.0 %
CD34+	13.3 %	15.5 %	1.52 %
CD45+	84.6 %	84.6 %	99.3 %
CD14+	36.9 %	42.3 %	16.1 %

Figure 12 - Flow cytometry analysis of UCB cells B. (**A**) Forward and side scatter plot of UCB cells B population. (**B**) Histogram analysis for CD34, CD31, CD45, and CD14 expression markers of UCB cells B. UCB cells B population in red, while isotype control is in blue. (**C**) Table with percentages of CD31, CD34, CD45, and C134 expression markers of UCB cells B for all cells, population 1 and 2.

The phenotypic profile of MNCs was also analyzed, as a control, to see the shift of the phenotypic marks with the differentiation protocol process. All four ligands changed their expression in the five days culture of UCB cells B and have a dramatic change in the final profile of UCB cells A. CD31, CD34, CD45 and CD14 showed to have expression values of

81.6%, 4.24%, 95.1%, and 20.5%, respectively (data not shown). The two UCB cell types A and B were also characterized by immunocytochemistry for different endothelial cell markers, namely CD31, VE-cad, and ac-LDL uptake (**Figure 13B)**. The UCB cell population A presented only a few cells stained for CD31, some ac-LDL uptake and were negative for VE-cad, while UCB cell population B were positive for CD31, showed ac-LDL uptake, but had little expression of VE-cad. In terms of CD31 expression, these results are in accordance with the flow cytometry results, with UCB cells A being negative and UCB cells B being positive.

Once again, UCB cells B expressed some ECs markers as described by other authors, while UCB cells A did not, since they should express CD31 in a great extent (*39, 44-49*). The morphology of UCB cells A and UCB cells B was also characterized by phase contrast microscopy. As depicted in **Figure 13A,** UCB cells A formed colonies, a feature described for OECs isolated by Silva *et al* (*163*) and had an elongated, fibroblast/mesenchymal-like shape, while UCB cells B presented a round shape and some were organized as multicellular agglomerates in certain regions of the well. The morphology of UCB cells A was another unexpected result. In fact, OECs are described as presenting a cobblestone-like morphology colonies that when isolated maintain the cobblestone-like morphology, similar to mature ECs. In contrast, UCB cells B have a morphology similar to that described for er-EPCs, being smaller and presenting a round shape (*38*).

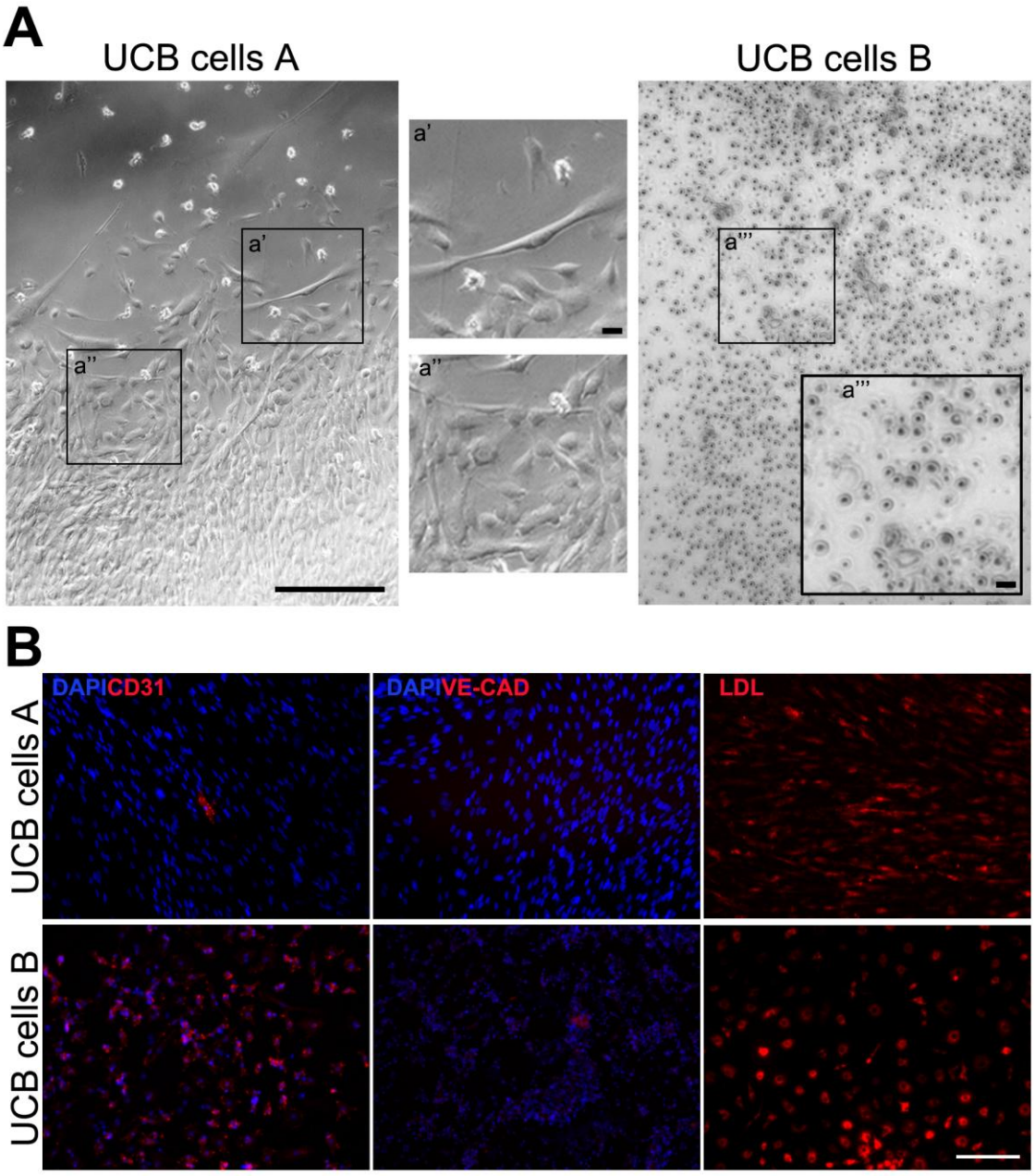

Figure 13 – UCB cells A and B morphologic and phenotypic characterization. (A) Contrast phase images of UCB cells A and B (scale bar: 100 μm). **a'** inset showing an UCB cell A with fibroblastic-like morphology in the periphery of a colony (scale bar: 10 μm). **a''** inset showing UCB cells A with a less elongated morphology (scale bar: 10 μm). **a'''** inset showing UCB cells B with round-shape (scale bar: 10 μm). **(B)** Immunocytochemstry of UCB cells A and B stained with primary antibodies for CD31 and VE-Cadherine, and Ac-LDL uptake (all in red). Nuclei stained with DAPI (in blue) (scale bar: 100 μm).

Taken together, these results lead us to conclude that UCB cells B have apparently differentiated as expected, according to what is described in the literature, including by Silva *et al* (*163*), resembling er-EPCs. In contrast, the UCB cells A population seems to be a heterogeneous population, presenting a few endothelial-like cells, but being mainly constituted by mesenchymal-like or fibroblastic-like cells.

2. 3D cocultures of HUVECs and MSCs

Our team has previously shown that MSCs in monoculture with 8 million/mL of cellular density were capable of producing their own ECM when cultured within RGD-alginate hydrogels with an optimized formulation (alginate 1% v/w with a ratio of 50:50 of HMW and LMW, with 200 μM of RGD (*90*)). Later, studies on how HUVECs and MSCs interact with each other in 3D, when cultured in the same RGD-alginate hydrogels, where performed. Joana Bianchi's thesis explored the cross-talk between these two cell types and described that when HUVECs and MSCs are both at 5 million/mL of cellular density in coculture within RGD-alginate hydrogels, they present higher metabolic activities and less cell death compared to both monocultures (5 million/mL of cellular density each). Moreover, their spatial rearrangement also changes when together. In coculture, these cells were able to significantly contract the hydrogel matrix, and to adopt some polarization of the actin filaments, with a superimposed mesh of Fn. Possibly, these changes were able to enhance HUVECs survival and drive them to form tubular structures in 3D, as observed by Bianchi's work (unpublished results).
Here, it was important to understand in more detail if MSCs were actually influencing HUVECs survival or if this effect would be only due to the increase of the cellular density (10 million/mL for the coculture and 5 million for monoculture in Bianchi's studies). Another important aspect to address was the culture time. Bianchi's results were obtained after only 1 and 3 days of culture, but it was important to know if the HUVECs survival and functionality could still be maintained after longer periods of time. In terms of a delivery system, the survival of cells along time is extremely important for a good therapeutic outcome. Following these questions, HUVECs and MSCs monocultures at 10 million/mL and HUVEC+MSC coculture at the same total density were established and maintained for 7 days in culture, being monitored at different levels.

The metabolic activity of cells entrapped in alginate hydrogels was assessed at days 1, 3 and 7. **Figure 14A** shows the metabolic activity values for 3D cultures of MSCs and HUVECs monocultures (10 million cells/mL), and HUVEC+MSC cocultures (10 million cells/mL of total density, each cell type at 5 million/mL), and also a theoretical value, corresponding to the sum of 50% of the values obtained with each monoculture.
The metabolic activity of HUVECs in monoculture decreases along the time, showing that these cells do not survive well under the 3D conditions established in this study. A drop in the metabolic activity of HUVECs monocultures at 5 million/mL had already been shown in Bianchi's thesis after 3 days of culture. Here, even if the cell density has been raised to 10 million/mL, no significant improvements were detected, and very low values of metabolic activity were still observed day 7. In previous studies from Bidarra *et al* (*124*), HUVECs were cultured at 20 million/mL within similar hydrogels, and their viability only dropped 10% along 2 days in culture, suggesting that in future studies higher cellular densities should be explored. In what concerns MSCs monocultures, their metabolic activity was higher than that

of HUVECs at day 1, and it was maintained essentially unchanged along the 7 days of culture. The opposite trend was reported in Bianchi's work, where MSCs metabolic activity decreased along the 3 days of culture. Most likely, this difference can be again explained by the cellular density used. Maia *et al* (*90*) used 8 million/mL as cellular density that is very close to 10 million/mL used here. However, in Bianchi's work, the cellular density used was 5 million/mL. In previous studies with MSCs, our group has demonstrated that higher cellular densities enhance MSCs activity in 3D, favoring cell-cell aggregation and production of endogenous ECM (*112*). Regarding the HUVEC+MSC coculture system, the metabolic activity slightly decreased from day 1 to day 3, being higher than the theoretical value. However, it decreased from day 3 to 7, reaching a value slightly below the theoretical level. Although it is not possible to discuss these differences in detail, as the values have not been normalized to the cell number, these results suggest that cells in coculture present acceptable levels of metabolic activity.

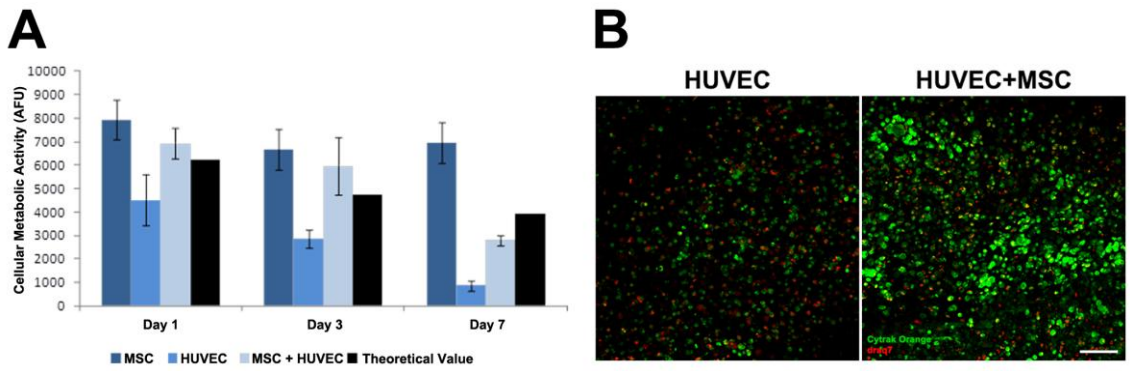

Figure 14 – Metabolic activity and viability of HUVECs and MSCs in 3D cultures. (A) Metabolic activity assessed at day 1, 3 and 7 of culture of HUVECs and MSCs monocultures and HUVEC+MSC cocultures. The theoretical value expected for the cocultures is also presented (black bar). **(B)** Cellular viability at day 3 of HUVEC+MSC and HUVECs alone assessed by LIVE/DEAD assay (cytrak orange in green (LIVE) and draq7 in red (DEAD)) (scale bar: 100 μm).

Figure 14B shows that the overall cellular viability was enhanced in HUVEC+MSC cocultures as compared with HUVECs monocultures. At day 3, it was possible to see that there were less dead cells (red) in cocultures as compared with HUVECs monoculture, where the number of dead cells was very high. This was also seen in Bianchi's results and it was expected, since in the coculture system half of the cells are MSCs, which survive better in this type of 3D microenvironment contributing to an increase of the total cellular viability.

At the macroscopic level (**Figure 15**), it was clear that a re-organization of cells rapidly occurred in the coculture system, as suggested by the contraction of the hydrogel matrix along the first 72 h of culture.

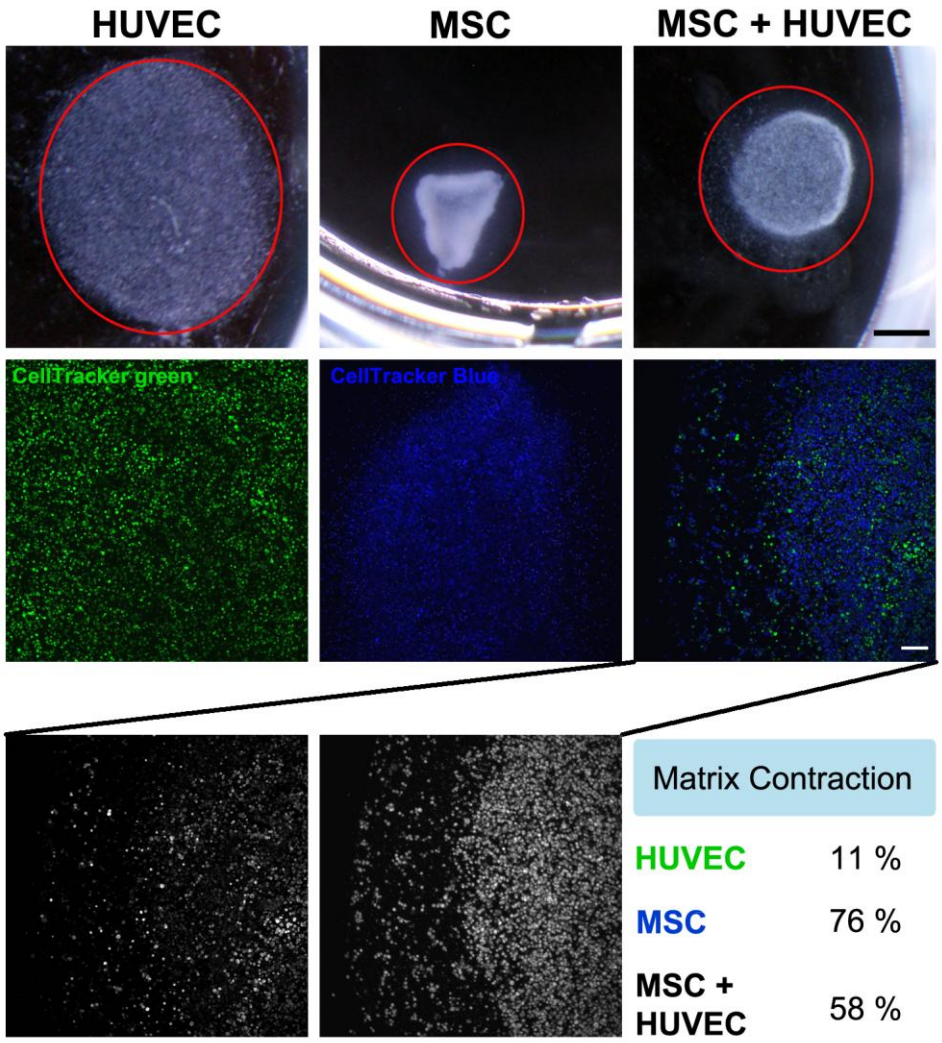

Figure 15 – Spatial re-organization of HUVECs and MSCs in 3D cultures. Images of the hydrogel matrices after 3 days in culture (red circles limiting disks periphery, scale bar: 500 μm) showing alterations at the macroscopic level (matrix contraction) and respective microscopic cellular organization (HUVECs labeled with cell tracker green® and MSCs with cell tracker blue®). Separate channels of coculture conditions show different cell migration pattern (grey scale) (scale bar: 100 μm). Matrix contraction is also presented in terms of percentage of contraction relatively to the original value.

This effect was probably mostly driven by the MSCs, as the same behavior was detected in MSCs monocultures but not in HUVECs monocultures. To better understand the contribution of each cell type to the disk's changes, MSCs were labeled with cell tracker blue™ and HUVECs with cell tracker green™. In fact, in the coculture, it is possible to see that MSCs (in blue) migrated towards the center of the disk and are closer to each other when comparing with HUVECs (in green), confirming our hypothesis. This can be even more clearly seen in the separated channels image (grey scale) that better depict the behavior of each cell type in terms of migration/aggregation. A high level of cell-cell aggregation, and matrix contraction, was also detected in MSCs monoculture, where cells also migrated to the center of disk forming a multicellular aggregate. In this case, the level of matrix contraction was even higher than that observed in the coculture system, as seen in **Figure 15**. This difference can

be explained by the number of MSCs, which was lower in coculture conditions. As suggested by previous results from our group (*90*), this cell migration towards the center of the disk creates a new microenvironment that certainly has an impact in HUVECs behavior. In particular, this process has been shown to be accompanied by the deposition of a Fn mesh, forming a microtissue (*90*). As already demonstrated, this effect is highly dependent on the viscoelastic properties of the hydrogel, occurring only within very soft matrices as the ones used in this study, and on the cellular density (*112*) (Neves *et al*, 2014, submitted). In HUVECs (in green) monocultures this phenomenon did not occur. Disks maintained the original size and cells remained dispersed throughout the matrix.

When cultured together, HUVECs and MSCs formed some clusters of cells within the hydrogel at day 1 that were not seen neither in HUVECs, nor in MSC monocultures (**Figure 16**). At day 3, the differences between the different formulations were even more pronounced. The morphology and distribution of HUVECs remained similar to that observed at day 1, showing a lack of cellular reorganization. In the coculture system, it was possible to see a complex structure that seemed to be growing outward the disk center, composed mainly of HUVECs (in green), suggesting that HUVECs are capable of re-organizing themselves within the hydrogel matrix. Unfortunately, these structures could no longer be detected at day 7 (data not shown), suggesting that their stability *in vitro* was lost after a certain period of time. In **Figure 14B**, it was seen that the overall cell viability was higher in coculture than HUVECs in monoculture, but it was not possible to distinguish between the two cell types. However, in this assay, a viability dye (DRAQ7, which do not permeates intact cell membranes) has been used in conjunction with the two cell trackers allowing a more detailed analysis of cellular viability. For MSCs, it seems that cell death was almost equal for monoculture and coculture. However, HUVECs showed some changes in cell viability. At day 1, in HUVECs monoculture, a great percentage of cells are dead or with compromised viability, contrasting with cocultures, where a lower percentage of HUVECs showed DRAQ7 permeation, particularly within the cell clusters. The same trend was also seen at day 3, where some HUVECs are stained in red, but not those within the multicellular structures. Thus, the coculture with MSCs seemed to contribute to the enhancement of HUVECs survival and function.

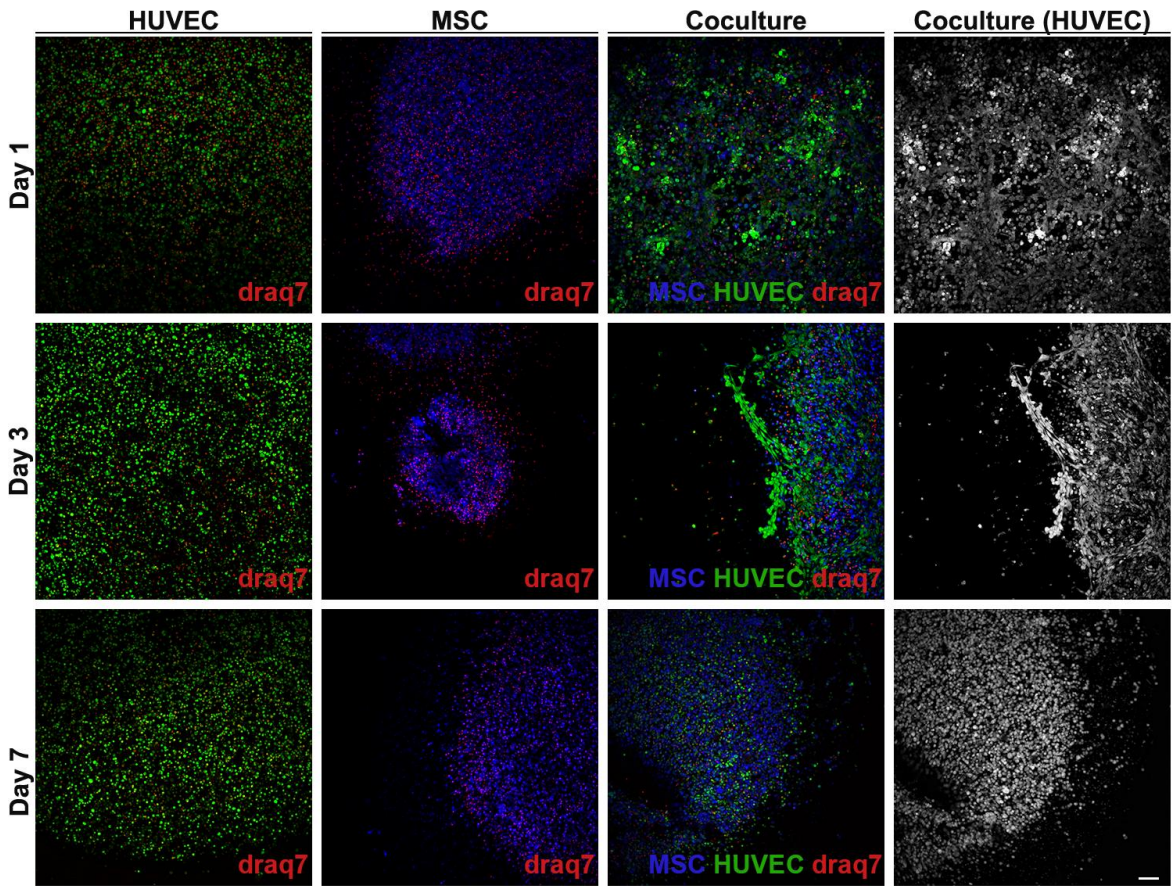

Figure 16 - Cellular re-organization in 3D. Confocal microscope images of HUVECs, MSCs and HUVEC+MSC cultures at days 1, 3 and 7. HUVECs were labeled with cell tracker green, MSCs with cell tracker blue, and Draq7 was used to detect dead cells. (scale bar: 100 μm)

The spatial cellular reorganization detected at day 3 was analyzed in more detail by labeling ECs with ac-LDL (**Figure 17**). In this way it was possible not only to detect HUVECs inside the disks, but also to address their functionality. When cocultured with MSCs, HUVECs form clusters inside the disk, detected by the intense levels of fluorescence at well-defined spots (**Figure 17A**). It was also possible to detect some tubular-like structures, often coming out from these clusters, showing that HUVECs, in the presence of MSCs, are able to reorganize and maintain functionality. In a higher magnification (**Figure 17A**), it is possible to see the alignment of HUVECs forming these tubular-like structures and their distribution in the z-axis, forming a three-dimensional network (**Figure 17B**). **Figure 17** also shows that MSCs (in blue) are in close contact with HUVECs.

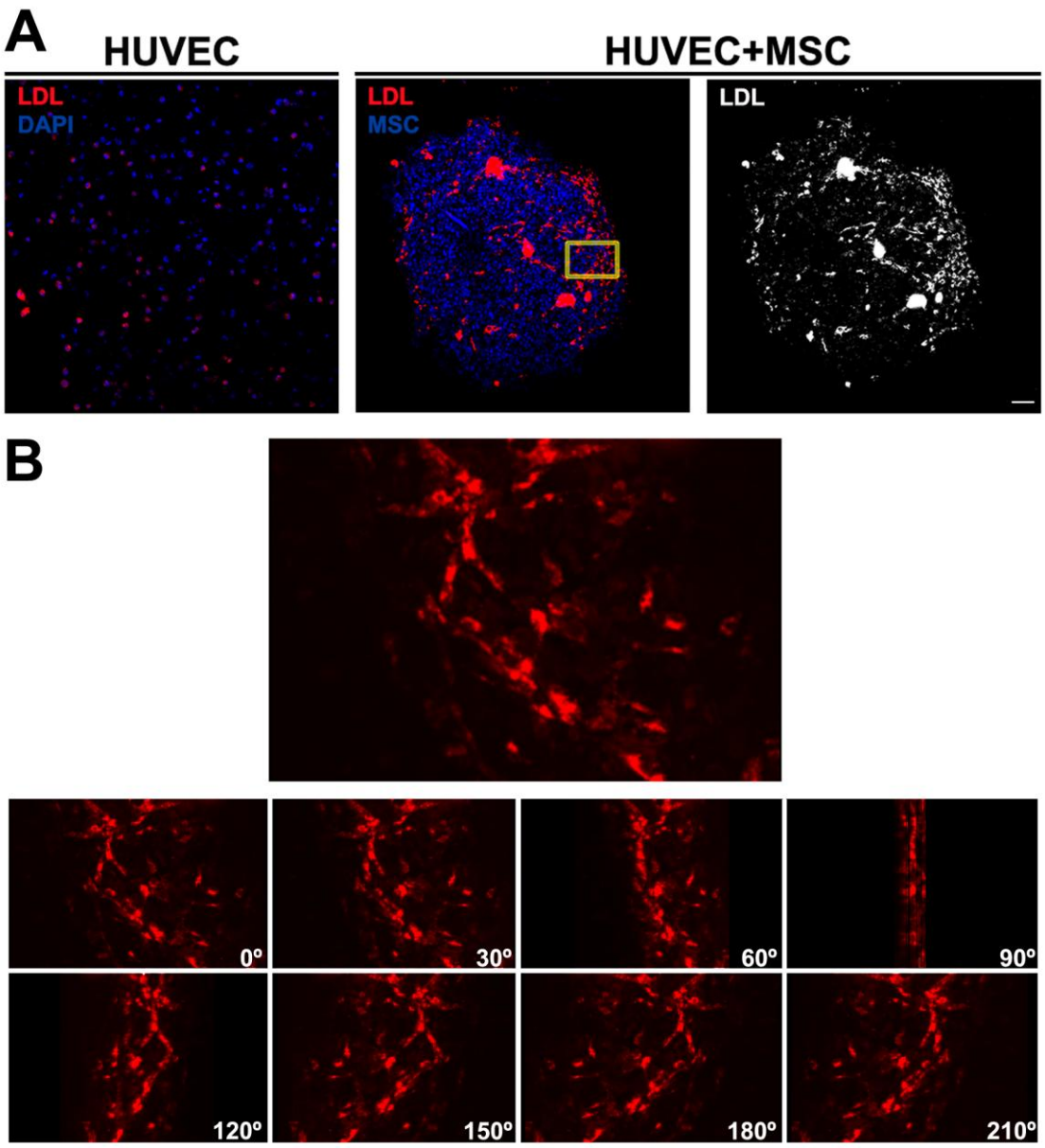

Figure 17 - HUVECs 3D arrangement and functionality. (A) Ac-LDL uptake and organization of HUVECs in monoculture and coculture at day 3. In monoclutures nuclei appear in blue (DAPI) and HUVECs in red (ac-LDL), in cocultures, MSCs appear in blue (cell tracker blue®) and HUVECs in red (ac-LDL) (scale bar: 100 µm). **(B)** Higher magnification images showing of aligned HUVECs aligned into tubular like structures in close proximity with MSCs. (scale bar: 10 µm)

Although they appear to exert a benefic effect over the cocultured HUVECs, the exact role(s) of MSCs remain unclear. As shown, MSCs promote HUVECs function, somehow providing them with cues that promote their assembly into organized structures. In the literature, MSCs have been described as mural cells that support other cellular types like HSCs, contributing for the bone marrow stem cell niche (*168*).

As mural cells, MSCs are known to produce ECM matrix and growth factors that stimulate, help, and respond to ECs (*169*). Fn is one of the most important proteins having a crucial role

in angiogenesis (*103*). Normally, ECs interact with a basement membrane rich in laminin, but when an angiogenic stimulus occur, Fn interact with ECs, working as a provisional matrix that is going to mediate proliferation and migration of ECs (*170-171*). Indeed, in a previous study from our group, Bianchi *et al* demonstrated that MSCs are able to assemble a Fn-rich network inside soft alginate hydrogels, both in monoculture and in coculture with HUVECs, which probably has a key role in promoting the organization of ECs into tubular-like structures.

MSCs have been also shown to be implicated in the stabilization and support of blood capillaries, acting as PCs or PVCs (*83, 172*). Indeed, some authors defend that all MSCs are PCs and contribute for the formation of new vasculature (*71*). It has been shown that PCs express the same markers as MSCs, and are able to differentiate into the three lineages related with MSC: osteogenic, chondrogenic and adipogenic lineages, showing that PCs are multipotent cells (*71*). These PCs that share a phenotypic profile with MSCs are found in the vasculature of all tissues in the body. Crisan *et al* (*71*) have explored the presence of these cells in human skeletal muscle, pancreas, placenta, white adipose tissue, heart, skin, lungs, among others, and all shared the same phenotypic markers. Indeed there are many evidences that PCs and MSCs are closely related or are the same cell. However it is not quite obvious if PCs come from MSCs, or if PCs are the cells less differentiated that can differentiate into MSCs. Not only these cells are found in the vasculature of tissues, but they are known to participate in the regeneration of wounded tissues, as MSCs are too (*71*). Here, we analyzed the expression of α-SMA, often considered as a PCs and PVCs marker (*72, 173*). As shown in **Figure 18**, MSCs are in fact expressing α-SMA. Some MSCs with spread-shape morphology that resemble that of PCs/PVCs-like cells were also detected, even if we were not able to detect them co-localizing with ECs structures. Although further studies have to be conducted to draw a convincing conclusion, these results suggest that MSCs in the coculture system might actually be acting as PCs/PVCs-like cells. However, this seems to be insufficient for the maturation of the ECs tubular structures, given that these were no longer detected after 7 days.

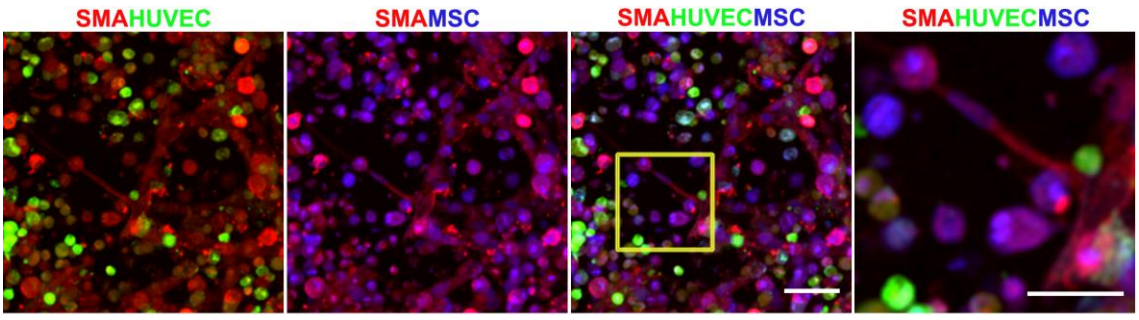

Figure 18 - MSCs functional behavior as PCs/PVCs cells in 3D. Immunocytochesmitry of α-SMA in cocultures of HUVECs (at green) with MSCs (at blue) at day 3 (scale bar: 100 μm). Inset (from the yellow square) showing a MSC with spread-shape morphology colocalizing α-SMA (scale bar: 10 μm).

3. 3D cultures of UCB Cells A and MSCs

Although we have been unable to fully characterize the phenotype of UCB cells A, we have decided to investigate the behavior of these cells in our 3D culture system, both in monoculture and in coculture with MSCs. After entrapment within the hydrogel, the metabolic activity of these cells was assessed after 4 hours, and at days 1, 2 and 3 (**Figure 19**).

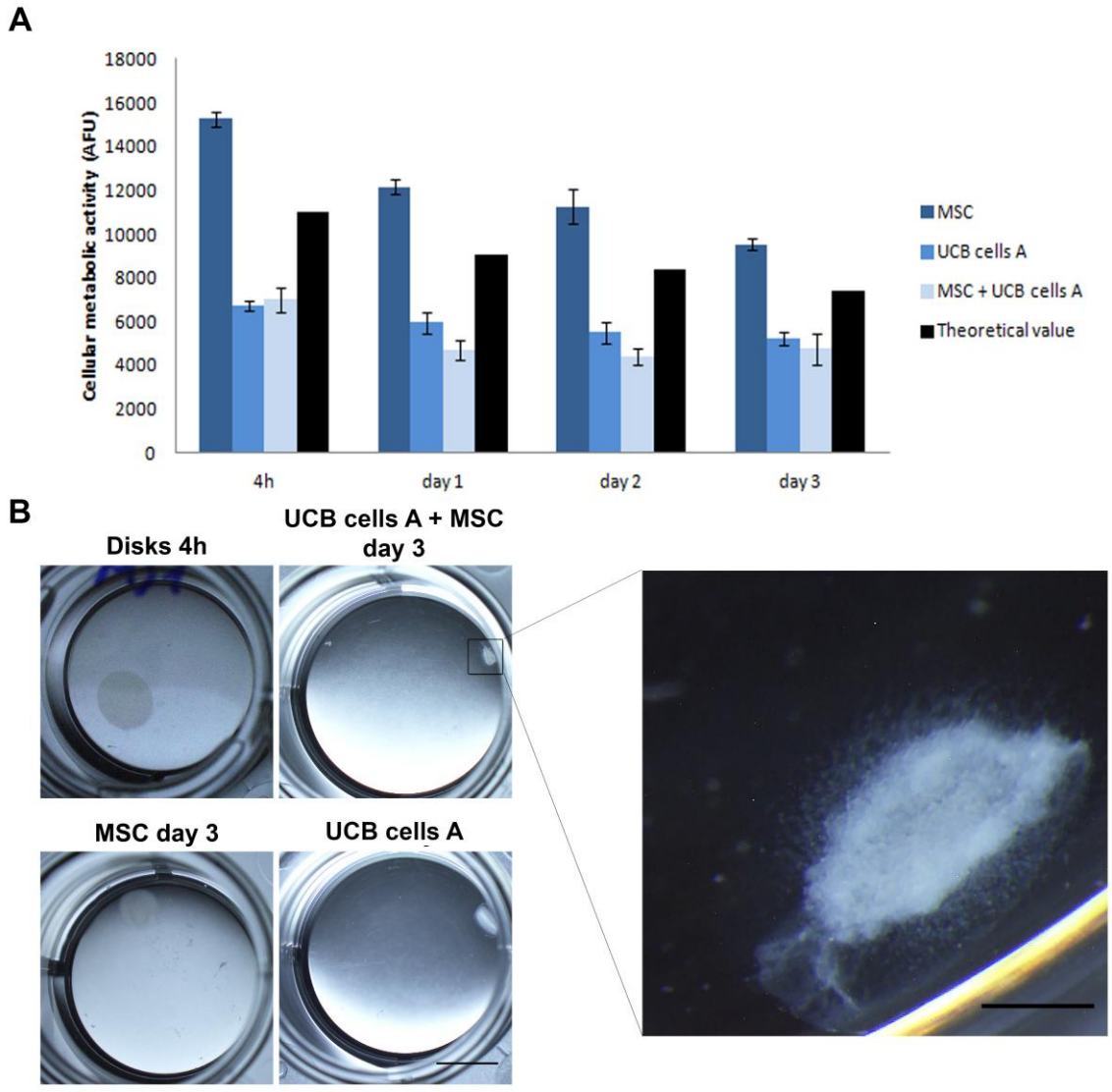

Figure 19 – Cellular metabolic activity and macroscopic organization of UCB Cells A and MSCs in 3D. (A) Metabolic activity of MSCs and UCB cells A in monocultures and in UCB cells A+MSC colculture after 4 h, and 1, 2 and 3 days after embedding. The theoretical value for the coculture is also represented in the graph in the black bar. **(B)** Macroscopic changes after 3 days in culture (scale bar: 500 μm). UCB cells A +MSC are depicted in a higher magnification at right (scale bar: 100 μm).

As depicted in **Figure 19A**, and in contrast with that observed for HUVECs, UCB cells A, were able to survive well in a 3D environment. Despite the slight decrease in metabolic activity observed after the first 24h, which is probably related with the embedding process and the adaptation of the cells to the new environment, UCB Cells A presented constant levels of metabolic activity until day 3. The same was observed in MSCs cultures, similarly to what had been previously shown in **Section 2**, and in the UCB cells A+MSC coculture. Yet, the theoretical value was always higher than the coculture value. As depicted in **Figure 19B**, which shows the macroscopic appearance of the disks after 3 days, extensive matrix contraction occurred in all conditions, including UCB-derived Cells A, which is a striking difference compared to the behavior of HUVECs. This result shows that these cells are able to exert traction/pulling forces in the matrix, which is a common feature of mesenchymal- and fibroblastic-like cells. The contraction of the coculture disks was higher than that of each individual monoculture, suggesting that both cell types are acting synergistically. So, effectively, UCB Cells A seem to behave more as mesenchymal or fibroblastic-like cells than as endothelial-like cells, as previously noticed.

In contrast with what was seen with MSCs monoculture, where the traction/pulling forces lead to the formation of a spherical mass at the center of the disk, UCB cells A in monoculture formed a more complex structure, with an elongated shape, that crossed the center of the disk from one edge to the other (**Figure 20**). This structure seemed to be quite well organized in terms of cellular alignment, with cells exhibiting actin filaments assembled with a specific orientation, while the cells outside this structure lack actin filaments organization. As it was described in **Section 1**, UCB cells A in 2D seem to have some ability to uptake ac-LDL. In 3D, some ac-LDL uptake was also detected, along with the expression of the ECs marker vWF, which was detected at very low levels at day 3. However, the expression of CD31 was not detected, similarly to that previously observed in 2D. So, strikingly, UCB cells A present a behavior that is similar to mesenchymal-like, fibroblastic-like cells or even SMCs, all of which have been already isolated from UCB (*174-175*), but concomitantly express, even if at low levels, some endothelial markers that are not characteristic of those cell types.

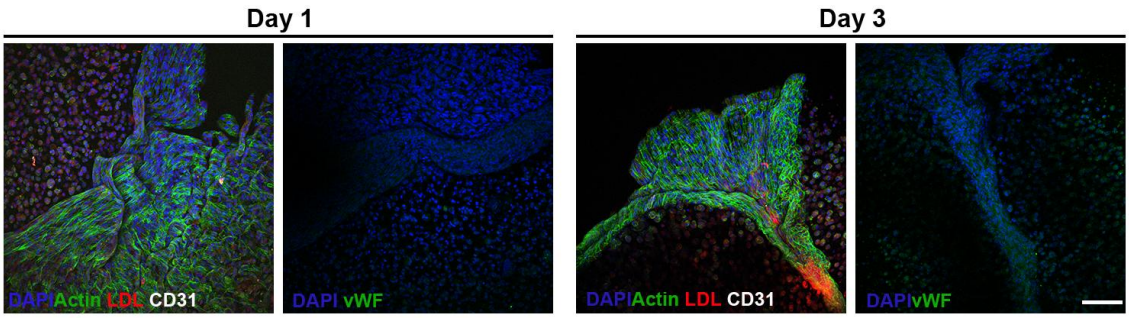

Figure 20 – UCB cells A phenotype and rearrangement in 3D. CLSM images of cell-laden hydrogel disks immunostained with primary antibodies for vWF, actin and CD31, and marked with ac-LDL uptake, at days 1 and 3 (scale bar: 100 μm).

In UCB cells A+MSC coculture, and as depicted in **Figure 19B,** some multicellular structures are growing outwards the center of the disk. These can be more easily observed in **Figure 21**, which shows the development of these structures in more detail, at days 1 and 3 of culture.

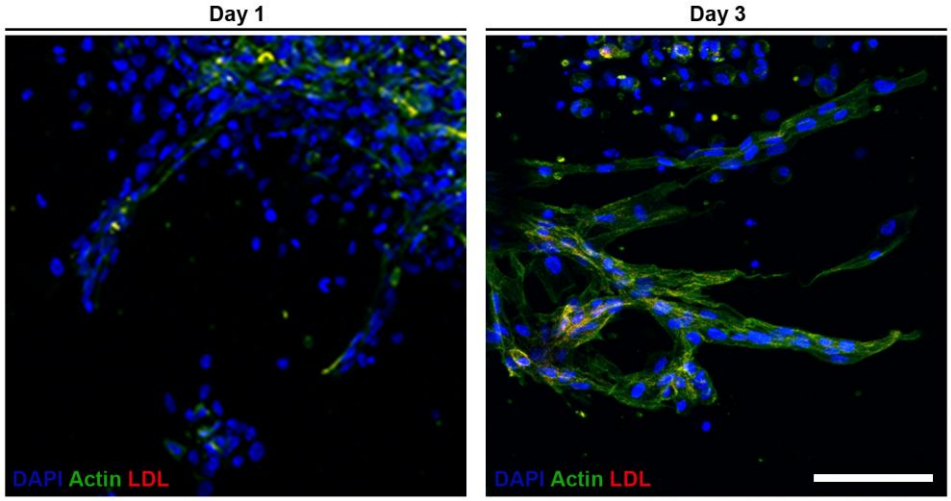

Figure 21 – UCB cells A and MSC cocultures: phenotype and rearrangement in 3D. CLSM images of cell-laden hydrogel disks immunostained for actin and labeled for ac-LDL uptake at days 1 and 3 (scale bar: 100 μm).

Actin staining shows that cells started aligning thus adapting their cytoskeleton to these organized structures. However, only at day 3 it was possible to detect cells with actin filaments with a specific orientation and cells arranged as multicellular structures, incorporating some ac-LDL-positive cells. Interestingly, such sprouting structures where not seen in UCB cells A or MSC monocultures (data not shown). So, it seems that the cross-talk between the two cell types promoted their formation. However, further characterization of UCB cells A both in 2D and in 3D has to be performed using complementary assays in order to better characterize these cells, and also to rule out the possibility of occurrence of technical artifacts.

4. 3D cultures of UCB cells B/HUVECs and UCB cells B /HUVECs/MSCs

In a 3D coculture microenvironment even if er-EPCs are not able to form vessels, they might secrete the appropriate factors (*37*) that will in turn stimulate ECs to form tubular-like structures.

Here, UCB cells B, which resemble er-EPCs, were cultured alone and in coculture with HUVECs and their metabolic activity was monitored along time (**Figure 22**). The metabolic activity of UCB cells B in monoculture decreased along the culture time, similarly to what has been observed for HUVECs, suggesting that these cells have a low survival rate when cultured alone in a 3D microenvironment. Moreover, they do not seem to contribute for HUVECs survival when in coculture, since, in this case, the metabolic activity in the coculture system also significantly decreased along the time.

These results can possibly be explained by the lack of newly-formed matrix. In the case of MSCs+HUVECs it was seen that MSCs enhance HUVECs survival, in part by producing Fn and probably other ECM proteins that apparently contribute to maintain HUVECs survival and function (Bianchi's thesis). In the absence of MSCs and their secreted ECM, HUVECs viability and metabolic activity in 3D are compromised. Thus, even though EPCs might secrete important factors that would be capable of enhancing HUVECs survival in 2D, this might be insufficient in such 3D environment.

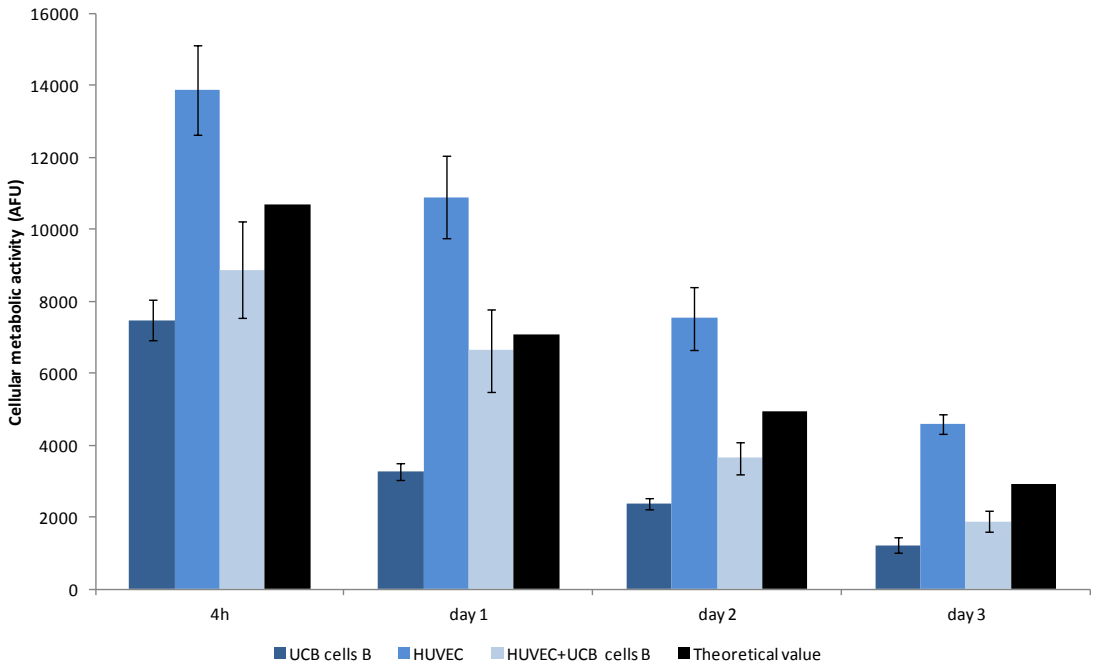

Figure 22 - Cellular metabolic activity of UCB cells B. UCB cells B and HUVECs in monocultures and of UCB cells B+HUVEC coculture after 4 h, and 1, 2 and 3 days after embedding. The theoretical value for the coculture is also represented in the graph (black bar).

Although we did not see any positive effect of UCB cells B in cocultured HUVECs, we decided to investigate if these cells could eventually display any synergistic effect in HUVEC+MSC cocultures, by promoting, for example, the formation and/or stabilization of ECs tubular structures. In fact, Burlacau *et al* (*176*) described that MSCs and er-EPCs have complementary paracrine effects on ECs. In particular, while MSCs support ECs adhesion, but not proliferation, EPCs promote proliferation, but do not sustain ECs adhesion.

Figure 23A shows the metabolic activity of MSC+HUVEC+UCB cells B triple-cultures along time. Although there was a significant decrease in metabolic activity after the first 24h in culture (-39%), from day 1 to day 2 the decrease was only -4% and from day 2 to day 3, there was no further decrease. This trend was not observed in either MSCs or HUVECs monocultures. As seen before, HUVECs presented higher cell death, while MSCs tend to have a high metabolic activity, but presented a higher decrease along the culture, namely ca. 14% between days 2 and 3. These results suggest that UCB cells B had a positive impact on the cells metabolic activity and survival in the triple-culture system. Even though MSC+HUVEC+UCB cells B do not have values higher than the theoretical value, it was the only condition presenting a rather constant metabolic activity over time.

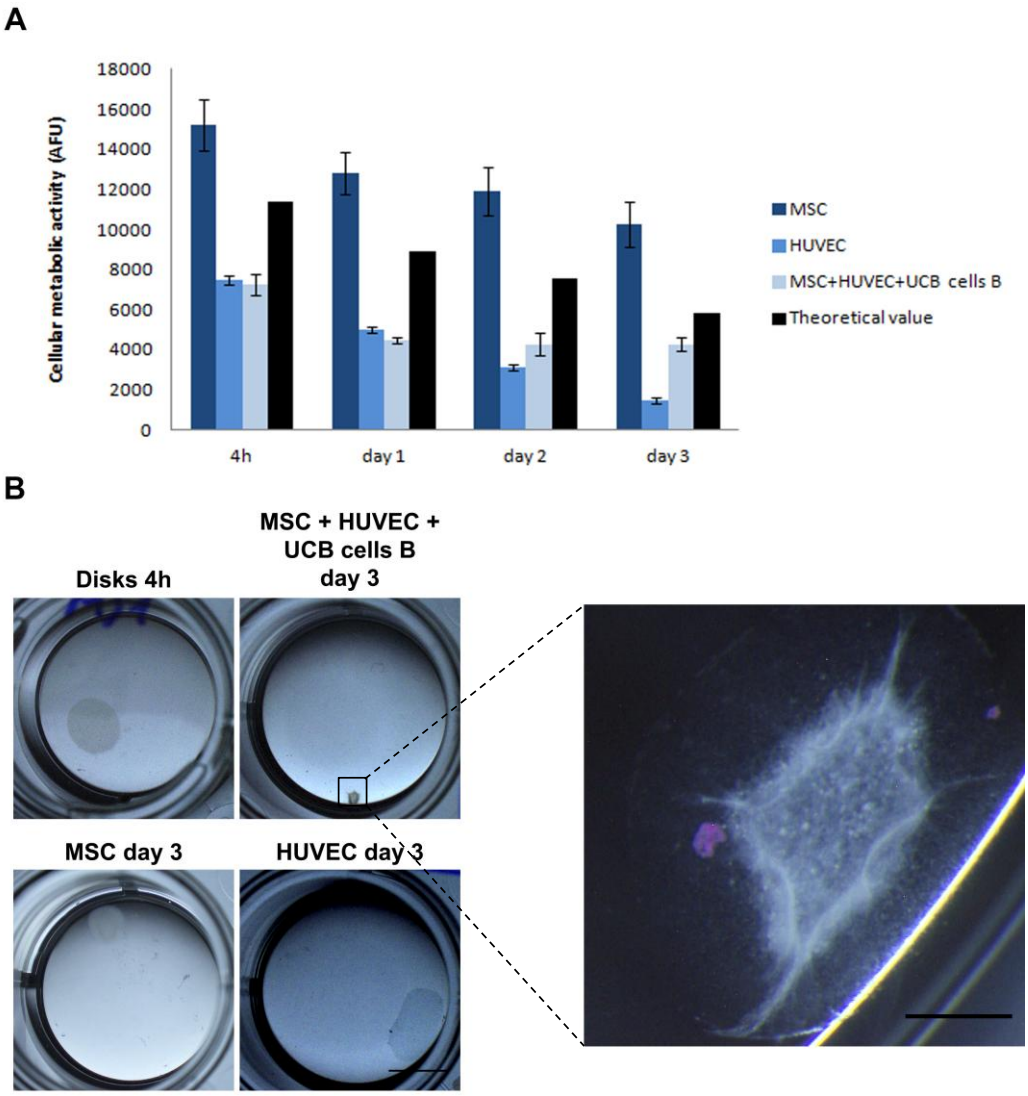

Figure 23 – Cellular metabolic activity and macroscopic organization of UCB Cells B, MSCs and HUVECs in 3D. (A) Metabolic activity of MSCs and HUVECs in monocultures and in UCB cells B+MSC+HUVEC triple-culture after 4 h, and 1, 2 and 3 days after embedding. The theoretical value for the coculture is also represented (black bar). **(B)** Macroscopic changes after 3 days in culture (scale bar: 500 μm). UCB cells B+MSC+HUVEC are depicted in a higher magnification at right (scale bar: 100 μm).

As depicted in **Figure 23B**, an extensive contraction of the hydrogel matrix was observed in the triple-culture, which was even higher than the contraction of MSCs monoculture disks. The presence of organized multicellular structures sprouting from the center of the disk could be observed at higher magnification (on the right). Since such dramatic changes were not previously observed in HUVEC+MSC cocultures, it is reasonable to assume that UCB cells B played a role on this process. In fact, Shi *et al* (*177*) described that when er-EPCs were triple-cultured with MSCs and OECs, the formation of prevascular structures at early stages of culture was enhanced, showing that er-EPCs have a synergistic effect in ECs-MSCs crosstalk, promoting ECs function.

Since CD45 is expressed by UCB cells B, but not by MSCs, nor HUVECs, this marker was used to distinguish between UCB cells B and other cells. **Figure 24A** shows that UCB cells B were widely distributed in the disk and in close proximity with the other cells, which is a relevant feature as it will certainly facilitate any paracrine effect that they might have over the other cells, particularly HUVECs. Indeed, the same effect was described for triple-cultures of MSCs, OECs and er-EPCs (*177*). Er-EPCs were found to be closely associated with angiogenic structures (in the tip or around vascular structures), suggesting their active role in the formation of vascular structures that can indicate the tight paracrine relation that er-EPCs can exert on ECs and MSCs (*177*).

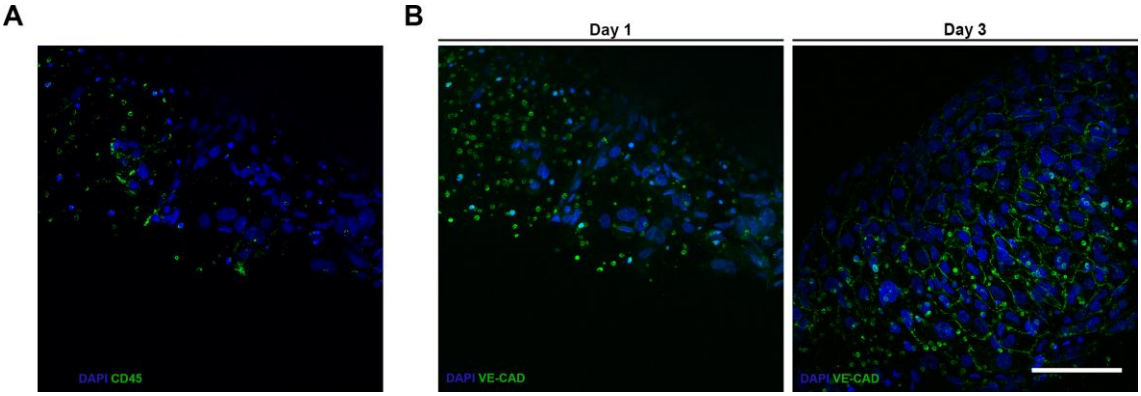

Figure 24 – 3D spatial rearrangement of cells in a UCB cells B+MSCs+HUVECs triple-culture. (A) Imunnocytochemistry of CD45 with DAPI at day 1 f culture **(B)** Imunnocytochemistry of VE-cad marked with DAPI at day 1 and 3 of culture (sacle bar: 100 μm).

To investigate HUVECs organization and functionality in the triple-culture system, the expression of VE-cad was analyzed, as this is an important EC marker implicated in the cohesion and organization of intercellular junctions, being indispensable for proper vascular development. **Figure 24B** shows that cells at day 1 did not present a specific organization and expressed low levels of VE-cad at the cell membrane. At day 3, however, VE-cad was expressed at the cell membrane in a network of ECs, confirming the tight interaction between them.

The EPC+HUVEC+MSC triple-culture was also stained for α-SMA expression at days 1 and 3 of culture (**Figure 25**). At day 1, the disks presented a lack of cell organization, but some α-SMA expression (in white) was detected throughout the disk, suggesting a homogeneous distribution of MSCs. Yet, α-SMA filaments were not fully organized, and did not display any specific orientation.

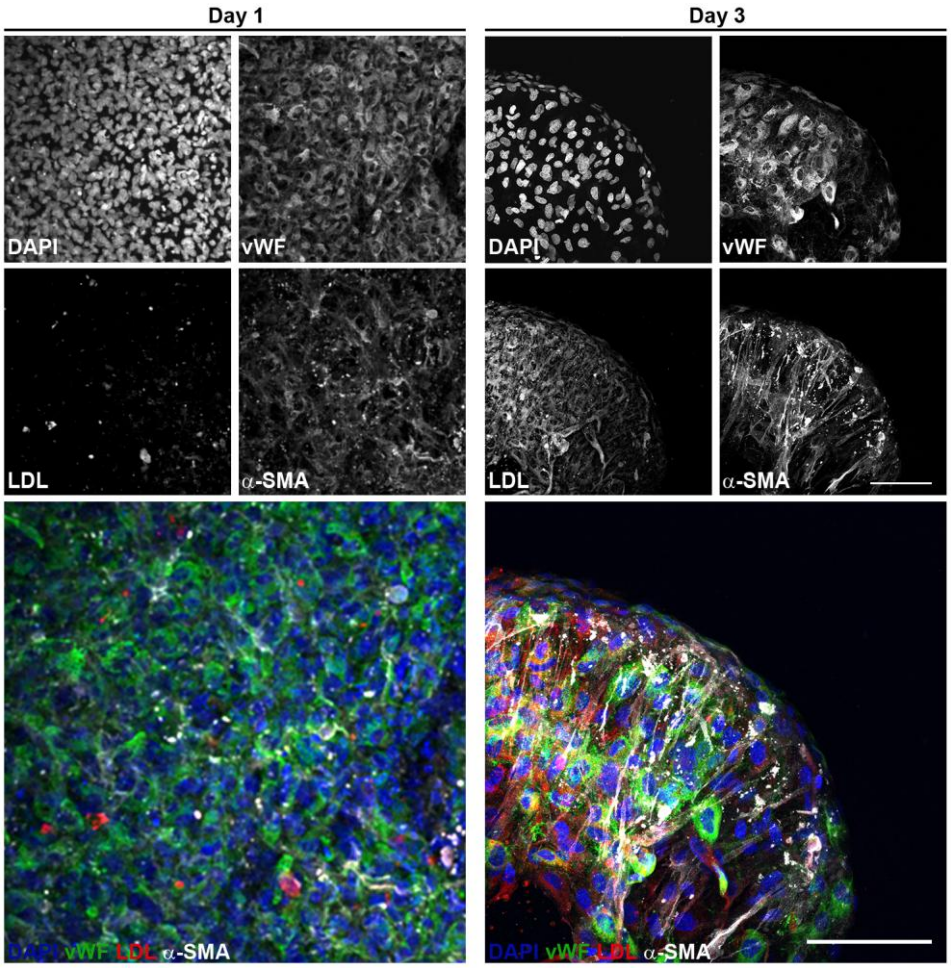

Figure 25 – UCB cells B, MSC, and HUVEC triple-culture 3D rearrangement. Imunnocytochemistry of vWF and α-SMA marked with DAPI and ac-LDL uptake at day 1 and 3 of culture (sacle bar: 100 μm).

However, at day 3, α-SMA filaments showed some alignment, and were in close proximity of cells that uptake ac-LDL and were positive for vWF expression – two major endothelial markers – which may indicate that MSCs were interacting with HUVECs.

Although the images have been obtained at the disks surface, the sprouting structures seen in **Figure 23B** (inset at higher magnification) were not possible to detect. During culture time, with the shrinking and reorganization of the disks, they fold under themselves, which posed some technical problems that unable the imaging of those structures. Even though, the new system described herein, which explores the cross-talk between HUVECs, MSCs and UCB cells B (that presumably are er-EPCs) might be potentially interesting for pro-angiogenic therapies.

Results and Discussion – Part II - Bioprinting of alginate-based bioinks

1. Rheological characterization of alginate solutions

The LAB technique is highly dependent of bioink's viscosity. The higher the viscosity, the higher the inertia felt by the solution during bubble formation. In order to overcome that extra inertia, more energy power has to be used. In what concerns the bioinks tested here, and as depicted in **Figure 26**, the viscosity of 2% (w/v) alginate solutions was higher than that of 1% (w/v) solutions, as expected. Also, the viscosity seemed to increase with the cell density. This may be explained by the presence of cells within the hydrogel, which behave like "particles" contributing to the viscous properties of the solution, as previously seen in other studies (*159*).

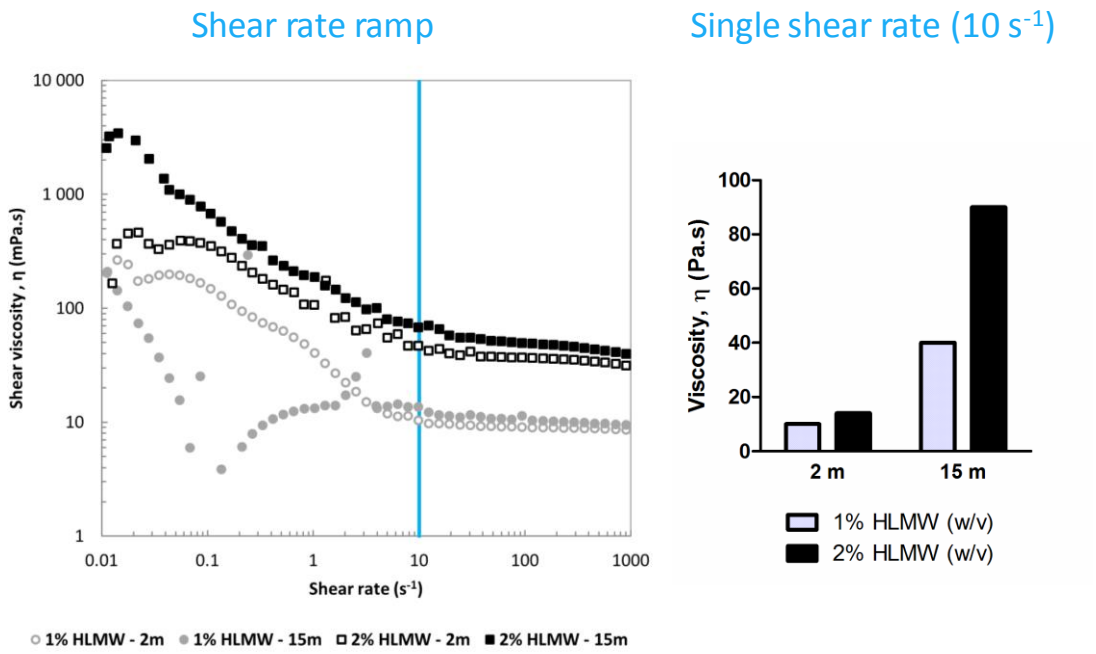

Figure 26 – Viscosity analysis. Viscosity of 1% and 2% (w/v) alginate solutions containing $CaCO_3$ and MSC at two different densities (2 and 15 million/mL). Left: Shear rate ramp; Right: single shear rate analysis.

2. Printing behavior of alginate solutions

In order to test the printability of alginate solutions; a preliminary assay was carried out using the 2% (w/v) alginate solution, since this solution was the most viscous one and would be in principle the most difficult to print. So, the laser conditions were initially tuned and analyzed with this formulation. A thickness of 20 µm was chosen for the solution layer, along with a standard laser energy of 28 A. As it is possible to see in **Figure 27**, all the expected printing steps occurred (*153*), namelly: 1) bubble formation (3 µs), 2) bubble collapsing (5 µs), 3) jet forming (10 µs), and 4) landing (50 µs). All the steps occurs within just 800 µs, showing not only that the tested alginate formulation was printable, but also that the printing process progressed in a HT manner, in less than 1 ms.

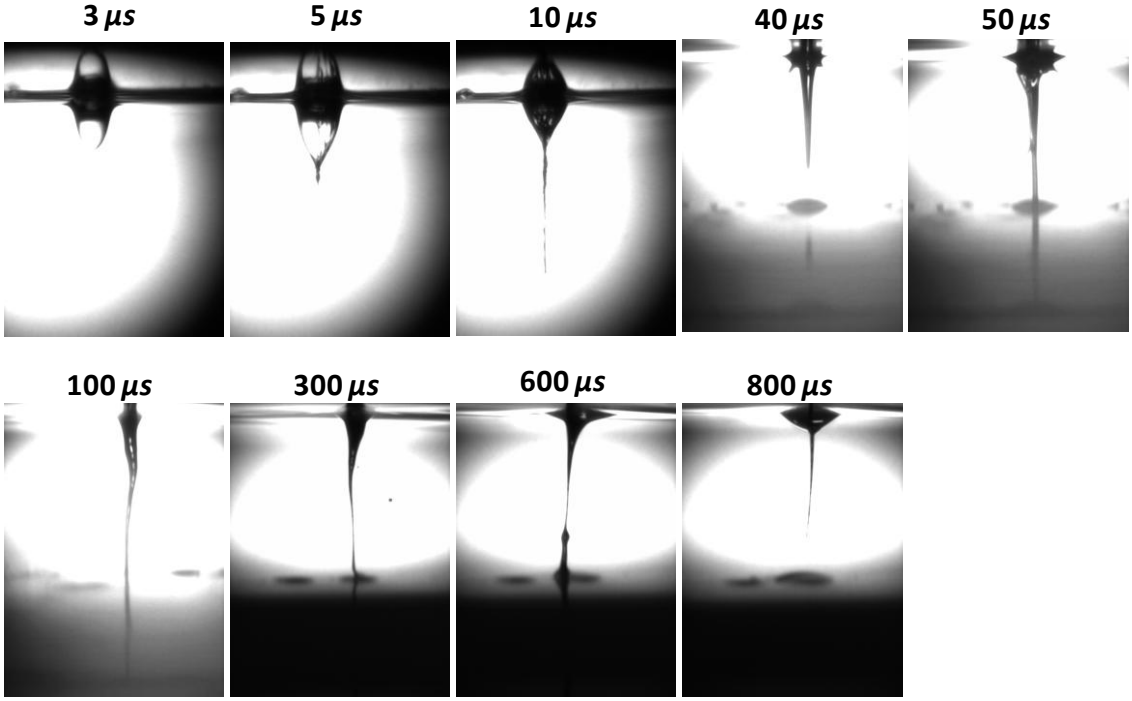

Figure 27 – TRI images taken over time. The images show the different stages of the printing process: **1)** bubble formation (3 µs), **2)** bubble collapsing (5 µs), **3)** jet forming (10 µs), and **4)** landing (50 µs).

3. Optimization of the bioprinting process

3.1. Morphology of the hydrogel spots

As described by Guillemot *et al* (*153*), the mechanical stress the cells suffer upon laser printing is the main factor affecting cellular viability during the printing process. Therefore, it was necessary to optimize the laser energy to be as low as possible, since more energy power leads to more mechanical stress. To address this, different laser energies were tested, namely 12, 23, 35, 46 and 58 µJ, and their effect on the hydrogel spots morphology and diameter was evaluated. This was performed using both alginate formulations (1% and 2% (w/v) alginate), which were spread in quartz slides (**Figure 28 and 29**).

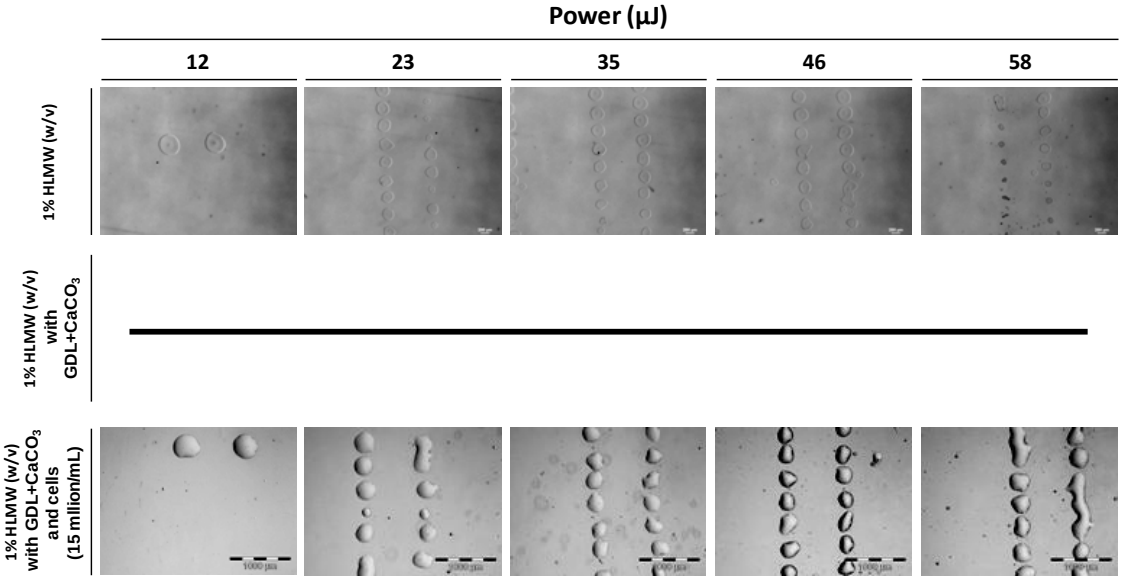

Figure 28 – Energy power effect in bioprinted spots formation. In the first row: 1% (w/v) alginate. Second row: 1% (w/v) alginate with GDL and CaCO3. Third row: 1% (w/v) alginate with GDL and CaCO3 and MSC at 15 million/mL.

As shown in **Figure 28**, 1% (w/v) alginate solutions were printable at the majority of the tested laser energies, except for the lowest and the highest values of 12 and 58 µJ, respectively. It seems that the energy of 12 µJ was insufficient to achieve the jetting regime. The opposite was observed at 58 µJ, where it was possible to see that only tiny droplets were formed, which are probably caused by a plume regime. Since one of the aims was to have a system that self-gelates after printing, the same energy spectrum was tested using 1% (w/v) alginate containing $CaCO_3$ and GDL. However, under such conditions, no printing was observed at none of the tested energies, because the bioink was not spreadable at the ribbon. This may be explained by differences in surface tensions that arise upon addition of $CaCO_3$ and GDL, but further confirmation has to be done in future studies. Finally, cell-loaded bionks were tested, and a preliminary printing with a cellular density of 2 million MSCs/mL in 1% (w/v)

alginate with $CaCO_3$ and GDL was performed (**Annex 1**). Once again, this bioink was printable at all the energies, with exception of 12 and 58 µJ. Yet, while some hydrogel spots were well defined, others had an irregular shape and/or fused. Later, the process was repeated using 15 million MSC/mL (**Figure 28**) and the same printing pattern was obtained. Although the spots obtained at 23, 35 and 46 µJ showed almost the same morphologies, the 35 µJ seemed to be the condition where the spots were in general more regular. The same process was repeated for the 2% (w/v) alginate solution (**Figure 29**).

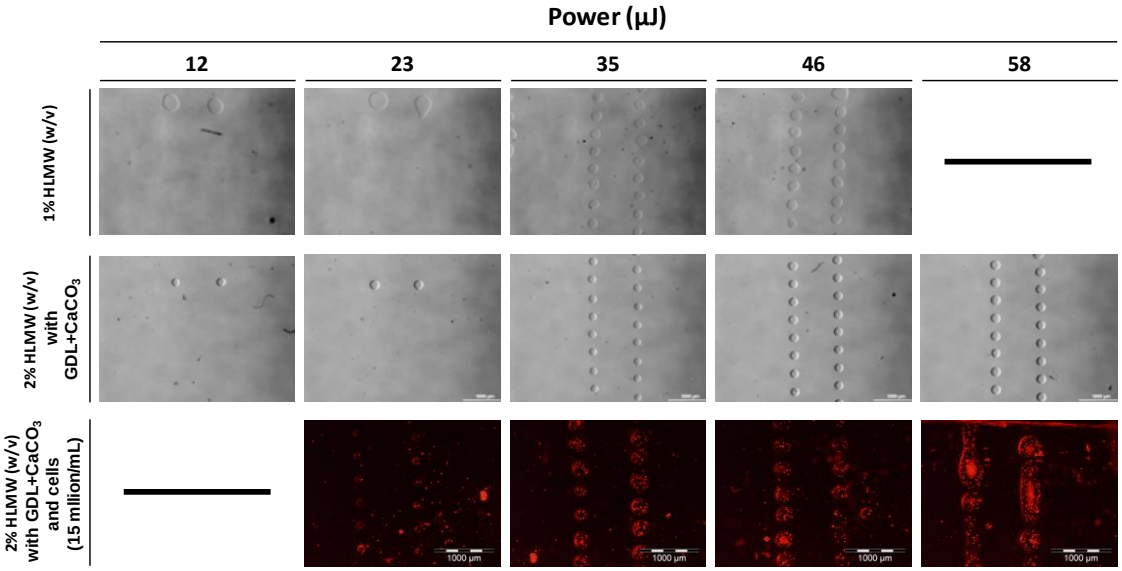

Figure 29 - Energy power effect in bioprinted spots formation. In the first row: 2% (w/v) alginate. Second row: 2% (w/v) alginate with GDL and CaCO3. Third row: 2% (w/v) alginate with GDL, CaCO3 and MSC (red) at 15 million/mL.

In this case, since there was an increase in the alginate concentration, 12 and 23 µJ proved to be insufficient energies to print adequate hydrogel spots in all the three conditions. Regarding the condition with 15 million MSCs/mL, 35 µJ seemed again to be the best laser energy for printing, since 46 and 56 µJ present some droplet abnormalities and 23 µJ seemed to give rise to very small hydrogel spots with few cells inside. Taking into consideration the results depicted in **Figure 28** and **29**, the energy chosen for the subsequent experiments was 35 µJ for both alginate concentrations.

3.2. Diameter of the hydrogel spots

The diameters of the hydrogel spots were measured for both alginate formulations, with and without cells (**Figure 30**). As expected, the average diameter of 1% (w/v) alginate spots is higher than those at 2% (w/v). This is probably related with the higher viscosity of the 2% (w/v) solution, which acts as an opposite force to bubble expansion. Also, at higher

viscosities, the hydrogel tends to recover better its shape, leading to a higher resistance to jet formation. The average diameter decreases in both formulations when cells are added, which is, again, probably explained by the associated increase in viscosity.

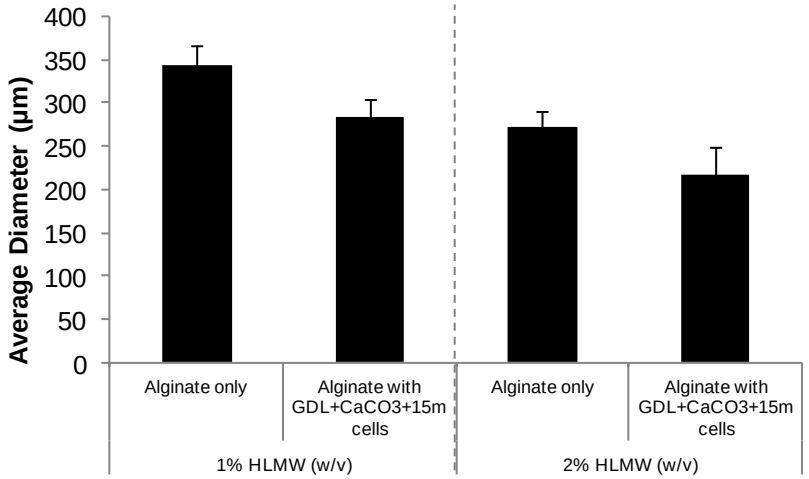

Figure 30 – Average diameters of the hydrogel. Hydrogel spots obtained with 1% and 2% (w/v) alginate solutions, without and with cells at 15 million/mL.

3.3. Volume of the hydrogel spots

Another important parameter is the hydrogel spots volume, which enables to estimate the real cellular density inside the gel spot. **Figure 31** shows the TRI images from which spots heights and diameters were obtained for the subsequent calculation of the spots volume. With these values, summarized in **Table 4,** it was possible to estimate the average cellular density of each printed alginate formulation. As expected from the previous results, the 2% (w/v) alginate spots presented lower volumes. In terms of cellular density, the 2% (w/v) alginate spots presented in average 28.2 million/mL, while the 1% (w/v) alginate spots presented in average 44.7 million/mL. Yet, even if the errors associated with the volume calculations were not very high, the values for the number of printed cells were very irregular and greatly affected the calculated densities, which are thus unreliable. This will have to be further optimized in the future.

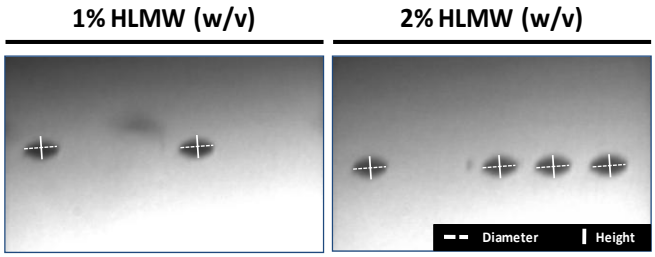

Table 4 – Cellular density Calculation

	Height (µm)	Volume (pL)	Aproximate Number of Printed Cells	Aproximate Cellular Density (millions/mL)
1% HLMW (w/v)	23 ± 0.5	107.7 ± 2.4	4.5 ± 1.5	44.7 ± 14.1
2% HLMW (w/v)	25.4 ± 1.2	73.0 ± 3.9	2.1 ± 1.4	28.2 ± 19.4

Figure 31 – Measurement of the height and diameter of hydrogel droplets from TRI images. Table 4 shows the hydrogel spots height and volume, the approximate number of printed cells, and the approximate cellular density for both alginate formulations.

4. *In vitro* culture of cell-laden hydrogel spots

After optimizing the printing conditions, MSCs-laden hydrogel spots were printed directly onto LabTek® slides and cultured under standard *in vitro* conditions. In this case, hydrogels were made of RGD-modified alginate, in order to promote cell-matrix adhesion.

4.1. Stability of hydrogel spots in culture

Since the hydrogel spots have to remain attached to the receiving substrate along the period of culture, a preliminary analysis on the spots stability over one week of culture was made. In order to have a stable microarray, LabTek® slides were pre-coated with PLL, which confers a positive charge to the surface and interact electrostatically with the negatively charged alginate droplets promoting an adequate spot-substrate adherence. After printing, the slides with attached spots were maintained for 7 days in cell culture medium, under standard incubation conditions, and pictures were taken over time.

Figure 32 shows that the hydrogel spots can be easily monitored during the culture period. Also, and more importantly, it shows that microarray can be maintained under standars culture conditions for at least one week, as the hydrogels spots remain attached to the substrate.

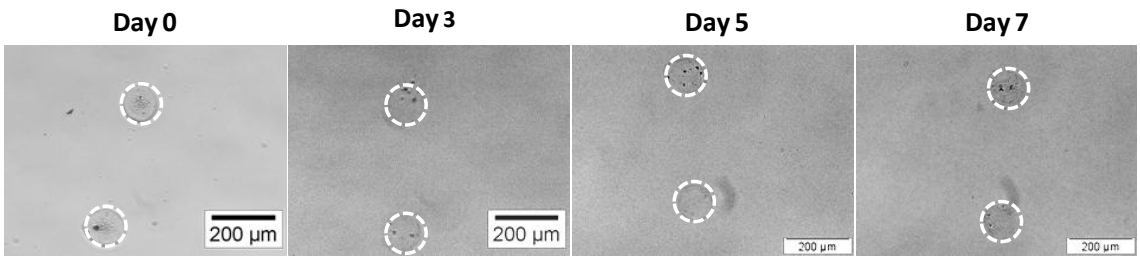

Figure 32 – Hydrogels stability. Stability of hydrogels spots attached to a PLL-coated LabTek® slides over 7 days of culture. The area of the spots is indicated by the dashed line circles.

4.2. Viability of bioprinted cells

One of the main problems of the LAB technique is that the printing process can detrimentally affect cell viability. In order to evaluate this possibility, the viability of the printed cells was analyzed by the LIVE/DEAD assay. As depicted in **Figure 33**, cells within the hydrogel spots remained alive after 7 days of culture, in both types of hydrogel formulations, as showed by the green fluorescence-staining from internalized calcein. These results were in accordance with the MT assay, which was used as a control, where entrapped cells also remained alive.

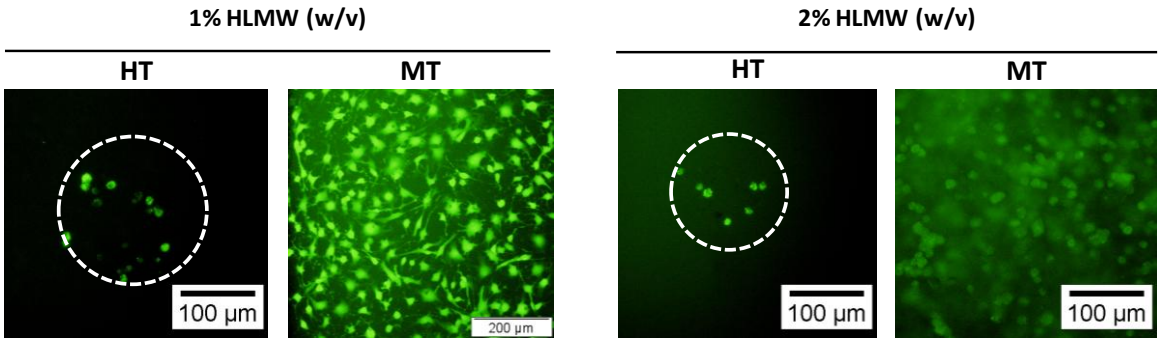

Figure 33 – Bioprinting cellular viability. Viability of MSCs entrapped in RGD-alginate hydrogels, after 7 days of culture in basal medium, in HT and MT formats, indicated by the green fluorescence of internalized calcein (LIVE/DEAD assay). HT: high-throughput; MT: medium-throughput. White circles indicate the area of the spots.

4.3. Validation of the microarray platform

In order to validate the use of the proposed HT platform in future studies it was important to guarantee that the behaviour of cells in this microarrays (cell-laden hydrogel spots) replicated the one typically observed in standard MT assays (cell-laden hydrogel disks). With this aim, we decide to analyze if this system supported the differentiation of entrapped MSCS into the osteoblastic lineage, as previously reported by our group for the hydrogel disks (*90*). Cell-laden hydrogels were cultured in osteoinductive medium and, after 7 days, MSCS osteogenic differentiation was assessed through the analysis of ALP activity expression. As depicted in **Figure 34**, MSCS entrapped in 1% (w/v) alginate hydrogel spots formed aggregates and expressed higher ALP activity than MSCS in 2% (w/v) RGD-alginate hydrogel spots. These results are in accordance with the ones obtained with the MT assay, depicted in the same figure (*90*).

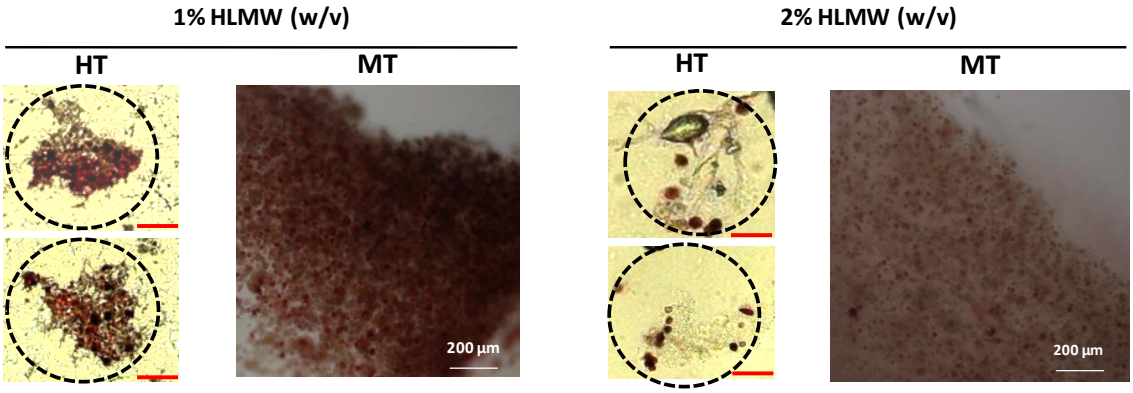

Figure 34 - Osteogenic differentiation assessment. ALP activity staining (dark pink) after 7 days of culture in osteogenic medium of cells cultured within both types of alginate formulations, HT and MT set ups. HT: high-throughput; MT: medium-throughput. Black circles indicate droplet' place and the red scales represent 50 µm.

5. Co-printing of ECs and MSCs

After optimizing the bioprinting and culture conditions for the MSCs-laden hydrogel microarrays, the feasibility of co-printing two cell types, MSCs and ECs, was evaluated. Cells were suspended in 1% (w/v) RGD-alginate hydrogels, at 50 million/mL of final cellular density and printed as previously described. As depicted in **Figure 35**, the obtained hydrogel spots were effectively loaded with the two types of cells, which were in close proximity.

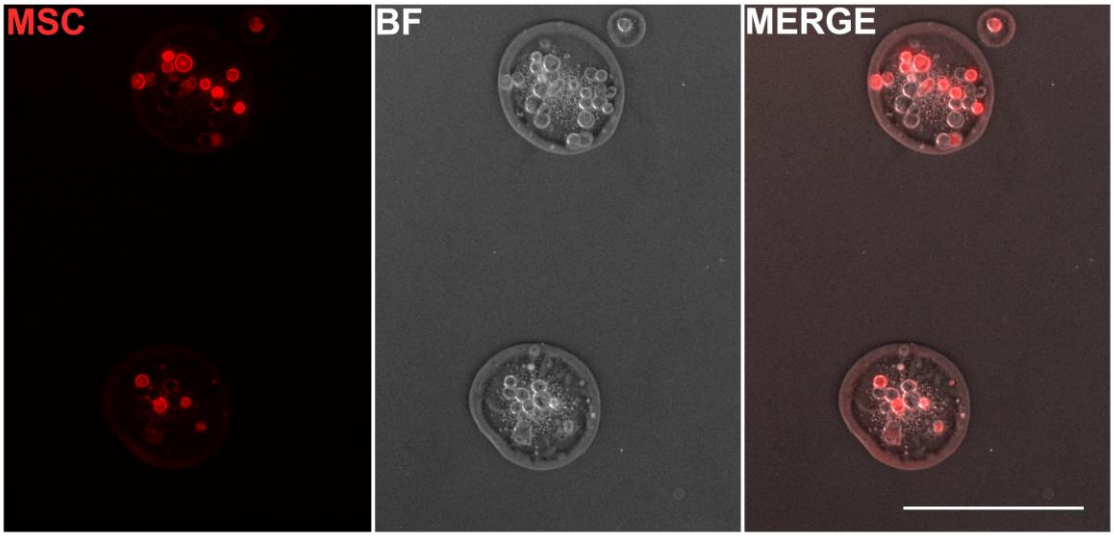

Figure 35 – Co-printing of ECs and MSCs. Left: fluoresce microscopy image of hydrogel spots showing entrapped MSCs expressing Tomato Fluorescent Protein (red); Center: Bright-field image of hydrogel spots with MSCs and ECs. Right: merged image, showing MSCs (red) and unlabeled ECs. (Scale bar: 200 µm).

Unfortunately, due to time constrains, it was not possible to advance further with the implementation of these coculture microarrays for the study of EC-MSC interactions in 3D. As it was demonstrated by Gruene *et al* (*161*), the development of this kind of microarrays has a great potential for tissue engineering to unravel how cells communicate with artificial biomimetic ECMs and how they communicate with each other. In this article, Gruene *et al* (*161*) show that direct cell–cell contacts trigger the development of stable vascular-like networks within spots around 200 µm. The number of cells and material used in this kind of techniques is so small that makes possible the up scaling of complex 3D experiments that are crucial for a more deep understanding of cell-cell and cell-matrix communication.

Conclusions and Future Work

Aiming towards the creation of a suitable ECs delivery system that could promote the neo-vascularization of injured/ischemic tissues, the goal of this work was to optimize, *in vitro*, 3D microenvironmental conditions that could improve ECs survival, as well as promote their capability to form tubular-structures. Using parameters already optimized by our team for HUVECs 3D culture, namely regarding the mechanical properties of the artificial ECM-like hydrogels and the density of available RGD peptides, a 3D system where ECs were combined with MSCs as supportive cells was successfully established in previous studies.

Despite these advances, a number of issues remained to be elucidated and further optimization of some parameters was still required. Here, additional studies were conducted to find an alternative source of ECs, as HUVECs are unsuitable for clinical applications due to their complex harvesting process and lower expansion potential. As alternative, we attempted to isolate two distinct populations of endothelial progenitor cells, early- and late-EPCs (or OEC) from UCB samples. Although we had difficulties to reproduce the differentiation protocol described in a previously published study, two different populations were isolated and characterized: UCB cells A, which presented both endothelial and mesenchymal/fibroblastic features; and UCB cells B which resembled early-EPCs. Both were used in subsequent 3D studies.

The important role of MSCs when in coculture with the different cell types was confirmed. In what concerns MSC+HUVEC cocultures, this study demonstrated that the differences between the mono- and cocultures effectively resulted from MSCs-HUVECs cross-talk and were not related with the total cell density. Expression of α-SMA suggests that MSCs might actually act as PCs/SMCs. Yet, although tubular structures were detected in MSC+HUVECs cocultures, their stability was lost after some days in culture. In future studies it will be important to extend their stability towards the formation of mature ECs structures, which might eventually be achieved by increasing even further the total cell density and/or change the MSCs/HUVECs ratio. In coculture with UCB cells A, MSCs seemed to assist the organization of these cells in 3D, resulting on the significant contraction of the hydrogel matrices and the formation of sprouting structures which were not present in UCB cells A monocultures. UCB cells B resembled er-EPCs, regarded as cells with paracrine potential to enhance ECs survival, but were not able to enhance HUVECs survival in coculture. However, these cells seemed to have a positive effect when triple-cultured with HUVECs and MSCs, HUVECs, which behavior was different from HUVECs+MSCs coculture, promoting a striking contraction of the hydrogel matrix with formation of sprouting structures, and also a tight interacting between HUVECs in proximity with MSCs expressing α-SMA.

Even thought we were able to isolate different cell populations with potential advantages for endothelial delivery and/or *in situ* endogenous stimulation, a more detailed characterization

of these populations must be carried as future work. Both UCB cells A and B have to be characterized regarding their doubling time, senescence, telomerase activity, and protein production, and in more detail, UCB cells A phenotype have to be further characterized by analyzing the expression of alternative endothelial markers along with fibroblastic/mesenchymal/SMC markers. Also, to overcome the difficulty of obtaining OECs, the use of cloning cylinders for harvesting cell colonies might present a good alternative for the standard cell trypsinization used in this work. In fact, after forming colonies, UCB cells A were harvest by trypsinization of the entire well, which could have led to contamination of the obtained population with fibroblastic/mesenchymal cells or SMC present outside the colony. Achieving a well-characterized OECs population would enable us to study the behavior of these cells in 3D, mono-, cocultured with MSCs, and triple-cultured with MSCs and er-EPCs as a fully competent ECs delivery system capable of providing supportive cells, endothelial stimulating cells (er-EPCs) and mature ECs (OECs).

Despite some new conditions and parameters could be optimized here, 3D cultures still continue to face the problem of being a technical challenging system. The amount of material and the number of cells that are needed to make these 3D systems lead to very slow progresses in finding an optimal approach for an ECs delivery system. As a solution, in the second part of this work, we aimed at developing a HTS platform, consisting on bioprinted cell-in-gel 3D microarrays that were prepared using the LAB technique. This was the first time that such an approach was tested and the developed microarrays are expected to serve us as a powerful tool for analyzing cell-ECM cross-talk behavior in 3D. Indeed, it was possible to replicate some previous results typically obtained with the standard MT approach (hydrogel discs), which was important for the validation of this new system. Not only it was possible to test different conditions in terms of alginate viscoelastic properties and cell densities, as it was also possible to co-print HUVECs and MSCs.

Although this study represents a first step towards the development of the proposed HTS platform further optimizations are needed. Some drawbacks, such as the difficulty to accurately control the droplets diameters and the high variability of cell numbers within the droplets, present inconsistencies to the final results that have to be further overcame. As future work we are planning to design a new bioprinter, in collaboration with Dr. Paulo Bartolo's team, at the Centre for Rapid and Sustainable Product Development (CDRSP). The aim is to develop a custom-made bioprinter integrating some important features, such as allowing different formulations of bioinks to be printed in the same chamber of a LabTek® (to more easily allow combinatorial analysis); and with the possibility of being used within a flow chamber hood.

We are also planning to carry out some modifications in our hydrogel formulations, in terms of the gelling mechanism. To avoid the limitation of having a working time window for the bioprinting process, as the current formulations start to gellify with time, we are planning to study a different gelation system. The idea is to use a photoacid generator (PAG) –

diphenyliodonium nitrate – that is triggered only by UV-light (*178*). This molecule would replace GDL, so that we could start the gelation on-demand, making the system even more controllable. With a more robust system it would be possible to combine different cell types (e.g. OECs, er-EPCs and MSCs) in a single droplet and more easily analyze the best conditions to promote the formation of stable ECs tubular structures to be further explored *in viv*o.

References

1. Harrison, R. H., St-Pierre, J. P., and Stevens, M. M. (2014) Tissue engineering and regenerative medicine: a year in review, *Tissue Eng Part B Rev 20*, 1-16.
2. Dijkgraaf, L. C., de Bont, L. G., Boering, G., and Liem, R. S. (1995) Normal cartilage structure, biochemistry, and metabolism: a review of the literature, *J Oral Maxillofac Surg 53*, 924-929.
3. Phelps, E. A., and Garcia, A. J. (2010) Engineering more than a cell: vascularization strategies in tissue engineering, *Curr Opin Biotechnol 21*, 704-709.
4. Kannan, R. Y., Salacinski, H. J., Sales, K., Butler, P., and Seifalian, A. M. (2005) The roles of tissue engineering and vascularisation in the development of micro-vascular networks: a review, *Biomaterials 26*, 1857-1875.
5. Sherwood, L. (2008) *Human physiology: from cells to systems*, Cengage Learning.
6. Novosel, E. C., Kleinhans, C., and Kluger, P. J. (2011) Vascularization is the key challenge in tissue engineering, *Adv Drug Deliv Rev 63*, 300-311.
7. Potente, M., Gerhardt, H., and Carmeliet, P. (2011) Basic and therapeutic aspects of angiogenesis, *Cell 146*, 873-887.
8. Jain, R. K. (2003) Molecular regulation of vessel maturation, *Nat Med 9*, 685-693.
9. Schwartz, S. M., Gajdusek, C. M., and Selden, S. C., 3rd. (1981) Vascular wall growth control: the role of the endothelium, *Arteriosclerosis 1*, 107-126.
10. Asahara, T., Murohara, T., Sullivan, A., Silver, M., van der Zee, R., Li, T., Witzenbichler, B., Schatteman, G., and Isner, J. M. (1997) Isolation of putative progenitor endothelial cells for angiogenesis, *Science 275*, 964-967.
11. Richardson, M. R., and Yoder, M. C. (2011) Endothelial progenitor cells: quo vadis?, *J Mol Cell Cardiol 50*, 266-272.
12. Yoder, M. C. (2009) Defining human endothelial progenitor cells, *J Thromb Haemost 7 Suppl 1*, 49-52.
13. Ingram, D. A., Caplice, N. M., and Yoder, M. C. (2005) Unresolved questions, changing definitions, and novel paradigms for defining endothelial progenitor cells, *Blood 106*, 1525-1531.
14. Naderi, H., Matin, M. M., and Bahrami, A. R. (2011) Review paper: critical issues in tissue engineering: biomaterials, cell sources, angiogenesis, and drug delivery systems, *J Biomater Appl 26*, 383-417.
15. Garlanda, C., and Dejana, E. (1997) Heterogeneity of endothelial cells. Specific markers, *Arterioscler Thromb Vasc Biol 17*, 1193-1202.
16. Belloni, P. N., and Tressler, R. J. (1990) Microvascular endothelial cell heterogeneity: interactions with leukocytes and tumor cells, *Cancer Metastasis Rev 8*, 353-389.
17. DeLisser, H. M., Newman, P. J., and Albelda, S. M. (1994) Molecular and functional aspects of PECAM-1/CD31, *Immunol Today 15*, 490-495.
18. Vecchi, A., Garlanda, C., Lampugnani, M. G., Resnati, M., Matteucci, C., Stoppacciaro, A., Schnurch, H., Risau, W., Ruco, L., Mantovani, A., and et al. (1994) Monoclonal antibodies specific for endothelial cells of mouse blood vessels. Their application in the identification of adult and embryonic endothelium, *Eur J Cell Biol 63*, 247-254.
19. Voyta, J. C., Via, D. P., Butterfield, C. E., and Zetter, B. R. (1984) Identification and isolation of endothelial cells based on their increased uptake of acetylated-low density lipoprotein, *J Cell Biol 99*, 2034-2040.
20. Jackson, C. J., Garbett, P. K., Nissen, B., and Schrieber, L. (1990) Binding of human endothelium to Ulex europaeus I-coated Dynabeads: application to the isolation of microvascular endothelium, *J Cell Sci 96 (Pt 2)*, 257-262.
21. Sahagun, G., Moore, S. A., Fabry, Z., Schelper, R. L., and Hart, M. N. (1989) Purification of murine endothelial cell cultures by flow cytometry using fluorescein-labeled griffonia simplicifolia agglutinin, *Am J Pathol 134*, 1227-1232.
22. Weibel, E. R., and Palade, G. E. (1964) New Cytoplasmic Components in Arterial Endothelia, *J Cell Biol 23*, 101-112.

23. Lampugnani, M. G., Resnati, M., Raiteri, M., Pigott, R., Pisacane, A., Houen, G., Ruco, L. P., and Dejana, E. (1992) A novel endothelial-specific membrane protein is a marker of cell-cell contacts, *J Cell Biol 118*, 1511-1522.
24. Krause, D. S., Fackler, M. J., Civin, C. I., and May, W. S. (1996) CD34: structure, biology, and clinical utility, *Blood 87*, 1-13.
25. Springer, T. A. (1990) Adhesion receptors of the immune system, *Nature 346*, 425-434.
26. Brooks, P. C., Stromblad, S., Sanders, L. C., von Schalscha, T. L., Aimes, R. T., Stetler-Stevenson, W. G., Quigley, J. P., and Cheresh, D. A. (1996) Localization of matrix metalloproteinase MMP-2 to the surface of invasive cells by interaction with integrin alpha v beta 3, *Cell 85*, 683-693.
27. Gougos, A., and Letarte, M. (1988) Identification of a human endothelial cell antigen with monoclonal antibody 44G4 produced against a pre-B leukemic cell line, *J Immunol 141*, 1925-1933.
28. Greenwalt, D. E., Lipsky, R. H., Ockenhouse, C. F., Ikeda, H., Tandon, N. N., and Jamieson, G. A. (1992) Membrane glycoprotein CD36: a review of its roles in adherence, signal transduction, and transfusion medicine, *Blood 80*, 1105-1115.
29. Airas, L., Salmi, M., and Jalkanen, S. (1993) Lymphocyte-vascular adhesion protein-2 is a novel 70-kDa molecule involved in lymphocyte adhesion to vascular endothelium, *J Immunol 151*, 4228-4238.
30. Bardin, N., Frances, V., Lesaule, G., Horschowski, N., George, F., and Sampol, J. (1996) Identification of the S-Endo 1 endothelial-associated antigen, *Biochem Biophys Res Commun 218*, 210-216.
31. Esmon, C. T. (1995) Thrombomodulin as a model of molecular mechanisms that modulate protease specificity and function at the vessel surface, *FASEB J 9*, 946-955.
32. Vainio, O., Dunon, D., Aissi, F., Dangy, J. P., McNagny, K. M., and Imhof, B. A. (1996) HEMCAM, an adhesion molecule expressed by c-kit+ hemopoietic progenitors, *J Cell Biol 135*, 1655-1668.
33. Yamamoto, Y., Yasumizu, R., Amou, Y., Watanabe, N., Nishio, N., Toki, J., Fukuhara, S., and Ikehara, S. (1996) Characterization of peripheral blood stem cells in mice, *Blood 88*, 445-454.
34. Beckner, M. E., Krutzsch, H. C., Stracke, M. L., Williams, S. T., Gallardo, J. A., and Liotta, L. A. (1995) Identification of a new immunoglobulin superfamily protein expressed in blood vessels with a heparin-binding consensus sequence, *Cancer Res 55*, 2140-2149.
35. Santos, M. I., and Reis, R. L. (2010) Vascularization in bone tissue engineering: physiology, current strategies, major hurdles and future challenges, *Macromol Biosci 10*, 12-27.
36. Kim, J., Jeon, Y. J., Kim, H. E., Shin, J. M., Chung, H. M., and Chae, J. I. (2013) Comparative proteomic analysis of endothelial cells progenitor cells derived from cord blood- and peripheral blood for cell therapy, *Biomaterials 34*, 1669-1685.
37. Goligorsky, M. S., and Salven, P. (2013) Concise review: endothelial stem and progenitor cells and their habitats, *Stem Cells Transl Med 2*, 499-504.
38. Fuchs, S., Dohle, E., Kolbe, M., and Kirkpatrick, C. J. (2010) Outgrowth endothelial cells: sources, characteristics and potential applications in tissue engineering and regenerative medicine, *Adv Biochem Eng Biotechnol 123*, 201-217.
39. Cheng, C. C., Chang, S. J., Chueh, Y. N., Huang, T. S., Huang, P. H., Cheng, S. M., Tsai, T. N., Chen, J. W., and Wang, H. W. (2013) Distinct angiogenesis roles and surface markers of early and late endothelial progenitor cells revealed by functional group analyses, *BMC Genomics 14*, 182.
40. Reagan, J., Foo, T., Tracy Watson, J., Jin, W., Moed, B. R., and Zhang, Z. (2011) Distinct phenotypes and regenerative potentials of early endothelial progenitor cells and outgrowth endothelial progenitor cells derived from umbilical cord blood, *J Tissue Eng Regen Med 5*, 620-628.
41. Eggermann, J., Kliche, S., Jarmy, G., Hoffmann, K., Mayr-Beyrle, U., Debatin, K. M., Waltenberger, J., and Beltinger, C. (2003) Endothelial progenitor cell culture and differentiation in vitro: a methodological comparison using human umbilical cord blood, *Cardiovasc Res 58*, 478-486.
42. Xu, Q. (2007) Progenitor cells in vascular repair, *Curr Opin Lipidol 18*, 534-539.

43. Lapergue, B., Mohammad, A., and Shuaib, A. (2007) Endothelial progenitor cells and cerebrovascular diseases, *Prog Neurobiol 83*, 349-362.
44. Ingram, D. A., Mead, L. E., Tanaka, H., Meade, V., Fenoglio, A., Mortell, K., Pollok, K., Ferkowicz, M. J., Gilley, D., and Yoder, M. C. (2004) Identification of a novel hierarchy of endothelial progenitor cells using human peripheral and umbilical cord blood, *Blood 104*, 2752-2760.
45. Lin, R. Z., Dreyzin, A., Aamodt, K., Dudley, A. C., and Melero-Martin, J. M. (2011) Functional endothelial progenitor cells from cryopreserved umbilical cord blood, *Cell Transplant 20*, 515-522.
46. Holnthoner, W., Hohenegger, K., Husa, A. M., Muehleder, S., Meinl, A., Peterbauer-Scherb, A., and Redl, H. (2012) Adipose-derived stem cells induce vascular tube formation of outgrowth endothelial cells in a fibrin matrix, *J Tissue Eng Regen Med*.
47. Stroncek, J. D., Grant, B. S., Brown, M. A., Povsic, T. J., Truskey, G. A., and Reichert, W. M. (2009) Comparison of endothelial cell phenotypic markers of late-outgrowth endothelial progenitor cells isolated from patients with coronary artery disease and healthy volunteers, *Tissue Eng Part A 15*, 3473-3486.
48. Moubarik, C., Guillet, B., Youssef, B., Codaccioni, J. L., Piercecchi, M. D., Sabatier, F., Lionel, P., Dou, L., Foucault-Bertaud, A., Velly, L., Dignat-George, F., and Pisano, P. (2011) Transplanted late outgrowth endothelial progenitor cells as cell therapy product for stroke, *Stem Cell Rev 7*, 208-220.
49. Mazzolai, L., Bouzourene, K., Hayoz, D., Dignat-George, F., Liu, J. W., Bounameaux, H., Dunoyer-Geindre, S., and Kruithof, E. K. (2011) Characterization of human late outgrowth endothelial progenitor-derived cells under various flow conditions, *J Vasc Res 48*, 443-451.
50. Yoon, C. H., Hur, J., Park, K. W., Kim, J. H., Lee, C. S., Oh, I. Y., Kim, T. Y., Cho, H. J., Kang, H. J., Chae, I. H., Yang, H. K., Oh, B. H., Park, Y. B., and Kim, H. S. (2005) Synergistic neovascularization by mixed transplantation of early endothelial progenitor cells and late outgrowth endothelial cells: the role of angiogenic cytokines and matrix metalloproteinases, *Circulation 112*, 1618-1627.
51. Lin, Y., Weisdorf, D. J., Solovey, A., and Hebbel, R. P. (2000) Origins of circulating endothelial cells and endothelial outgrowth from blood, *J Clin Invest 105*, 71-77.
52. Rehman, J., Li, J., Orschell, C. M., and March, K. L. (2003) Peripheral blood "endothelial progenitor cells" are derived from monocyte/macrophages and secrete angiogenic growth factors, *Circulation 107*, 1164-1169.
53. Gulati, R., Jevremovic, D., Peterson, T. E., Chatterjee, S., Shah, V., Vile, R. G., and Simari, R. D. (2003) Diverse origin and function of cells with endothelial phenotype obtained from adult human blood, *Circ Res 93*, 1023-1025.
54. Ingram, D. A., Mead, L. E., Moore, D. B., Woodard, W., Fenoglio, A., and Yoder, M. C. (2005) Vessel wall-derived endothelial cells rapidly proliferate because they contain a complete hierarchy of endothelial progenitor cells, *Blood 105*, 2783-2786.
55. Yoder, M. C., Mead, L. E., Prater, D., Krier, T. R., Mroueh, K. N., Li, F., Krasich, R., Temm, C. J., Prchal, J. T., and Ingram, D. A. (2007) Redefining endothelial progenitor cells via clonal analysis and hematopoietic stem/progenitor cell principals, *Blood 109*, 1801-1809.
56. Hur, J., Yoon, C. H., Kim, H. S., Choi, J. H., Kang, H. J., Hwang, K. K., Oh, B. H., Lee, M. M., and Park, Y. B. (2004) Characterization of two types of endothelial progenitor cells and their different contributions to neovasculogenesis, *Arterioscler Thromb Vasc Biol 24*, 288-293.
57. Kalka, C., Masuda, H., Takahashi, T., Kalka-Moll, W. M., Silver, M., Kearney, M., Li, T., Isner, J. M., and Asahara, T. (2000) Transplantation of ex vivo expanded endothelial progenitor cells for therapeutic neovascularization, *Proc Natl Acad Sci U S A 97*, 3422-3427.
58. Fuchs, S., Hermanns, M. I., and Kirkpatrick, C. J. (2006) Retention of a differentiated endothelial phenotype by outgrowth endothelial cells isolated from human peripheral blood and expanded in long-term cultures, *Cell Tissue Res 326*, 79-92.
59. Timmermans, F., Van Hauwermeiren, F., De Smedt, M., Raedt, R., Plasschaert, F., De Buyzere, M. L., Gillebert, T. C., Plum, J., and Vandekerckhove, B. (2007) Endothelial outgrowth cells are not derived from CD133+ cells or CD45+ hematopoietic precursors, *Arterioscler Thromb Vasc Biol 27*, 1572-1579.

60. Gehling, U. M., Ergun, S., Schumacher, U., Wagener, C., Pantel, K., Otte, M., Schuch, G., Schafhausen, P., Mende, T., Kilic, N., Kluge, K., Schafer, B., Hossfeld, D. K., and Fiedler, W. (2000) In vitro differentiation of endothelial cells from AC133-positive progenitor cells, *Blood 95*, 3106-3112.
61. Delorme, B., Basire, A., Gentile, C., Sabatier, F., Monsonis, F., Desouches, C., Blot-Chabaud, M., Uzan, G., Sampol, J., and Dignat-George, F. (2005) Presence of endothelial progenitor cells, distinct from mature endothelial cells, within human CD146+ blood cells, *Thromb Haemost 94*, 1270-1279.
62. Peichev, M., Naiyer, A. J., Pereira, D., Zhu, Z., Lane, W. J., Williams, M., Oz, M. C., Hicklin, D. J., Witte, L., Moore, M. A., and Rafii, S. (2000) Expression of VEGFR-2 and AC133 by circulating human CD34(+) cells identifies a population of functional endothelial precursors, *Blood 95*, 952-958.
63. Urbich, C., and Dimmeler, S. (2004) Endothelial progenitor cells: characterization and role in vascular biology, *Circ Res 95*, 343-353.
64. Assmus, B., Schachinger, V., Teupe, C., Britten, M., Lehmann, R., Dobert, N., Grunwald, F., Aicher, A., Urbich, C., Martin, H., Hoelzer, D., Dimmeler, S., and Zeiher, A. M. (2002) Transplantation of Progenitor Cells and Regeneration Enhancement in Acute Myocardial Infarction (TOPCARE-AMI), *Circulation 106*, 3009-3017.
65. Mukai, N., Akahori, T., Komaki, M., Li, Q., Kanayasu-Toyoda, T., Ishii-Watabe, A., Kobayashi, A., Yamaguchi, T., Abe, M., Amagasa, T., and Morita, I. (2008) A comparison of the tube forming potentials of early and late endothelial progenitor cells, *Exp Cell Res 314*, 430-440.
66. Sieveking, D. P., Buckle, A., Celermajer, D. S., and Ng, M. K. (2008) Strikingly different angiogenic properties of endothelial progenitor cell subpopulations: insights from a novel human angiogenesis assay, *J Am Coll Cardiol 51*, 660-668.
67. Nuzzolo, E. R., Capodimonti, S., Martini, M., Iachininoto, M. G., Bianchi, M., Cocomazzi, A., Zini, G., Leone, G., Larocca, L. M., and Teofili, L. (2014) Adult and cord blood endothelial progenitor cells have different gene expression profiles and immunogenic potential, *Blood Transfus 12 Suppl 1*, s367-374.
68. da Silva, C. L., Goncalves, R., Porada, C. D., Ascensao, J. L., Zanjani, E. D., Cabral, J. M., and Almeida-Porada, G. (2009) Differences amid bone marrow and cord blood hematopoietic stem/progenitor cell division kinetics, *J Cell Physiol 220*, 102-111.
69. Kurtzberg, J., Laughlin, M., Graham, M. L., Smith, C., Olson, J. F., Halperin, E. C., Ciocci, G., Carrier, C., Stevens, C. E., and Rubinstein, P. (1996) Placental blood as a source of hematopoietic stem cells for transplantation into unrelated recipients, *N Engl J Med 335*, 157-166.
70. De Smedt, M., Leclercq, G., Vandekerckhove, B., Kerre, T., Taghon, T., and Plum, J. (2011) T-lymphoid differentiation potential measured in vitro is higher in CD34+CD38-/lo hematopoietic stem cells from umbilical cord blood than from bone marrow and is an intrinsic property of the cells, *Haematologica 96*, 646-654.
71. Crisan, M., Corselli, M., Chen, W. C., and Peault, B. (2012) Perivascular cells for regenerative medicine, *J Cell Mol Med 16*, 2851-2860.
72. Ribatti, D., Nico, B., and Crivellato, E. (2011) The role of pericytes in angiogenesis, *Int J Dev Biol 55*, 261-268.
73. Nehls, V., Denzer, K., and Drenckhahn, D. (1992) Pericyte involvement in capillary sprouting during angiogenesis in situ, *Cell Tissue Res 270*, 469-474.
74. Betsholtz, C. (2004) Insight into the physiological functions of PDGF through genetic studies in mice, *Cytokine Growth Factor Rev 15*, 215-228.
75. Yamagishi, S., Yonekura, H., Yamamoto, Y., Fujimori, H., Sakurai, S., Tanaka, N., and Yamamoto, H. (1999) Vascular endothelial growth factor acts as a pericyte mitogen under hypoxic conditions, *Lab Invest 79*, 501-509.
76. Ghajar, C. M., Kachgal, S., Kniazeva, E., Mori, H., Costes, S. V., George, S. C., and Putnam, A. J. (2010) Mesenchymal cells stimulate capillary morphogenesis via distinct proteolytic mechanisms, *Exp Cell Res 316*, 813-825.
77. Carrion, B., Kong, Y. P., Kaigler, D., and Putnam, A. J. (2013) Bone marrow-derived mesenchymal stem cells enhance angiogenesis via their alpha6beta1 integrin receptor, *Exp Cell Res 319*, 2964-2976.
78. Strassburg, S., Nienhueser, H., Bjorn Stark, G., Finkenzeller, G., and Torio-Padron, N. (2013) Co-culture of adipose-derived stem cells and endothelial cells in fibrin induces

angiogenesis and vasculogenesis in a chorioallantoic membrane model, *J Tissue Eng Regen Med*.
79. Aguirre, A., Planell, J. A., and Engel, E. (2010) Dynamics of bone marrow-derived endothelial progenitor cell/mesenchymal stem cell interaction in co-culture and its implications in angiogenesis, *Biochem Biophys Res Commun 400*, 284-291.
80. Ma, J., Yang, F., Both, S. K., Prins, H. J., Helder, M. N., Pan, J., Cui, F. Z., Jansen, J. A., and van den Beucken, J. J. (2014) In vitro and in vivo angiogenic capacity of BM-MSCs/HUVECs and AT-MSCs/HUVECs cocultures, *Biofabrication 6*, 015005.
81. Anfuso, C. D., Motta, C., Satriano, C., Gennaro, S., Marletta, G., Giurdanella, G., Alberghina, M., and Lupo, G. (2012) Microcapillary-like structures prompted by phospholipase A2 activation in endothelial cells and pericytes co-cultures on a polyhydroxymethylsiloxane thin film, *Biochimie 94*, 1860-1870.
82. Trkov, S., Eng, G., Di Liddo, R., Parnigotto, P. P., and Vunjak-Novakovic, G. (2010) Micropatterned three-dimensional hydrogel system to study human endothelial-mesenchymal stem cell interactions, *J Tissue Eng Regen Med 4*, 205-215.
83. Crisan, M., Yap, S., Casteilla, L., Chen, C. W., Corselli, M., Park, T. S., Andriolo, G., Sun, B., Zheng, B., Zhang, L., Norotte, C., Teng, P. N., Traas, J., Schugar, R., Deasy, B. M., Badylak, S., Buhring, H. J., Giacobino, J. P., Lazzari, L., Huard, J., and Peault, B. (2008) A perivascular origin for mesenchymal stem cells in multiple human organs, *Cell Stem Cell 3*, 301-313.
84. Corselli, M., Chen, C. W., Sun, B., Yap, S., Rubin, J. P., and Peault, B. (2012) The tunica adventitia of human arteries and veins as a source of mesenchymal stem cells, *Stem Cells Dev 21*, 1299-1308.
85. Duttenhoefer, F., Lara de Freitas, R., Meury, T., Loibl, M., Benneker, L. M., Richards, R. G., Alini, M., and Verrier, S. (2013) 3D scaffolds co-seeded with human endothelial progenitor and mesenchymal stem cells: evidence of prevascularisation within 7 days, *Eur Cell Mater 26*, 49-64; discussion 64-45.
86. Saleh, F. A., Whyte, M., and Genever, P. G. (2011) Effects of endothelial cells on human mesenchymal stem cell activity in a three-dimensional in vitro model, *Eur Cell Mater 22*, 242-257; discussion 257.
87. Li, Q., and Wang, Z. (2013) Influence of mesenchymal stem cells with endothelial progenitor cells in co-culture on osteogenesis and angiogenesis: an in vitro study, *Arch Med Res 44*, 504-513.
88. Liu, K., Ji, K., Guo, L., Wu, W., Lu, H., Shan, P., and Yan, C. (2014) Mesenchymal stem cells rescue injured endothelial cells in an in vitro ischemia-reperfusion model via tunneling nanotube like structure-mediated mitochondrial transfer, *Microvasc Res 92*, 10-18.
89. Ranganath, S. H., Levy, O., Inamdar, M. S., and Karp, J. M. (2012) Harnessing the mesenchymal stem cell secretome for the treatment of cardiovascular disease, *Cell Stem Cell 10*, 244-258.
90. Maia, F. R., Fonseca, K. B., Rodrigues, G., Granja, P. L., and Barrias, C. C. (2014) Matrix-driven formation of mesenchymal stem cell-extracellular matrix microtissues on soft alginate hydrogels, *Acta Biomater 10*, 3197-3208.
91. Nassiri, S. M., and Rahbarghazi, R. (2014) Interactions of mesenchymal stem cells with endothelial cells, *Stem Cells Dev 23*, 319-332.
92. Montesano, R., Orci, L., and Vassalli, P. (1983) In vitro rapid organization of endothelial cells into capillary-like networks is promoted by collagen matrices, *J Cell Biol 97*, 1648-1652.
93. Elsdale, T., and Bard, J. (1972) Collagen substrata for studies on cell behavior, *J Cell Biol 54*, 626-637.
94. Justice, B. A., Badr, N. A., and Felder, R. A. (2009) 3D cell culture opens new dimensions in cell-based assays, *Drug Discov Today 14*, 102-107.
95. Even-Ram, S., and Yamada, K. M. (2005) Cell migration in 3D matrix, *Curr Opin Cell Biol 17*, 524-532.
96. Cukierman, E., Pankov, R., and Yamada, K. M. (2002) Cell interactions with three-dimensional matrices, *Curr Opin Cell Biol 14*, 633-639.
97. Griffith, L. G., and Swartz, M. A. (2006) Capturing complex 3D tissue physiology in vitro, *Nat Rev Mol Cell Biol 7*, 211-224.
98. Owen, S. C., and Shoichet, M. S. (2010) Design of three-dimensional biomimetic scaffolds, *J Biomed Mater Res A 94*, 1321-1331.

99. Ehrbar, M., Sala, A., Lienemann, P., Ranga, A., Mosiewicz, K., Bittermann, A., Rizzi, S. C., Weber, F. E., and Lutolf, M. P. (2011) Elucidating the role of matrix stiffness in 3D cell migration and remodeling, *Biophys J 100*, 284-293.
100. Peppas, N. A., Huang, Y., Torres-Lugo, M., Ward, J. H., and Zhang, J. (2000) Physicochemical foundations and structural design of hydrogels in medicine and biology, *Annu Rev Biomed Eng 2*, 9-29.
101. Vats, K., and Benoit, D. S. (2013) Dynamic manipulation of hydrogels to control cell behavior: a review, *Tissue Eng Part B Rev 19*, 455-469.
102. Tibbitt, M. W., and Anseth, K. S. (2009) Hydrogels as extracellular matrix mimics for 3D cell culture, *Biotechnol Bioeng 103*, 655-663.
103. Zhou, X., Rowe, R. G., Hiraoka, N., George, J. P., Wirtz, D., Mosher, D. F., Virtanen, I., Chernousov, M. A., and Weiss, S. J. (2008) Fibronectin fibrillogenesis regulates three-dimensional neovessel formation, *Genes Dev 22*, 1231-1243.
104. Urech, L., Bittermann, A. G., Hubbell, J. A., and Hall, H. (2005) Mechanical properties, proteolytic degradability and biological modifications affect angiogenic process extension into native and modified fibrin matrices in vitro, *Biomaterials 26*, 1369-1379.
105. Califano, J. P., and Reinhart-King, C. A. (2010) Exogenous and endogenous force regulation of endothelial cell behavior, *J Biomech 43*, 79-86.
106. Yang, S., Graham, J., Kahn, J. W., Schwartz, E. A., and Gerritsen, M. E. (1999) Functional roles for PECAM-1 (CD31) and VE-cadherin (CD144) in tube assembly and lumen formation in three-dimensional collagen gels, *Am J Pathol 155*, 887-895.
107. Satake, S., Kuzuya, M., Ramos, M. A., Kanda, S., and Iguchi, A. (1998) Angiogenic stimuli are essential for survival of vascular endothelial cells in three-dimensional collagen lattice, *Biochem Biophys Res Commun 244*, 642-646.
108. Bayless, K. J., and Davis, G. E. (2003) Sphingosine-1-phosphate markedly induces matrix metalloproteinase and integrin-dependent human endothelial cell invasion and lumen formation in three-dimensional collagen and fibrin matrices, *Biochem Biophys Res Commun 312*, 903-913.
109. Nakatsu, M. N., Sainson, R. C., Aoto, J. N., Taylor, K. L., Aitkenhead, M., Perez-del-Pulgar, S., Carpenter, P. M., and Hughes, C. C. (2003) Angiogenic sprouting and capillary lumen formation modeled by human umbilical vein endothelial cells (HUVEC) in fibrin gels: the role of fibroblasts and Angiopoietin-1, *Microvasc Res 66*, 102-112.
110. Nehls, V., and Drenckhahn, D. (1995) A novel, microcarrier-based in vitro assay for rapid and reliable quantification of three-dimensional cell migration and angiogenesis, *Microvasc Res 50*, 311-322.
111. Passaniti, A., Taylor, R. M., Pili, R., Guo, Y., Long, P. V., Haney, J. A., Pauly, R. R., Grant, D. S., and Martin, G. R. (1992) A simple, quantitative method for assessing angiogenesis and antiangiogenic agents using reconstituted basement membrane, heparin, and fibroblast growth factor, *Lab Invest 67*, 519-528.
112. Maia, F. R., Lourenco, A. H., Granja, P. L., Goncalves, R. M., and Barrias, C. C. (2014) Effect of Cell Density on Mesenchymal Stem Cells Aggregation in RGD-Alginate 3D Matrices under Osteoinductive Conditions, *Macromol Biosci 14*, 759-771.
113. Nakatsu, M. N., and Hughes, C. C. (2008) An optimized three-dimensional in vitro model for the analysis of angiogenesis, *Methods Enzymol 443*, 65-82.
114. Grellier, M., Granja, P. L., Fricain, J. C., Bidarra, S. J., Renard, M., Bareille, R., Bourget, C., Amedee, J., and Barbosa, M. A. (2009) The effect of the co-immobilization of human osteoprogenitors and endothelial cells within alginate microspheres on mineralization in a bone defect, *Biomaterials 30*, 3271-3278.
115. Kawada, A., Hiura, N., Tajima, S., and Takahara, H. (1999) Alginate oligosaccharides stimulate VEGF-mediated growth and migration of human endothelial cells, *Arch Dermatol Res 291*, 542-547.
116. Khalil, S., and Sun, W. (2009) Bioprinting endothelial cells with alginate for 3D tissue constructs, *J Biomech Eng 131*, 111002.
117. Lee, K. H., Shin, S. J., Park, Y., and Lee, S. H. (2009) Synthesis of cell-laden alginate hollow fibers using microfluidic chips and microvascularized tissue-engineering applications, *Small 5*, 1264-1268.
118. Augst, A. D., Kong, H. J., and Mooney, D. J. (2006) Alginate hydrogels as biomaterials, *Macromol Biosci 6*, 623-633.

119. Evangelista, M. B., Hsiong, S. X., Fernandes, R., Sampaio, P., Kong, H. J., Barrias, C. C., Salema, R., Barbosa, M. A., Mooney, D. J., and Granja, P. L. (2007) Upregulation of bone cell differentiation through immobilization within a synthetic extracellular matrix, *Biomaterials 28*, 3644-3655.
120. Fonseca, K. B., Bidarra, S. J., Oliveira, M. J., Granja, P. L., and Barrias, C. C. (2011) Molecularly designed alginate hydrogels susceptible to local proteolysis as three-dimensional cellular microenvironments, *Acta Biomater 7*, 1674-1682.
121. Rowley, J. A., Madlambayan, G., and Mooney, D. J. (1999) Alginate hydrogels as synthetic extracellular matrix materials, *Biomaterials 20*, 45-53.
122. Hsiong, S. X., Huebsch, N., Fischbach, C., Kong, H. J., and Mooney, D. J. (2008) Integrin-adhesion ligand bond formation of preosteoblasts and stem cells in three-dimensional RGD presenting matrices, *Biomacromolecules 9*, 1843-1851.
123. Rowley, J. A., and Mooney, D. J. (2002) Alginate type and RGD density control myoblast phenotype, *J Biomed Mater Res 60*, 217-223.
124. Bidarra, S. J., Barrias, C. C., Fonseca, K. B., Barbosa, M. A., Soares, R. A., and Granja, P. L. (2011) Injectable in situ crosslinkable RGD-modified alginate matrix for endothelial cells delivery, *Biomaterials 32*, 7897-7904.
125. Ranga, A., and Lutolf, M. P. (2012) High-throughput approaches for the analysis of extrinsic regulators of stem cell fate, *Curr Opin Cell Biol 24*, 236-244.
126. Harris, A. (1973) Behavior of cultured cells on substrata of variable adhesiveness, *Exp Cell Res 77*, 285-297.
127. Yliperttula, M., Chung, B. G., Navaladi, A., Manbachi, A., and Urtti, A. (2008) High-throughput screening of cell responses to biomaterials, *Eur J Pharm Sci 35*, 151-160.
128. Flaim, C. J., Chien, S., and Bhatia, S. N. (2005) An extracellular matrix microarray for probing cellular differentiation, *Nat Methods 2*, 119-125.
129. Soen, Y., Mori, A., Palmer, T. D., and Brown, P. O. (2006) Exploring the regulation of human neural precursor cell differentiation using arrays of signaling microenvironments, *Mol Syst Biol 2*, 37.
130. Anderson, D. G., Putnam, D., Lavik, E. B., Mahmood, T. A., and Langer, R. (2005) Biomaterial microarrays: rapid, microscale screening of polymer-cell interaction, *Biomaterials 26*, 4892-4897.
131. Fernandes, T. G., Kwon, S. J., Bale, S. S., Lee, M. Y., Diogo, M. M., Clark, D. S., Cabral, J. M., and Dordick, J. S. (2010) Three-dimensional cell culture microarray for high-throughput studies of stem cell fate, *Biotechnol Bioeng 106*, 106-118.
132. Fernandes, T. G., Diogo, M. M., Clark, D. S., Dordick, J. S., and Cabral, J. M. (2009) High-throughput cellular microarray platforms: applications in drug discovery, toxicology and stem cell research, *Trends Biotechnol 27*, 342-349.
133. Fernandes, T. G., Kwon, S. J., Lee, M. Y., Clark, D. S., Cabral, J. M., and Dordick, J. S. (2008) On-chip, cell-based microarray immunofluorescence assay for high-throughput analysis of target proteins, *Anal Chem 80*, 6633-6639.
134. Dolatshahi-Pirouz, A., Nikkhah, M., Gaharwar, A. K., Hashmi, B., Guermani, E., Aliabadi, H., Camci-Unal, G., Ferrante, T., Foss, M., Ingber, D. E., and Khademhosseini, A. (2014) A combinatorial cell-laden gel microarray for inducing osteogenic differentiation of human mesenchymal stem cells, *Sci Rep 4*, 3896.
135. Tasoglu, S., and Demirci, U. (2013) Bioprinting for stem cell research, *Trends Biotechnol 31*, 10-19.
136. Xu, F., Moon, S. J., Emre, A. E., Turali, E. S., Song, Y. S., Hacking, S. A., Nagatomi, J., and Demirci, U. (2010) A droplet-based building block approach for bladder smooth muscle cell (SMC) proliferation, *Biofabrication 2*, 014105.
137. Mironov, V., Boland, T., Trusk, T., Forgacs, G., and Markwald, R. R. (2003) Organ printing: computer-aided jet-based 3D tissue engineering, *Trends Biotechnol 21*, 157-161.
138. Mironov, V., Kasyanov, V., Drake, C., and Markwald, R. R. (2008) Organ printing: promises and challenges, *Regen Med 3*, 93-103.
139. Moon, S., Hasan, S. K., Song, Y. S., Xu, F., Keles, H. O., Manzur, F., Mikkilineni, S., Hong, J. W., Nagatomi, J., Haeggstrom, E., Khademhosseini, A., and Demirci, U. (2010) Layer by layer three-dimensional tissue epitaxy by cell-laden hydrogel droplets, *Tissue Eng Part C Methods 16*, 157-166.
140. Demirci, U., and Montesano, G. (2007) Single cell epitaxy by acoustic picolitre droplets, *Lab Chip 7*, 1139-1145.

141. Fang, Y., Frampton, J. P., Raghavan, S., Sabahi-Kaviani, R., Luker, G., Deng, C. X., and Takayama, S. (2012) Rapid generation of multiplexed cell cocultures using acoustic droplet ejection followed by aqueous two-phase exclusion patterning, *Tissue Eng Part C Methods 18*, 647-657.
142. Boland, T., Xu, T., Damon, B., and Cui, X. (2006) Application of inkjet printing to tissue engineering, *Biotechnol J 1*, 910-917.
143. Nakamura, M., Kobayashi, A., Takagi, F., Watanabe, A., Hiruma, Y., Ohuchi, K., Iwasaki, Y., Horie, M., Morita, I., and Takatani, S. (2005) Biocompatible inkjet printing technique for designed seeding of individual living cells, *Tissue Eng 11*, 1658-1666.
144. Demirci, U., and Montesano, G. (2007) Cell encapsulating droplet vitrification, *Lab Chip 7*, 1428-1433.
145. Song, Y. S., Adler, D., Xu, F., Kayaalp, E., Nureddin, A., Anchan, R. M., Maas, R. L., and Demirci, U. (2010) Vitrification and levitation of a liquid droplet on liquid nitrogen, *Proc Natl Acad Sci U S A 107*, 4596-4600.
146. Moon, S., Kim, Y. G., Dong, L., Lombardi, M., Haeggstrom, E., Jensen, R. V., Hsiao, L. L., and Demirci, U. (2011) Drop-on-demand single cell isolation and total RNA analysis, *PLoS One 6*, e17455.
147. Odde, D. J., and Renn, M. J. (1999) Laser-guided direct writing for applications in biotechnology, *Trends Biotechnol 17*, 385-389.
148. Nahmias, Y., Schwartz, R. E., Verfaillie, C. M., and Odde, D. J. (2005) Laser-guided direct writing for three-dimensional tissue engineering, *Biotechnol Bioeng 92*, 129-136.
149. Guillotin, B., Souquet, A., Catros, S., Duocastella, M., Pippenger, B., Bellance, S., Bareille, R., Remy, M., Bordenave, L., Amedee, J., and Guillemot, F. (2010) Laser assisted bioprinting of engineered tissue with high cell density and microscale organization, *Biomaterials 31*, 7250-7256.
150. Gaebel, R., Ma, N., Liu, J., Guan, J., Koch, L., Klopsch, C., Gruene, M., Toelk, A., Wang, W., Mark, P., Wang, F., Chichkov, B., Li, W., and Steinhoff, G. (2011) Patterning human stem cells and endothelial cells with laser printing for cardiac regeneration, *Biomaterials 32*, 9218-9230.
151. Wilson, W. C., Jr., and Boland, T. (2003) Cell and organ printing 1: protein and cell printers, *Anat Rec A Discov Mol Cell Evol Biol 272*, 491-496.
152. Nahmias, Y., and Odde, D. J. (2006) Micropatterning of living cells by laser-guided direct writing: application to fabrication of hepatic-endothelial sinusoid-like structures, *Nat Protoc 1*, 2288-2296.
153. Guillemot, F., Souquet, A., Catros, S., and Guillotin, B. (2010) Laser-assisted cell printing: principle, physical parameters versus cell fate and perspectives in tissue engineering, *Nanomedicine (Lond) 5*, 507-515.
154. Barron, J. A., Ringeisen, B. R., Kim, H., Spargo, B. J., and Chrisey, D. B. (2004) Application of laser printing to mammalian cells, *Thin Solid Films 453-454*, 383-387.
155. Duocastella, M., Colina, M., Fernández-Pradas, J. M., Serra, P., and Morenza, J. L. (2007) Study of the laser-induced forward transfer of liquids for laser bioprinting, *Applied Surface Science 253*, 7855-7859.
156. Gruene, M., Unger, C., Koch, L., Deiwick, A., and Chichkov, B. (2011) Dispensing pico to nanolitre of a natural hydrogel by laser-assisted bioprinting, *Biomed Eng Online 10*, 19.
157. Koch, L., Deiwick, A., Schlie, S., Michael, S., Gruene, M., Coger, V., Zychlinski, D., Schambach, A., Reimers, K., Vogt, P. M., and Chichkov, B. (2012) Skin tissue generation by laser cell printing, *Biotechnol Bioeng 109*, 1855-1863.
158. Michael, S., Sorg, H., Peck, C. T., Koch, L., Deiwick, A., Chichkov, B., Vogt, P. M., and Reimers, K. (2013) Tissue engineered skin substitutes created by laser-assisted bioprinting form skin-like structures in the dorsal skin fold chamber in mice, *PLoS One 8*, e57741.
159. Keriquel, V., Guillemot, F., Arnault, I., Guillotin, B., Miraux, S., Amedee, J., Fricain, J. C., and Catros, S. (2010) In vivo bioprinting for computer- and robotic-assisted medical intervention: preliminary study in mice, *Biofabrication 2*, 014101.
160. Gruene, M., Pflaum, M., Deiwick, A., Koch, L., Schlie, S., Unger, C., Wilhelmi, M., Haverich, A., and Chichkov, B. N. (2011) Adipogenic differentiation of laser-printed

3D tissue grafts consisting of human adipose-derived stem cells, *Biofabrication 3*, 015005.
161. Gruene, M., Pflaum, M., Hess, C., Diamantouros, S., Schlie, S., Deiwick, A., Koch, L., Wilhelmi, M., Jockenhoevel, S., Haverich, A., and Chichkov, B. (2011) Laser printing of three-dimensional multicellular arrays for studies of cell-cell and cell-environment interactions, *Tissue Eng Part C Methods 17*, 973-982.
162. Evangelista, M. B., Hsiong, S. X., Fernandes, R., Sampaio, P., Kong, H.-J., Barrias, C. C., Salema, R., Barbosa, M. A., Mooney, D. J., and Granja, P. L. (2007) Upregulation of bone cell differentiation through immobilization within a synthetic extracellular matrix, *Biomaterials 28*, 3644-3655.
163. Silva, E. A., Kim, E. S., Kong, H. J., and Mooney, D. J. (2008) Material-based deployment enhances efficacy of endothelial progenitor cells, *Proc Natl Acad Sci U S A 105*, 14347-14352.
164. Bouhadir, K. H., Hausman, D. S., and Mooney, D. J. (1999) Synthesis of cross-linked poly(aldehyde guluronate) hydrogels, *Polymer 40*, 3575-3584.
165. Kuo, C. K., and Ma, P. X. (2001) Ionically crosslinked alginate hydrogels as scaffolds for tissue engineering: part 1. Structure, gelation rate and mechanical properties, *Biomaterials 22*, 511-521.
166. Oliveira, S. M., Barrias, C. C., Almeida, I. F., Costa, P. C., Ferreira, M. R., Bahia, M. F., and Barbosa, M. A. (2008) Injectability of a bone filler system based on hydroxyapatite microspheres and a vehicle with in situ gel-forming ability, *J Biomed Mater Res B Appl Biomater 87*, 49-58.
167. Bidarra, S. J., Barrias, C. C., Barbosa, M. A., Soares, R., and Granja, P. L. (2010) Immobilization of human mesenchymal stem cells within RGD-grafted alginate microspheres and assessment of their angiogenic potential, *Biomacromolecules 11*, 1956-1964.
168. Mendez-Ferrer, S., Michurina, T. V., Ferraro, F., Mazloom, A. R., Macarthur, B. D., Lira, S. A., Scadden, D. T., Ma'ayan, A., Enikolopov, G. N., and Frenette, P. S. (2010) Mesenchymal and haematopoietic stem cells form a unique bone marrow niche, *Nature 466*, 829-834.
169. Nassiri, S. M., and Rahbarghazi, R. (2013) Interactions of mesenchymal stem cells with endothelial cells, *Stem cells and development 23*, 319-332.
170. Kumar, V. B., Viji, R. I., Kiran, M. S., and Sudhakaran, P. R. (2012) Angiogenic response of endothelial cells to fibronectin, *Adv Exp Med Biol 749*, 131-151.
171. Zou, L., Cao, S., Kang, N., Huebert, R. C., and Shah, V. H. (2012) Fibronectin induces endothelial cell migration through beta1 integrin and Src-dependent phosphorylation of fibroblast growth factor receptor-1 at tyrosines 653/654 and 766, *J Biol Chem 287*, 7190-7202.
172. Caplan, A. I. (2008) All MSCs Are Pericytes?, *Cell Stem Cell 3*, 229-230.
173. Mills, S. J., Cowin, A. J., and Kaur, P. (2013) Pericytes, mesenchymal stem cells and the wound healing process, *Cells 2*, 621-634.
174. Gang, E. J., Jeong, J. A., Hong, S. H., Hwang, S. H., Kim, S. W., Yang, I. H., Ahn, C., Han, H., and Kim, H. (2004) Skeletal myogenic differentiation of mesenchymal stem cells isolated from human umbilical cord blood, *Stem Cells 22*, 617-624.
175. Moonen, J. R., Krenning, G., Brinker, M. G., Koerts, J. A., van Luyn, M. J., and Harmsen, M. C. (2010) Endothelial progenitor cells give rise to pro-angiogenic smooth muscle-like progeny, *Cardiovasc Res 86*, 506-515.
176. Burlacu, A., Grigorescu, G., Rosca, A. M., Preda, M. B., and Simionescu, M. (2013) Factors secreted by mesenchymal stem cells and endothelial progenitor cells have complementary effects on angiogenesis in vitro, *Stem Cells Dev 22*, 643-653.
177. Shi, Y., Kramer, G., Schroder, A., Kirkpatrick, C. J., Seekamp, A., Schmidt, H., and Fuchs, S. (2014) Early endothelial progenitor cells as a source of myeloid cells to improve the pre-vascularisation of bone constructs, *Eur Cell Mater 27*, 64-79; discussion 79-80.
178. Javvaji, V., Baradwaj, A. G., Payne, G. F., and Raghavan, S. R. (2011) Light-activated ionic gelation of common biopolymers, *Langmuir 27*, 12591-12596.

***Annex I** – Laser power influence in printing 1% HLMW (w/v) alginate with gelation agents and cells at 2 million/mL as cell density*